REPORT SAMSO-TR-78-42

Theoretical Pressure Correlation Functions in Turbulent Boundary Layers

W. C. MEECHAM, Consultant, and M. T. TAVIS
Electronics Research Laboratory
The Ivan A. Getting Laboratories
The Aerospace Corporation
El Segundo, Calif. 90245

8 June 1978

Interim Report

Prepared for

AIR FORCE WEAPONS LABORATORY
Kirtland Air Force Base, N. Mex. 87117

SPACE AND MISSILE SYSTEMS ORGANIZATION
AIR FORCE SYSTEMS COMMAND
Los Angeles Air Force Station
P.O. Box 92960, Worldway Postal Center
Los Angeles, Calif. 90009

This interim report was submitted by The Aerospace Corporation, El Segundo, CA 90245, under Contract No. F04701-77-C-0078 with the Space and Missile Systems Organization, Deputy for Advanced Space Programs, P.O. Box 92960, Worldway Postal Center, Los Angeles, CA 90009. It was reviewed and approved for The Aerospace Corporation by A. H. Silver, Director, Electronics Research Laboratory. Lieutenant Dara Batki, SAMSO/YCPT, was the project officer for Advanced Space Programs.

This report has been reviewed by the Information Office (OI) and is releasable to the National Technical Information Service (NTIS). At NTIS, it will be available to the general public, including foreign nations.

This technical report has been reviewed and is approved for publica tion. Publication of this report does not constitute Air Force approval of the report's findings or conclusions. It is published only for the exchange and stimulation of ideas.

Dara Batki
Dara Batki, Lt, USAF
Project Officer

Robert W. Lindemuth
Robert W. Lindemuth, Lt Col, USAF
Chief, Technology Plans Division

FOR THE COMMANDER

Leonard E. Baltzell
LEONARD E. BALTZELL, Col, USAF
Asst. Deputy for Advanced Space Programs

UNCLASSIFIED

SECURITY CLASSIFICATION OF THIS PAGE (When Data Entered)

REPORT DOCUMENTATION PAGE		READ INSTRUCTIONS BEFORE COMPLETING FORM
1. REPORT NUMBER SAMSO-TR-78-42	2. GOVT ACCESSION NO.	3. RECIPIENT'S CATALOG NUMBER
4. TITLE (and Subtitle) THEORETICAL PRESSURE CORRELATION FUNCTIONS IN TURBULENT BOUNDARY LAYERS		5. TYPE OF REPORT & PERIOD COVERED Interim 6. PERFORMING ORG. REPORT NUMBER TR-0078(3606)-2
7. AUTHOR(s) William C. Meecham (Consultant) and Michael T. Tavis		8. CONTRACT OR GRANT NUMBER(s) F04701-77-C-0078
9. PERFORMING ORGANIZATION NAME AND ADDRESS The Aerospace Corporation El Segundo, Calif. 90245		10. PROGRAM ELEMENT, PROJECT, TASK AREA & WORK UNIT NUMBERS
11. CONTROLLING OFFICE NAME AND ADDRESS Air Force Weapons Laboratory Kirtland Air Force Base, N. Mex. 87117		12. REPORT DATE 8 June 1978 13. NUMBER OF PAGES 89
14. MONITORING AGENCY NAME & ADDRESS(if different from Controlling Office) Space and Missile Systems Organization Air Force Systems Command Los Angeles, Calif. 90009		15. SECURITY CLASS. (of this report) Unclassified 15a. DECLASSIFICATION/DOWNGRADING SCHEDULE

16. DISTRIBUTION STATEMENT (of this Report)

Approved for public release; distribution unlimited.

17. DISTRIBUTION STATEMENT (of the abstract entered in Block 20, if different from Report)

18. SUPPLEMENTARY NOTES

19. KEY WORDS (Continue on reverse side if necessary and identify by block number.)

Boundary Layer
Pressure Correlation
Navier-Stokes Equation

20. ABSTRACT (Continue on reverse side if necessary and identify by block number)

A Poisson equation is constructed for the pressure in terms of velocity fluctuations, and solved. The pressure correlation has a second-order velocity fluctuation contribution (usually assumed dominant in past work) and a fourth-order velocity correlation contribution. The velocity correlations are assumed to be those--suitably weighted—found from homogeneous turbulence measurements. Results are computed for two boundary layers: an idealized (canonical) turbulent boundary layer and a deliberately thickened boundary layer. The pressure variances are found to be essentially the same as

DD FORM 1473 (FACSIMILE)

UNCLASSIFIED

SECURITY CLASSIFICATION OF THIS PAGE (When Data Entered)

19. KEY WORDS (Continued)

20. ABSTRACT (Continued)

measured values. The correlations have scales equal to the displacement thickness of the boundary layer. All correlations are positive except the streamwise, x-correlation for the thickened boundary layer. The canonical layer shows a pressure variance that peaks very close to the wall, near the laminar sublayer. The fourth-order velocity fluctuations may be generally neglected for the thickened boundary layer; close to the wall it is an important part of the variance and correlation for the canonical layer.

CONTENTS

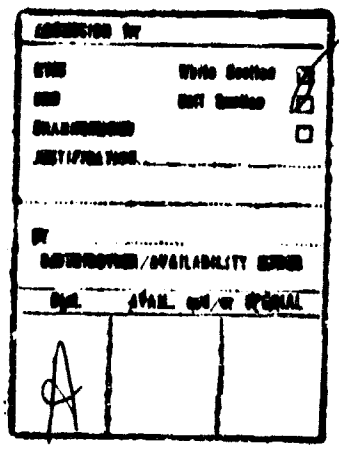

FIGURES

I. INTRODUCTION

In this paper, the pressure correlation function for a single boundary layer over a flat plate will be derived for the subsonic flow regime. Numerical results will be given based on experimental measurements of the magnitude of the mean and fluctuation velocities in the boundary layer. One application for this work is that of the propagation of a laser beam through a turbulent boundary layer. Another important application is that of the generation of sound by boundary layers over flat surfaces.

There has been a tremendous amount of work directed toward questions relating to such boundary layers. This work has in the main been experimental, because of the complexity of the equations governing fluid flow. Kraichnan [1-2] has produced theoretical estimates of pressure correlations at the boundary. Other literature can be found in standard references.

Index of refraction fluctuations, important to optical propagation, are primarily dependent upon density changes. Density fluctuations can be caused by pressure and/or by temperature fluctuations. As a result of recent experimental information and some estimates, it has seemed reasonable to concentrate first upon the effects of pressure fluctuations. For now we neglect temperature effects and treat these effects in a later paper; in effect we suppose that the flow is adiabatic. We assume air is an ideal gas. A sketch of the boundary layer is shown in Fig. 1.

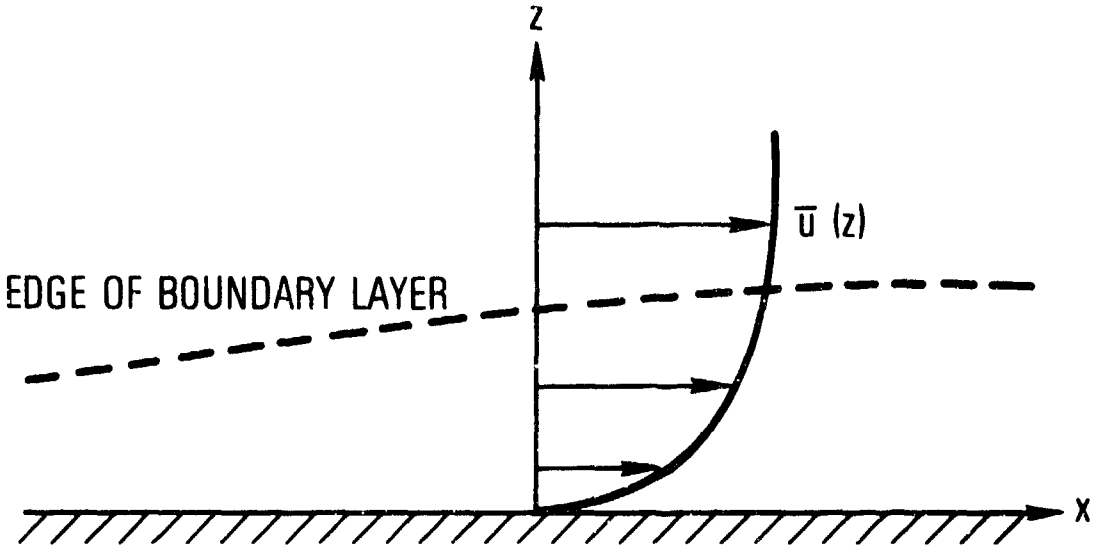

Fig. 1. Sketch of Turbulent Boundary Layer

Since we are interested here in subsonic flow regimes, it is possible to treat the fluid as approximately incompressible. It is true that the mean flow Mach number approaches unity. Nevertheless, the velocity fluctuations (determining the pressure fluctuations) are considerably smaller than mean flow values and their Mach number is small. (The question of whether or not one can treat a flow as incompressible is governed mainly by the Mach number.) The incompressible equations of motion, the Navier-Stokes equations, and the equation of continuity can be written

$$\dot{\underline{u}} + \underline{u} \cdot \nabla \underline{u} = - \frac{1}{\rho_o} \nabla p + \nu \nabla^2 \underline{u} \qquad (1)$$

and

$$\nabla \cdot \underline{u} = 0 \qquad (2)$$

The notation in these equations is standard. The density ρ_o is assumed constant; the dot over the velocity in Eq. (1) represents the time derivative of that quantity.

The equations of motion are of course very complicated at this level of generality. For turbulent boundary layers there are some useful and realistic simplifying assumptions. The boundary layer grows very slowly in the down-stream direction: the characteristic length in that direction is much greater than the thickness of the boundary layer. To good approximation we may assume that the averages of all quantities are functions only of the direction perpendicular to the wall; the mean flow in particular depends mainly on that direction. Consequently, the drag on the flow is approximately

constant in the down-stream direction; hence the pressure gradient (which overcomes that drag) is likewise constant. The Poiseuille flow problem fulfills these approximations exactly and is discussed in this connection in Appendix A. We assume that the flow is statistically stationary, so that averages are independent of the time at which they are taken.

The definitions of some quantities to be discussed here are shown in the figure. The y-direction is perpendicular to the plane of the page.

The components of the position vector and of the velocity in the three Cartesian directions are

$$\underline{r} = (x,\ y,\ z) = (r_1,\ r_2,\ r_3)$$

and (3)

$$\underline{u} = (u,\ v,\ w) = (u_1,\ u_2,\ u_3)\ ;$$

the choice of component representation is made as convenient. Other vectors below have similar representation. We write the velocity and pressure in terms of mean values and fluctuations

$$\underline{u} = \overline{\underline{u}} + \underline{u}' = \overline{u}\ (z)\ \hat{i} + \underline{u}'$$

$$p = \overline{p} + p' \qquad (4)$$

Here $\underline{u}'$ is taken at $\underline{r}'$ and (later) $\underline{u}''$ at $\underline{r}''$ and similarly for p' and p''.

The essential method to be employed in this work is the following: take the divergence of the incompressible Navier-Stokes equation. One finds a Poisson equation for the pressure where the right side (source term) under our assumptions consists of second-order velocity fluctuations and terms quartic in such fluctuations. The former have mean-velocity gradients

as coefficients. The Poisson equation is solved for the pressure fluctuations; the correlations (and variances) of the pressure are constructed from this solution. The quantities so found are integrated numerically.

In Section II the pressure correlation function will be derived with contributions retained through the fourth order in velocity fluctuations. Section III is concerned with evaluation of the fourth-order contribution to the pressure correlation while Section IV deals with the second order term. Numerical techniques used in calculating the correlation function are given in Appendix E. Numerical results and conclusions are presented in Section V.

II. DERIVATION OF THE PRESSURE CORRELATION

From the above assumptions (see Appendix A)

$$\bar{p} = -ax - \overline{w'^2(z')} \tag{5}$$

where we refer pressures to the pressure at the origin. Now take the divergence of Eq. (1) using the incompressibility condition given by Eq. (2) and find (with ∇'^2 the Laplacian in $\underline{r}'$ - space)

$$\nabla'^2 p(\underline{r}', t) = -\rho_o \frac{\partial^2}{\partial r'_\alpha \partial r'_\beta} u_\alpha(r', t)\, u_\beta(\underline{r}', t) \tag{6}$$

written at the point $\underline{r}'$. We use the summation convention: a repeated index in a single term is to be summed from one to three. If now we substitute Eq. (4) in Eq. (6) and average we obtain an expression for the average pressure, noting from Eq. (4) that averages of the fluctuations, $\underline{u}'$ and p', vanish.

Subtract the averaged equation from Eq. (6) to find the following relation for the pressure fluctuation (the time-dependence is implicit),

$$\nabla'^2 p' = -\rho_o \frac{\partial^2}{\partial r'_\alpha \partial r'_\beta} \left[2\bar{u}(z') \delta_{\alpha 1} u'_\beta + u'_\alpha u'_\beta - \langle u'_\alpha u'_\beta \rangle \right]$$

$$\equiv -\rho_o \frac{\partial^2 H_{\alpha\beta}(\underline{r}')}{\partial r'_\alpha \partial r'_\beta} \quad . \tag{7}$$

We use the brackets, $\langle\ \rangle$, or the overbar for time averages, as convenient. The last (average) term in Eq. (7) is a function of z' alone under our boundary layer assumptions. The Kronecker delta has values: $\delta_{ij} = 1$, $i = j$ and equal zero otherwise.

In order to solve Eq. (7) we need the Green's function for the problem. It is recalled that the flow is confined to the half-space above the plane (see Fig. 1). The boundary conditions on the pressure at the plane are not simple and, in fact, stated exactly would involve fluctuating quantities. An approach, which in some ways simplifies the treatment, is the following. First, our problem consists of a plane which exerts drag upon the flow, and the complicated flow above the plane, confined of course mainly to the boundary layer. This problem can be replaced by an equivalent problem. Suppose that we construct a flow below the plane which is the mirror image of the actual one above it, and replace our problem by the original flow plus the imaged flow plus a force; the boundary-layer plane of course exerts a drag upon the flow and when we remove that plane we must insert a force equal to that drag. Fortunately this force is negligible (see Appendix B). We proceed with the

situation as described consisting of the actual, physical flow and the mirror-imaged flow. Then the Green's function needed for the solution of Eq. (7) is the free space Green's function for the Laplacian operator--essentially $\frac{1}{r}$. Further, we suppose that all fluctuating quantities, pressure and velocity, vanish sufficiently far outside the boundary layer regions, whether in the physical flow or the mirrored flow. Then all solutions of the homogeneous equation derived from Eq. (7) (that is, solutions of Eq. (7) with the right side equal to zero) must vanish. The solution of that equation becomes [4]

$$p'(\underline{r}') = \frac{\rho_o}{4\pi} \int |\underline{r}' - \underline{r}'_0|^{-1} \frac{\partial^2}{\partial r'_{0\alpha} \partial r'_{0\beta}} H_{\alpha\beta}(\underline{r}'_0)\, d\underline{r}'_0$$

with, as above,

$$H_{\alpha\beta} = 2\bar{u}(z')\delta_{\alpha 1} u'_\beta + u'_\alpha u'_\beta - \langle u'_\alpha u'_\beta \rangle \tag{8}$$

The velocity functions, and integrals involving them, extend now over all space (they are, as stated, primarily confined within the boundary layer and the mirrored boundary layer).

To find the pressure correlation from this, write Eq. (8) for the pressure at the point $\underline{r}''$ and multiply that equation by Eq. (8) at the point $\underline{r}'$ and average to find

$$C_{pp} = \langle p'(\underline{r}')\, p''(\underline{r}'')\rangle$$

$$= \left(\frac{\rho_o}{4\pi}\right)^2 \iint |\underline{r}' - \underline{r}'_0|^{-1}\, |\underline{r}'' - \underline{r}''_0|^{-1} \tag{9}$$

$$\times \frac{\partial^4}{\partial r'_{0\alpha}\, \partial r'_{0\beta}\, \partial r''_{0\gamma}\, \partial r''_{0\delta}} \langle H_{\alpha\beta}(\underline{r}'_0)\, H_{\gamma\delta}(\underline{r}''_0)\rangle\, d\underline{r}'_0\, d\underline{r}''_0 \quad .$$

The question of convergence of these integrals is of primary importance. Suppose the integral over $\underline{r}''_0$ is performed first; we can expect that the correlation in the integrand will vanish for $\underline{r}''_0$ sufficiently different from $\underline{r}'_0$, so that the integral will be convergent at infinity. Furthermore there is a question of convergence when $\underline{r}'' - \underline{r}''_0$ vanishes. The differential element of volume $d\underline{r}''_0$ will take care of this apparent singularity. There is however, more difficulty with the outer integral over $\underline{r}'_0$, in particular at infinity for that integral. This is a familiar problem if one attempts to deal seriously with a pressure representation as given in Eq. (8). The fact is that there is a considerable amount of cancellation in that integration process which results from the fact that the integrand of Eq. (8) is a quadrupole source for the pressure field. The proper way to deal with this difficulty is to integrate Eq. (9) by parts using the derivatives with respect to $\underline{r}'_0$. This is what will be done below. When that manipulation is carried out we have the factor $|\underline{r}' - \underline{r}'_0|^{-1}$ replaced, for $\underline{r}'_0$ large, by something like $|\underline{r}'_0|^{-3}$ which will give a convergent result at infinity. Then one might expect difficulties at the singular point $|\underline{r}'_0 - \underline{r}''_0| = 0$. Fortunately, the integral is also convergent there, because of angular cancellations. The difficulties, which arise at the singular point when we integrate by parts, are discussed in Appendix D.

Consider the correlation in the integral (9). It consists of second-order, third-order and fourth-order velocity correlations, the second- and third-order with coefficients involving the mean flow. To begin, we note that third-order velocity correlations are usually very small compared with even order correlations. Indeed, for a velocity field with Gaussian statistics, odd moments would vanish. In actual flows the odd moments of fluctuating quantities are typically very small. We neglect them.

There have been many measurements made of second-order velocity correlations but rather few of fourth-order correlations. We make the reasonable assumption that the velocity field is not too far from Gaussian; then the fourth-order velocity correlation can be written as follows

$$\begin{aligned}\langle u'_\alpha u'_\beta u''_\gamma u''_\delta \rangle &= Q_{\alpha\gamma}(\underline{r}'_0, \underline{r}''_0)\, Q_{\beta\delta}(\underline{r}'_0, \underline{r}''_0) \\ &+ Q_{\alpha\delta}(\underline{r}'_0, \underline{r}''_0)\, Q_{\beta\gamma}(\underline{r}'_0, \underline{r}''_0) \\ &+ Q_{\alpha\beta}(\underline{r}'_0, \underline{r}'_0)\, Q_{\gamma\delta}(\underline{r}''_0, \underline{r}''_0)\ ;\end{aligned} \tag{10}$$

the result of this Gaussianity assumption is that the fourth-order velocity correlation can be written in terms of quadratic expressions involving the second-order correlation. We have defined the second-order velocity correlation:

$$Q_{ij}(\underline{r}'_0, \underline{r}''_0) = \langle u'_i u''_j \rangle \quad . \tag{11}$$

We let the pressure correlation be represented by

$$C_{pp} = C^{(1)}_{pp} + C^{(2)}_{pp} \tag{12}$$

where

$$C_{pp}^{(1)} = \left(\frac{\rho_o}{4\pi}\right)^2 \iint |\underline{r}' - \underline{r}_0'|^{-1} \; |\underline{r}'' - \underline{r}_0''|^{-1} \; \frac{\partial^4}{\partial r_{0\alpha}' \, \partial r_{0\beta}' \, \partial r_{0\gamma}'' \, \partial r_{0\delta}''}$$

$$\times \left[4 \bar{u}(z_0') \, \bar{u}(z_0'') \, \delta_{\alpha 1} \, \delta_{\gamma 1} \, Q_{\beta\delta}(\underline{r}_0', \underline{r}_0'')\right] d\underline{r}_0' \, d\underline{r}_0'' \tag{13}$$

$$C_{pp}^{(2)} = \left(\frac{\rho_o}{4\pi}\right)^2 \iint |\underline{r}' - \underline{r}_0'|^{-1} \; |\underline{r}'' - \underline{r}_0''|^{-1} \; \frac{\partial^4}{\partial r_{0\alpha}' \, \partial r_{0\beta}' \, \partial r_{0\gamma}'' \, \partial r_{0\delta}''}$$

$$\times \left[2 \, Q_{\alpha\gamma}(\underline{r}_0', \underline{r}_0'') \; Q_{\beta\delta}(\underline{r}_0', \underline{r}_0'')\right] d\underline{r}_0' \, d\underline{r}_0'' \; . \tag{14}$$

In this last equation the symmetry under index interchange has been utilized. Further, the last term in the fourth-order correlation given in Eq. (10) (that last term representing simple averages) is cancelled by the last term in the function $H_{\alpha\beta}$ given in Eq. (8). Kraichnan [1-2] has considered the problem of the pressure correlation at the boundary-layer wall. He made some progress in the estimation of the size of the correlation coefficients. One of his conclusions was that the first integral, $C_{pp}^{(1)}$, was more important than the second discussed here, the reason being that the first involves the mean-flow velocity whereas the second involves only the (smaller) velocity fluctuations. We carry both of the contributions to the pressure correlation and will determine through computation whether the assertion is justified or not. There is some reason to question it, despite its apparent reasonableness. Measurements of rms pressure fluctuations at the wall give values which appear to be $\frac{1}{2} \rho_o u'^2$ rather than $\frac{1}{2} \rho_o u'\bar{u}$, as would be the case if the mean flow term dominated the result. To proceed, further (reasonable) simplifying assumptions are required. First, for the

integral $c_{pp}^{(1)}$ we suppose that the second-order velocity correlation can be written,

$$Q_{\beta\delta}(\underline{r}_0', \underline{r}_0'') = u'(z_0')\, u'(z_0'')\, Q_{\beta\delta}^*(\underline{r}_0),$$

with $$\underline{r}_0 = \underline{r}_0'' = \underline{r}_0' ,$$

$$u'(z_0') = \langle \tfrac{1}{3} \underline{u}'^2 (z_0') \rangle^{1/2} \qquad (15)$$

and $$u''(z_0'') = \langle \tfrac{1}{3} \underline{u}''^2 (z_0'') \rangle^{1/2}$$

where $Q_{\beta\delta}^*(\underline{r}_0')$ is the normalized second-order velocity correlation for homogeneous and isotropic turbulence (normalized by the rms values of the velocity fluctuation in one direction). Here we have used a normalization involving the velocity fluctuations at the two points $\underline{r}_0'$ and $\underline{r}_0''$. The normalized second-order velocity correlation has an outer scale which is approximately the distance from the wall; for that scale we choose M. The scale M is defined as $M^{-1} = [(z_0')^{-1} + T^{-1}]^{-1}$ where T is the thickness of the fluctuating boundary layer, defined as the distance from the wall where $\bar{u}$ attains 0.9 of its maximum value. This T is greater than δ (the displacement thickness defined by $\delta = \int_0^\infty [1 - \frac{\bar{u}(z)}{u_\infty}] dz$). It was felt that this value T was appropriate here, rather than the smaller δ. The substance of this assumed form is that we propose that the second-order velocity correlation is locally isotropic, but corrected for the variation in strength of the velocity fluctuation over the displacement vector $\underline{r}_0$. The nature of the second-order velocity correlation for homogeneous and isotropic turbulence is well known through wind tunnel

measurements. Later we shall take numerical values from standard literature references [5]. In fact, for our incompressible flow problem, the correlation function becomes, for large Reynold's numbers, essentially independent of the Reynold's number: a universal function. Consequently, for different boundary layer measurements it will not be necessary to change these functions. The normalized velocity correlations for homogeneous and isotropic turbulence can be written [5]

$$Q^*_{ij}(\underline{r}) = \frac{f(r/M) - g(r/M)}{r^2} r_i r_j + g(r/M)\delta_{ij} \tag{16}$$

The f and g and $Q^*_{ij}(\underline{r})$ are simply behaved functions of r/M where M, the "distance" from the wall is the outer scale for the velocity correlation as proposed above.

For the second-order velocity correlation (dropping the scaling factor for now) it will be convenient sometimes to use the notation

$$Q^*_{ij}(\underline{r}) = Q_1(r) r_i r_j + Q_2(r)\delta_{ij} \tag{17}$$

with the functions Q_1, Q_2 f and g related as shown. Finally for incompressible flow one can write the function g in terms of the function f as follows [5]

$$g(\bar{r}) = f + 1/2\,\bar{r}\,f' \tag{18}$$

and of course there is a corresponding relation between Q_1 and Q_2. The

relation Eq. (18) follows, as indicated, directly from incompressibility. That condition can be written

$$\frac{\partial}{\partial r_i} Q^*_{ij} = \frac{\partial}{\partial r_j} Q^*_{ij} = 0; \tag{19}$$

The relation, Eq. (18) is obtained from this by differentiating Eq. (16).

If we substitute from Eq. (15) to Eq. (19) into Eq. (13) we find

$$C^{(1)}_{pp} = \left(\frac{\rho_o}{4\pi}\right)^2 \iint d\underline{r}'_0 \, d\underline{r}''_0 \, |\underline{r}' - \underline{r}'_0|^{-1} \, |\underline{r}'' - \underline{r}''_0|^{-1}$$
$$\times \left\{ 4 \left[\frac{\partial}{\partial z'_0} \overline{u}(z'_0)\right] u'(z'_0) \left[\frac{\partial}{\partial z''_0} \overline{u}(z''_0)\right] u''(z''_0) \right\} \tag{20}$$
$$\times \left[- \frac{\partial^2}{\partial x''^2_0} Q^*_{33}(\underline{r}''_0 - \underline{r}'_0) \right]$$

In order to proceed further with this term, simplifying assumptions must be made. For now we will consider the more complicated fourth-order contribution and return to the evaluation of Eq. (20) in Section IV.

III. DETERMINATION OF THE FOURTH-ORDER CONTRIBUTION TO THE PRESSURE CORRELATION

Continue now with a discussion of the term $C^{(2)}_{pp}$ given in Eq. (14). For the term $C^{(2)}_{pp}$ we take for the second-order velocity correlation the following

$$Q_{ij}(\underline{r}'_0, \underline{r}''_0) = u'^2 Q^*_{ij}(\underline{r}_0) \tag{21}$$

where our boundary layer assumptions mean that u'^2 is a function of only z'_o. Substitute this relation for the velocity correlation into Eq. (14). Then integrate by parts and use Gauss' theorem to obtain the result (see below for I),

$$C_{pp}^{(2)} = 2\left(\frac{\rho_o}{4\pi}\right)^2 \int d\underline{r}'_0 \; u'^4 \; (z'_0) \left[\frac{\partial^2}{\partial r'_\alpha \, \partial r'_\beta} \, |\underline{r}' - \underline{r}'_0|^{-1}\right] \frac{\partial^2}{\partial \xi_\gamma \, \partial \xi_\delta} \, I_{\alpha\gamma\beta\delta}(\underline{\xi}) \qquad (22)$$

From Gauss' theorem one also obtains integrals over the surfaces bounding the region of turbulence. Those surfaces are taken outside the physical flow and the image flow; on those surfaces all the fluctuations vanish so the surface integrals vanish. There is also the question of the singular points which arise when the denominators of Eq. (10) vanish. It is shown in Appendix D that these singularities in fact cause no difficulty. We have used new variables in Eq. (22) (as above and as follows),

$$\underline{r}_0 = \underline{r}''_0 - \underline{r}'_0 \qquad (23)$$

and

$$\underline{\xi} = \underline{r}'' - \underline{r}'_0$$

and defined the integral

$$I_{\alpha\gamma\beta\delta}(\underline{\xi}) = \int d\underline{r}_0 \, | \, \underline{\xi} - \underline{r}_0 \, |^{-1} Q^*_{\alpha\gamma}(\underline{r}_0) \, Q^*_{\beta\delta}(\underline{r}_0). \qquad (24)$$

Substituting from Eq. (18) into Eq. (24) we identify the following different types of terms for that integral:

$$I_{\alpha\nu\beta\delta} = I^{(a)}_{\alpha\nu\beta\delta} + I^{(b1)}_{\alpha\nu\beta\delta} + I^{(b2)}_{\alpha\nu\beta\delta} + I^{(c)}_{\alpha\gamma\beta\delta} \quad , \tag{25}$$

$$I^{(a)}_{\alpha\nu\beta\delta} = \int d\underline{r}_0 \, |\underline{\xi} - \underline{r}_0|^{-1} \, Q_1^2 \, (r_0) \, r_{0\alpha} \, r_{0\beta} \, r_{0\nu} \, r_{0\delta} \quad , \tag{26}$$

$$= A_1(\xi) \, \xi_\alpha \, \xi_\beta \, \xi_\nu \, \xi_\delta + A_2(\xi) \left[\xi_\alpha \, \xi_\beta \, \delta_{\nu\delta} + \ldots\ldots \right] \tag{26a}$$

$$+ A_3(\xi) \left[\delta_{\alpha\beta} \, \delta_{\nu\delta} + \delta_{\alpha\nu} \, \delta_{\beta\delta} + \delta_{\alpha\delta} \, \delta_{\beta\gamma} \right],$$

where the coefficient of $A_2(\xi)$ has the six permutations of the indices, two-by-two

$$I^{(b1)}_{\alpha\nu\beta\delta} = \int d\underline{r}_0 \, |\underline{\xi} - \underline{r}_0|^{-1} \, Q_1(r_0) \, Q_2(r_0) \, r_{0\alpha} \, r_{0\nu} \, \delta_{\beta\delta} \quad , \tag{27}$$

$$= \left[B_1(\xi) \, \xi_\alpha \, \xi_\nu + B_2(\xi) \, \delta_{\alpha\nu} \right] \delta_{\beta\delta} \quad ; \tag{27a}$$

$$I^{(b2)}_{\alpha\nu\beta\delta} = I^{(b1)}_{\beta\delta\alpha\nu} \quad ; \tag{28}$$

$$I^{(c)}_{\alpha\nu\beta\delta} = \int d\underline{r}_0 \, |\underline{\xi} - \underline{r}_0|^{-1} \, Q_2^2 \, (r_0) \, \delta_{\alpha\nu} \, \delta_{\beta\delta} \tag{29}$$

$$= C(\xi) \, \delta_{\alpha\nu} \, \delta_{\beta\delta} \quad . \tag{29a}$$

We know the integrals must be of the forms of Eqs. (26a), (27a) and (29a) because of their vector (transformation) properties. One must now find the functions A_1, A_2, A_3, B_1, B_2 and C. These functions are evaluated in Appendix C. For substitution in the integrand of Eq. (22) we must evaluate the second-order derivatives of the integrals given in Eqs. (25) - (29a). Again, by the vector properties of the expression we know

$$\frac{\partial^2}{\partial \xi_\gamma \partial \xi_\delta} I_{\alpha\gamma\beta\delta}(\underline{\xi}) = D_1(\xi)\xi_\alpha \xi_\beta + D_2(\xi)\delta_{\alpha\beta} \quad , \tag{30}$$

Substituting the results given in Appendix C into Eq. (30) and adding the coefficients of corresponding terms, we find for the functions D_1 and D_2

$$D_1(\xi) = 4\pi \left\{ \frac{12}{5} E_1(\xi) + \frac{2}{5}\xi^{-5} E_6 + 2\xi^{-5} F_4 + 3\xi^{-5} G_2 - \left[\xi Q_1(\xi) + \xi^{-1} Q_2(\xi)\right]^2 \right\} \tag{31}$$

$$D_2(\xi) = 4\pi \left\{ -\frac{4}{5}\xi^2 E_1 + \frac{2}{3} E_3 - \frac{2}{15}\xi^{-3} E_6 + \frac{4}{3} F_1 - \frac{2}{3}\xi^{-3} F_4 - \xi^{-3} G_2 \right\} \tag{32}$$

These expressions may be simplified by the use of Eqs. (16) - (18) yielding

$$D_1(\xi) = \frac{4\pi}{5} \left| 12\, E_1(\xi) + 7\xi^{-5} E_6(\xi) \right| \tag{31a}$$

$$D_2(\xi) = \frac{-4\pi\xi^2}{15} \left| 12\, E_1(\xi) + 7\xi^{-5} E_6(\xi) + 10\xi^{-2} E_3(\xi) + 10\xi^{-2} f^2(\xi) \right| \tag{32a}$$

Equation (31a) unlike Eq. (31) is easy to evaluate at $\xi = 0$ and differentiation w.r.t. ξ is more easily accomplished.

Here $E_n(x)$, $F_n(x)$ and $G_n(x)$ are defined by the expressions

$$\int_x^\infty r^n\, q(r)\, dr, \quad n \text{ odd}$$

and (33)

$$\int_0^x r^n\, q(r)\, dr, \quad n \text{ even}$$

with $q(r) = Q_1^2(r)$ for E_n; $q(r) = Q_1(r)\, Q_2(r)$ for F_n; $q(r) = Q_2^2(r)$ for G_n.

Substitute Eq. (30) into Eq. (22), use the known relation

$$\nabla^2 |\underline{r}' - \underline{r}_0'|^{-1} = -4\pi\, \delta(\underline{r}' - \underline{r}_0'), \tag{34}$$

define

$$C_{pp}^{(2)} = C_{pp}^{(2a)} + C_{pp}^{(2b)} + C_{pp}^{(2c)} \tag{35}$$

and find for the term involving D_2,

$$C_{pp}^{(2a)} = -4\pi\left(\frac{\rho_o}{4\pi}\right)^2 2\,[u'(z')]^4\, D_2(r) \tag{35a}$$

with $\underline{r} = \underline{r}'' - \underline{r}'$. The other contribution, from D_1, $\left[C_{pp}^{(2b)} \text{ and } C_{pp}^{(2c)}\right]$ is more complicated. To simplify, use the definition of $\underline{\xi}$ [Eq. (23)] to write $\underline{r}_0' - \underline{r}' = \underline{r} - \underline{\xi}$ and noting that $\frac{\partial^2}{\partial r_\alpha' \partial r_\beta'} |\underline{r}' - \underline{r}_0'|^{-1} = \frac{\partial^2}{\partial \xi_\alpha \partial \xi_\beta} |\underline{r} - \underline{\xi}|$ find

$$\xi_\alpha \xi_\beta \frac{\partial^2}{2\xi_\alpha \partial \xi_\beta} |\underline{r} - \underline{\xi}|^{-1} = \frac{3[\underline{\xi} \cdot (\underline{r} - \underline{\xi})]^2}{|\underline{r} - \underline{\xi}|^5} - \frac{\xi^2}{|\underline{r} - \underline{\xi}|^3} \tag{36}$$

Using $\xi \cdot r = \frac{1}{2}\left(\xi^2 + r^2 - |\underline{r} - \underline{\xi}|^2\right)$ we have for the right hand side of Eq. (36),

$$\frac{3}{4}\left[\frac{(r^2-\xi^2)^2}{|\underline{r}-\underline{\xi}|^5} - \frac{2(r^2-\xi^2)}{|\underline{r}-\underline{\xi}|^3} + \frac{1}{|r-\underline{\xi}|}\right] - \frac{\xi^2}{|\underline{r}-\underline{\xi}|^3} \tag{37}$$

Substitute Eq. (37) and the first term of Eq. (30) into Eq. (22) to find (aside from the delta function contribution at the singular point $\underline{r}' - \underline{r}_0'$, given below)

$$C_{pp}^{(2b)}\left(z',\ (x^2+y^2)^{1/2},\ z\right) = \frac{\rho_o^2}{4\pi^2}\int_{-\infty}^{\infty} d\xi_3 \frac{u'^4(|z''-\xi_3|)}{M^2}\int_0^{\infty}\rho d\rho D_1\left(\frac{(\rho^2+\xi_3^2)^{1/2}}{M}\right)$$

$$\times\int_0^{\pi} d\phi\left\{\frac{3}{4}\left[\frac{(r^2-\xi^2)^2}{|\underline{r}-\underline{\xi}|^5} - \frac{2(r^2-\xi^2)}{|\underline{r}-\underline{\xi}|^3} + \frac{1}{|\underline{r}-\underline{\xi}|}\right] - \frac{\xi^2}{|\underline{r}-\underline{\xi}|^3}\right\} \tag{38a}$$

where $\underline{\xi} = \underline{\rho} + \xi_3\underline{k}$ and $M = (T^{-1} + |z'' - \xi_3|^{-1})^{-1}$. Note the scaling factor used in Eq. (16) has been used explicitly in Eq. (38). This scaling also applies to Eq. (35a) and Eq. (38b) though it is not shown there. The apparent singularity in the neighborhood of $\underline{r} = \underline{\xi}$ in the $\underline{\rho}$ and ξ_3 integration is in fact in integrable. This is most easily shown by using spherical coordinates about the origin; convergence results from the angular integrations.

The last contribution comes from the delta-function at $\underline{r} = \underline{\xi}$; care must be exercised in order not to lose this portion--as cautioned at the end of Appendix D. It can be found by taking the integral of the term involving $D_1(\xi)$ in the volume $|\underline{r}' - \underline{r}_0'| \leq \epsilon$, ϵ very small. We have for it from Eq. (22) and the first term of Eq. (30),

$$C_{pp}^{(2c)} = 2\left(\frac{\rho_o}{4\pi}\right)^2 \int_{|\underline{r}' - \underline{r}_0'| \le \epsilon} d\underline{r}_0'\, u'^4(z_0') \left[\frac{\partial^2}{\partial r_\alpha' \partial r_\beta'} |\underline{r}' - \underline{r}_0'|^{-1}\right] D_1(\xi)\, \xi_\alpha \xi_\beta. \qquad (38b)$$

Following the result given in (D-7) this is

$$C_{pp}^{(2c)} = -\frac{\rho_o^2}{6\pi} u'^4(z')\, r^2\, D_1(r). \qquad (38c)$$

In Appendix F, the techniques used in the calculation of Eq. (38) will be discussed. Consider now the second order contribution.

IV. DETERMINATION OF THE SECOND-ORDER VELOCITY CONTRIBUTION TO THE PRESSURE CORRELATION

It is plausible to expect that the second-order velocity fluctuation terms will dominate the fourth-order; this has often been suggested in the literature (see e.g. Ref. 1). We shall see from our computations that this is usually--though not always--the case.

In the determination of the second-order contribution several different assumptions were considered. The assumption finally chosen as the most tractable was that the prime location replaces the double prime location except in Q^*_{33}.

$$\left[\frac{\partial}{\partial z_0''} \bar{u}(z_0'')\right] u''(z_0'') \frac{\partial^2}{\partial x_0''^2} Q^*_{33}(\underline{r}_0'' - \underline{r}_0') \cong$$

$$\left[\frac{\partial}{\partial z_0'} \bar{u}(z_0')\right] u'(z_0') \frac{\partial^2}{\partial x_0'^2} Q^*_{33}(\underline{r}_0'' - \underline{r}_0') \qquad (39)$$

This is reasonable for $Q_{33} \to 0$ as $\underline{r}_0'' - \underline{r}_0'$ becomes large; it is consistant with the approximation made for the fourth order contribution in Eq. (21). Inserting Eqs. (39), (23) into Eq. (20) yields

$$C_{pp}^{(1)} = \frac{\rho_o^2}{4\pi^2} \int d\underline{r}_0' \left[\frac{\partial}{\partial z_0'} \bar{u}(z_0') u'(z_0') \right]^2 |\underline{r} - \underline{\xi}|^{-1} \frac{\partial^2}{\partial \xi_1^2} \int \frac{d\underline{r}_0 Q_{33}^*(\underline{r}_0)}{|\underline{\xi} - \underline{r}_0|} \tag{40}$$

Analogous to treatment of the fourth order contribution, define

$$I_{\alpha\beta}(\xi) = \int d\underline{r}_0 |\underline{\xi} - \underline{r}_0|^{-1} Q_{\alpha\beta}^*(\underline{r}_0) = A_1(\xi) \xi_\alpha \xi_\beta + A_2(\xi) \delta_{\alpha\beta} + B_2(\xi) \delta_{\alpha\beta} \tag{41}$$

where A_2 is determined first by using the double cross-product with the vector $\underline{\xi}$ and then A_1 is determined by taking the inner product (summing on the indices). Using results from Appendix C.

$$B_2(\xi) = 4\pi \left| \xi^{-1} \bar{F}_2 + \bar{F}_1 \right|$$

$$A_2(\xi) = \frac{4\pi}{15} \left| 5[\xi^{-1} \bar{E}_4 + \bar{E}_3] - [\xi^{-3} \bar{E}_6 + \bar{E}_1 \right|$$

$$A_1(\xi) = \frac{4\pi}{5} \left| \xi^{-5} \bar{E}_6 + \bar{E}_1 \right|$$

where $\bar{E}$, $\bar{F}$ are defined as in Eq. (33) except that here $q(r) = Q_1(r)$ for $\bar{E}_n$ and

$q(r) = Q_2(r)$ for $\overline{F}_n$. Using these expressions and Eqs. (16) - (18) we have the scalar function

$$\underline{D}_1(\xi) = \frac{\partial^2}{\partial \xi_1^2} I_{33}(\xi) = 4\pi \left(\xi_3^2 \left\{ \frac{\xi_1^2}{\xi^2} [7\xi^{-7}\overline{E}_6(\xi) - Q_1(\xi)] - \xi^{-7}\overline{E}_6(\xi) \right\} \right.$$

$$\left. + \frac{\xi_1^2}{\xi^2} [f(\xi) - Q_2(\xi) - \xi^{-5}\overline{E}_6(\xi)] - [2f(\xi) - \xi^{-5}\overline{E}_6(\xi)]/5 \right) \quad (42)$$

Substituting Eq. (42) into Eq. (40) and taking into account scaling results in

$$C_{pp}^{(1)} = \frac{\rho_o^2}{2\pi^2} \int_{-\infty}^{\infty} d\xi_3 [\bar{u}'(|z'' - \xi_3|)\, u'(|z'' - \xi_3|)]^2 \int_0^{\infty} \rho d\rho \int_0^{\pi} \underline{D}_1\left(\frac{|\xi|}{M}\right) |\underline{r} - \underline{\xi}|^{-1} d\phi \quad (43)$$

where ϕ is the angle between the projections of $\underline{\xi}$ and $\underline{r}$ in the x-y plane. Noting that $\xi_1^2 = \rho^2 \cos^2(\alpha - \phi)$ with α is the angle between the projection of $\underline{r}$ in the x-y plane and the x axis unit vector allows Eq. (43) to be written as

$$C_{pp}^{(1)}(x, y. z, z') = C_{pp}^{(1)}(\eta, 0, z, z') \cos^2\alpha + C_{pp}^{(1)}(0, \eta, z, z') \sin^2\alpha \quad (44)$$

where $\eta = \sqrt{x^2 + y^2}$ and ξ_1^2 is replaced by $\rho^2 \cos^2\phi$ for the argument $y = 0$

and $\rho^2 \sin^2 \phi$ for $x = 0$. The cross term vanishes for integration over ϕ.

V. NUMERICAL RESULTS AND CONCLUSIONS

This section contains numerical results and conclusions based on calculating the pressure variance and correlation function from Eq. (38) and Eq. (44). For the interested reader the details of the calculation may be found in Appendix E and supplemental numerical results may be found in Appendix F. In order tc present results which are cohesive a brief step-by-step procedure for obtaining the numerical results is presented with equation and figure numbers prefixed by letters referring to the corresponding appendix. Some of the results presented here should more reasonably have been presented in Appendix F; however, they are presented here to show the reader how to calculate the pressure variance for his own boundary layer data without referring to the cited appendices.

In order to obtain numerical results, all intermediate functions were calculated and stored in the computer in tabular form. Numerical integrations were preformed by Gaussian Quadrature integration techniques with the interval step size determined by an accuracy criteria of one part in 10^3. Values of the functions not in the table were obtained by linear interpolation of the log of the function for positive functions. Close to the origin or for negative functions second to fourth-order Lagrange interpolation techniques were used. The calculation starts with the definition of the longitudinal, f(r), and transverse, g(r), velocity correlations (16). These may be taken from experiments. In our calculations we must

differentiate these functions: a smooth representation is needed. Thus we use the calculation which has been made using the Weiner Hermite expansion[6]. Those results fitted large Reynolds' number experiments very well and were differentiable. The second step in the calculation is the definition of $Q_1(r)$ Eqs. (16)-(17). Using f, g, and Q_1 the functions $D_1(r)$ Eq. (31a) and $D_2(r)$ Eq. (32a) are determined by numerical integration Figure 2 shows the results for $D_1(r)$. After the angular integration in Eq. (38a) has been performed analytically and the results expressed in terms of the complete elliptic integrals, a change of variables and an integration by parts is made on the ρ coordinate. This technique removes a numerical convergence problem but requires the evaluation of the first derivation of $D_1(r)$ which can be obtained from Eq. (31a). Once the flow field turbulent velocity, $u'(z)$, is determined, the fourth-order contribution to the pressure correlation and variance can be obtained directly (see Appendix E). Results for this calculation are presented later in this section. As an aside the fourth-order contribution to the pressure variance can be written as

$$C_{pp}^{(2)}(z',\ o) = \frac{\rho_o^2}{2\pi} \left\{ -[u'(z')]\, D_2(o) + \int_{-\infty}^{\infty} d\xi_3\, [u'(|z' + \xi_3|)]^4 M(xx) M^{-1} \right\} \quad \text{(E3)}$$

where

$$M(xx) = \int_{xx}^{\infty} d\xi\, D_1(\xi)$$

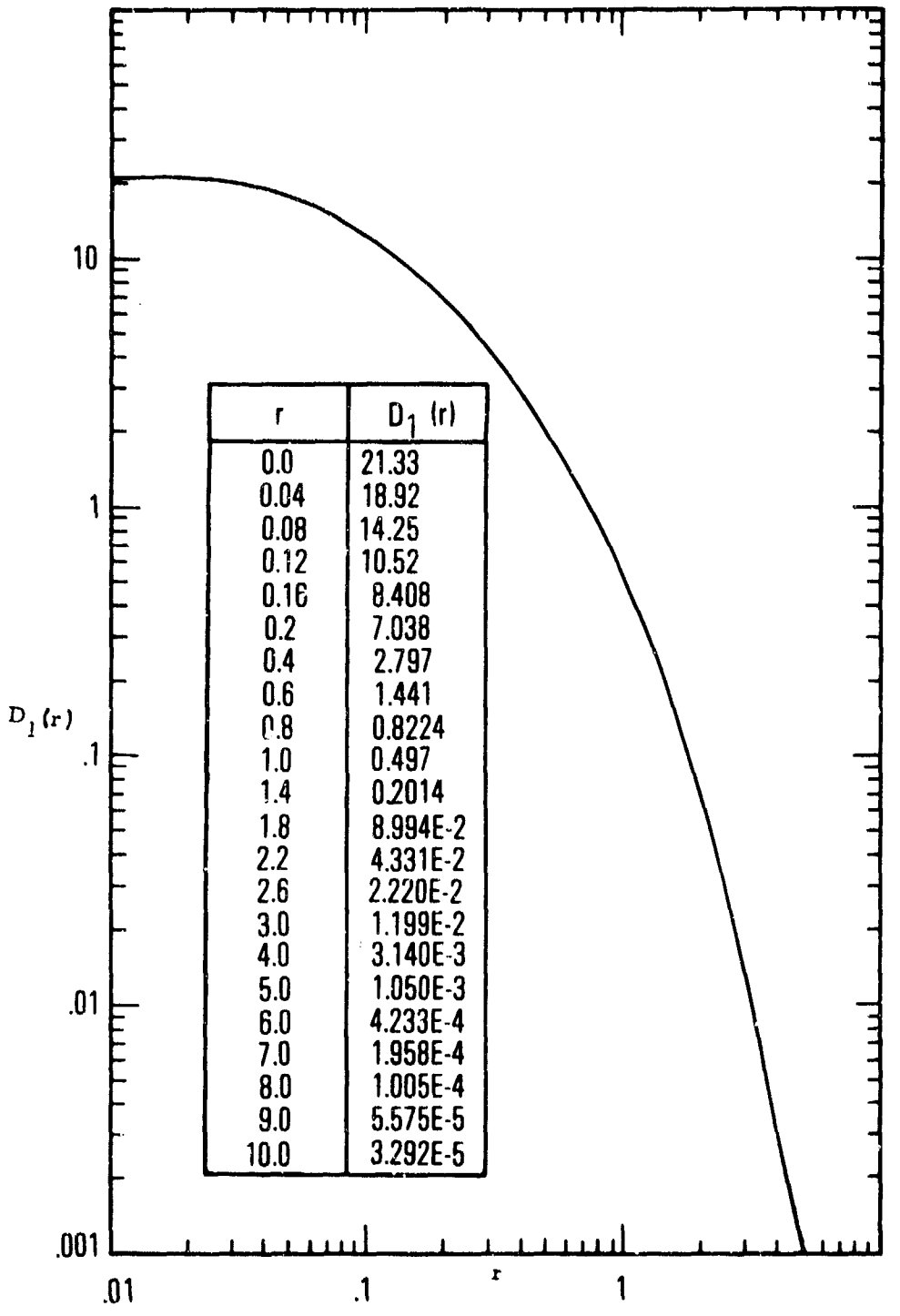

r	D_1 (r)
0.0	21.33
0.04	18.92
0.08	14.25
0.12	10.52
0.16	8.408
0.2	7.038
0.4	2.797
0.6	1.441
0.8	0.8224
1.0	0.497
1.4	0.2014
1.8	8.994E-2
2.2	4.331E-2
2.6	2.220E-2
3.0	1.199E-2
4.0	3.140E-3
5.0	1.050E-3
6.0	4.233E-4
7.0	1.958E-4
8.0	1.005E-4
9.0	5.575E-5
10.0	3.292E-5

Fig. 2. D_1 (r) vs r

$$xx = \xi_3 M^{-1} \tag{E4}$$

$$M = (T^{-1} + | z' + \xi_3 |^{-1})^{-1}$$

$$D_2(0) = -0.54154$$

and T is the thickness of the boundary layer. The function M is plotted in Fig. 3; the reader may obtain the fourth-order variance for other, particular, experimental values of $u'(z)$.

We now consider the second-order contribution to the pressure variance and correlation functions. From Eqs. (43)-(44) it is seen that $\underline{D}(\xi)$ is required. This scalar function is obtained using Eq. (42) and the definition of $\xi^{-7}\bar{E}_6(\xi)$ [defined after Eq. (41)]. The interested reader may then obtain the second-order pressure variance directly from Eq. (43). First it is noted that $\underline{r} = 0$ implies that the angular integration can be performed analytically yielding a factor π for terms not including ξ_1^2 and $\pi/2$ for terms with ξ_1^2. The integral over ρ is then calculated as a function of ξ_3 and normalized by $4\pi^2 M^{-1}$. This function is tabulated in the computer and used in Eq. (43) to obtain the variance for any boundary layer. This function is plotted in Fig. 4. In order to obtain the second-order correlation the angular integrations for Eqs. (43)-(44) are also performed analytically and lead to the tabular function $\bar{B}(x)$ Eq. (E10). The calculation of $C_{pp}^{(1)}$ then proceeds via a double numerical, integration (E12), given the flow

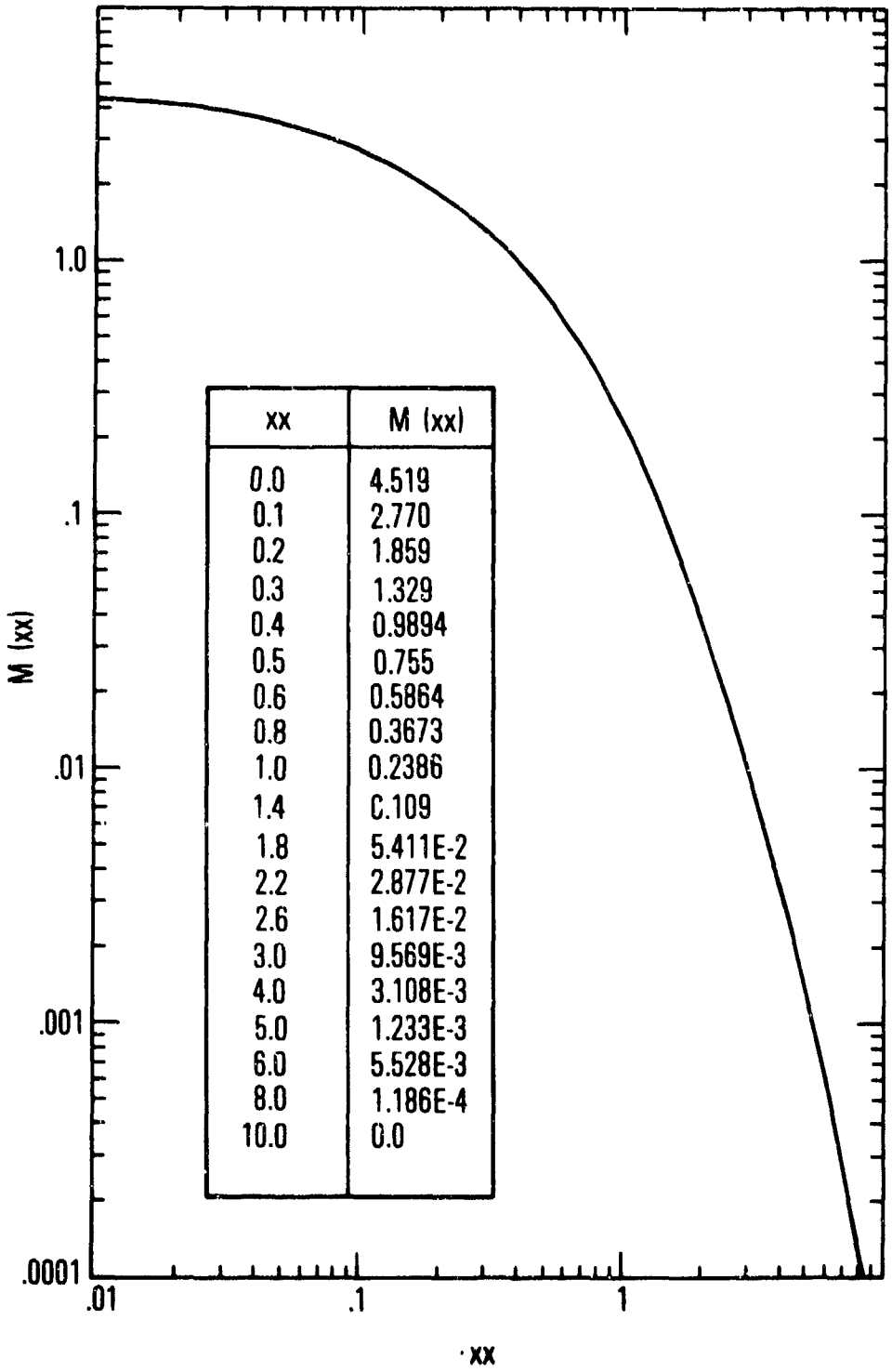

xx	M (xx)
0.0	4.519
0.1	2.770
0.2	1.859
0.3	1.329
0.4	0.9894
0.5	0.755
0.6	0.5864
0.8	0.3673
1.0	0.2386
1.4	C.109
1.8	5.411E-2
2.2	2.877E-2
2.6	1.617E-2
3.0	9.569E-3
4.0	3.108E-3
5.0	1.233E-3
6.0	5.528E-3
8.0	1.186E-4
10.0	0.0

Fig. 3. Function M (xx)

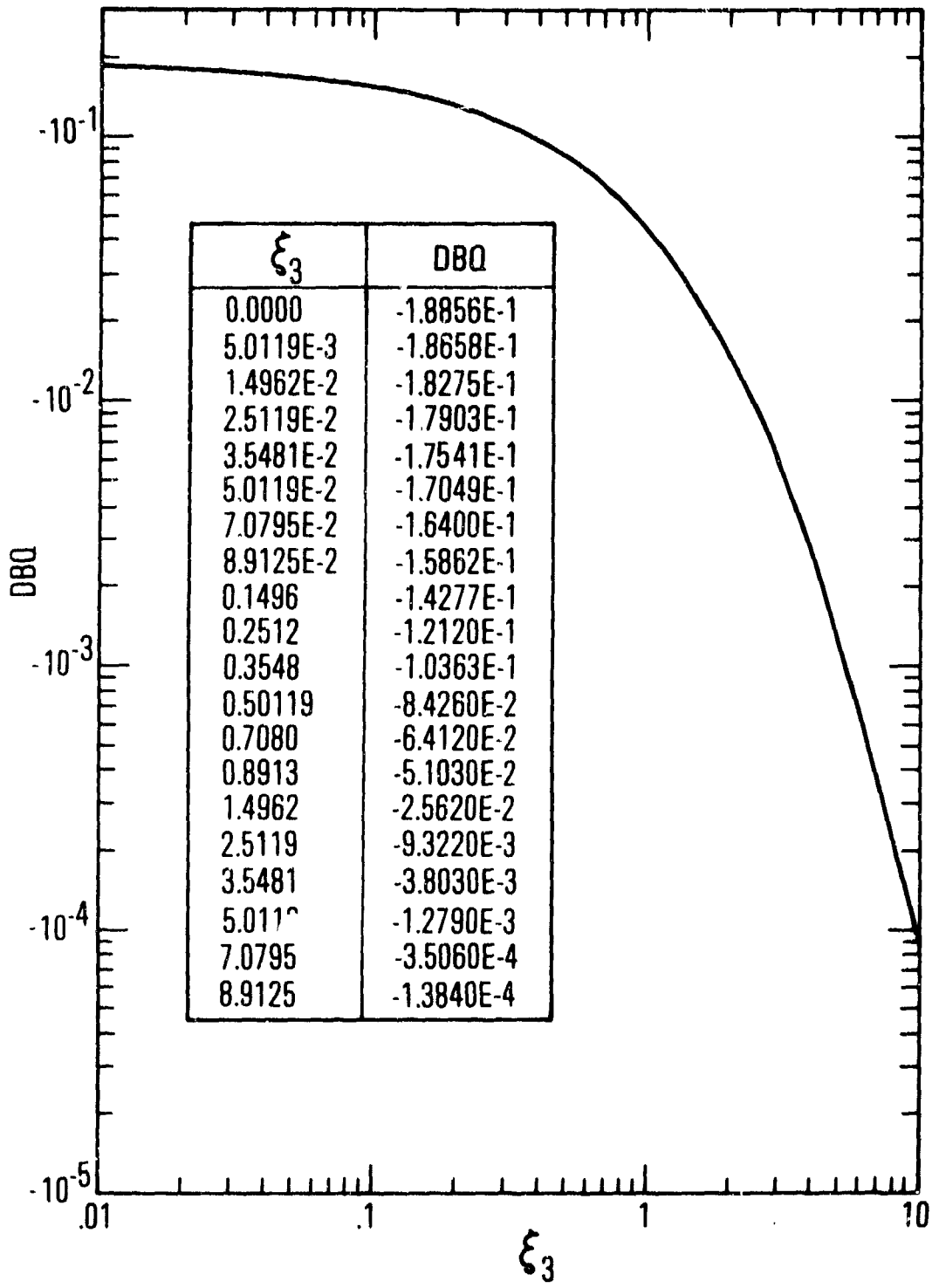

ξ_3	DBQ
0.0000	-1.8856E-1
5.0119E-3	-1.8658E-1
1.4962E-2	-1.8275E-1
2.5119E-2	-1.7903E-1
3.5481E-2	-1.7541E-1
5.0119E-2	-1.7049E-1
7.0795E-2	-1.6400E-1
8.9125E-2	-1.5862E-1
0.1496	-1.4277E-1
0.2512	-1.2120E-1
0.3548	-1.0363E-1
0.50119	-8.4260E-2
0.7080	-6.4120E-2
0.8913	-5.1030E-2
1.4962	-2.5620E-2
2.5119	-9.3220E-3
3.5481	-3.8030E-3
5.011[illegible]	-1.2790E-3
7.0795	-3.5060E-4
8.9125	-1.3840E-4

Fig. 4. Normalized Integrated Value of D_1 (ξ) as a Function of $|\xi_3|$

field data $u_3' \overline{u}'$. Graphical results for f(r), g(r), $Q_1(r)$, $D_2(r)$, $D_1(r)$, and $\xi^{-7}\overline{E}_6(\xi)$ are found in Appendix F.

In order to obtain specific numerical results, flow field quantities must be given.

The flow field quantities necessary to perform the calculations are the normalized mean turbulent velocity used for the calculation of the $C_{pp}^{(2)}$ term and the burbulent fluctuation velocity in the z direction multiplied by the derivative of the flow velocity in the x-direction, which is used in the calculation of the $C_{pp}^{(1)}$ term.

Our calculations were carried out for two separate boundary layer flows: first, for a thickened turbulent boundary layer relating to experiments carried out at NASA-Ames.[7] The thickened layer was generated by a flow of approximately Mach 0.9 and a Reynolds number of 3×10^6/ft. The thickening came as a result of upstream pins and spoilers projecting from the wall over which the boundary layer formed. The second boundary layer for which calculations were made was an idealized one (called here the canonical boundary layer). Data were taken from earlier experimental work with such boundary layers (Hinze, Ref. 8, Figs. 7-4 and 7-10). The flow field quantities necessary for the calculation are presented in Figs. 5-8 vs. the normalized distance from the wall. The normalizing factor for all distance measurements is the displacement thickness δ defined previously. Figures 5-6 are for the experimental case while Figs. 7-8 are for the canonical case. For these two flow fields the normalized (normalization factor $\rho_o^{2-4}\overline{u}^{4}/4$)

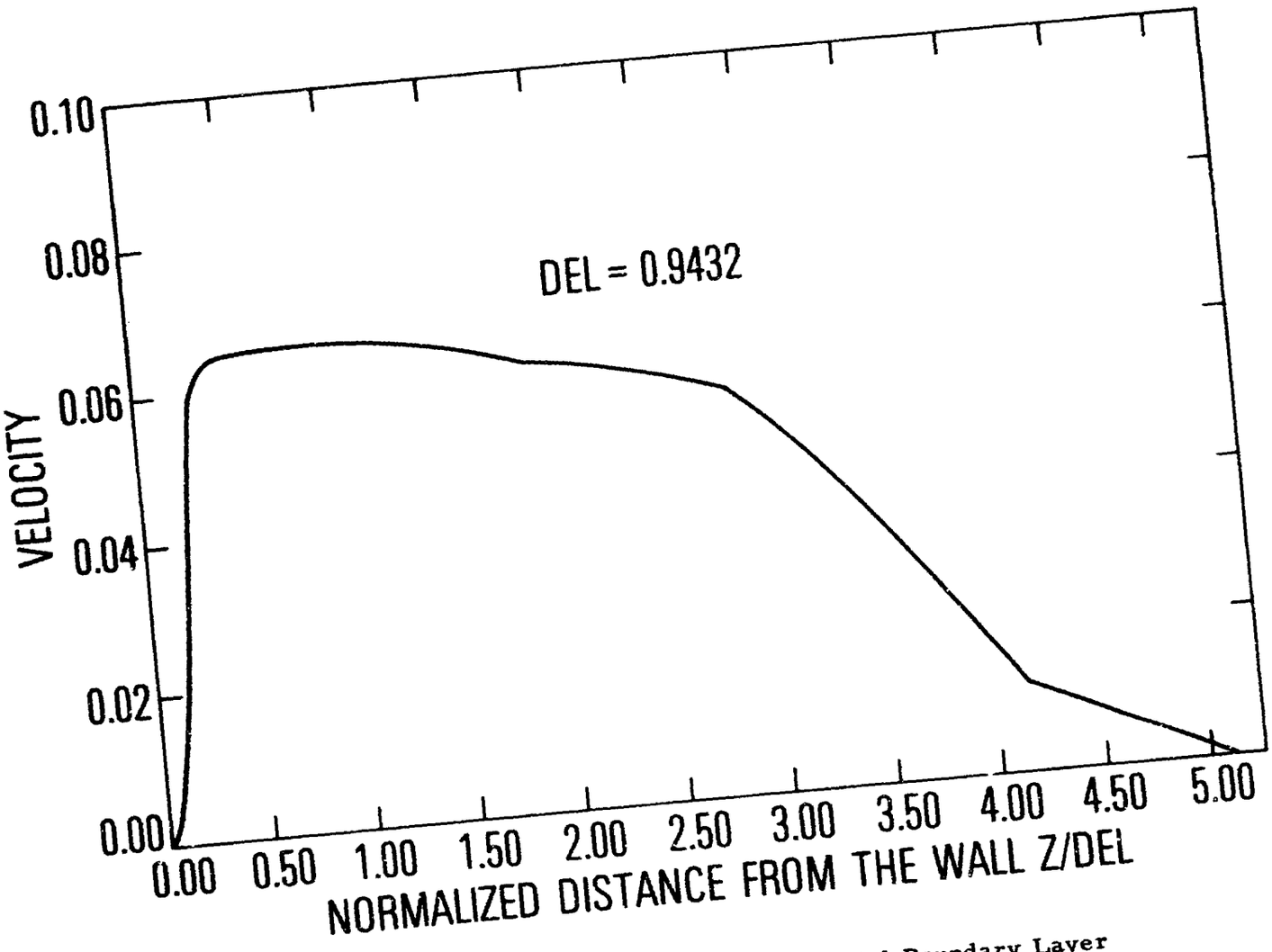

Fig. 5. Mean Turbulent Velocity - Experimental Boundary Layer

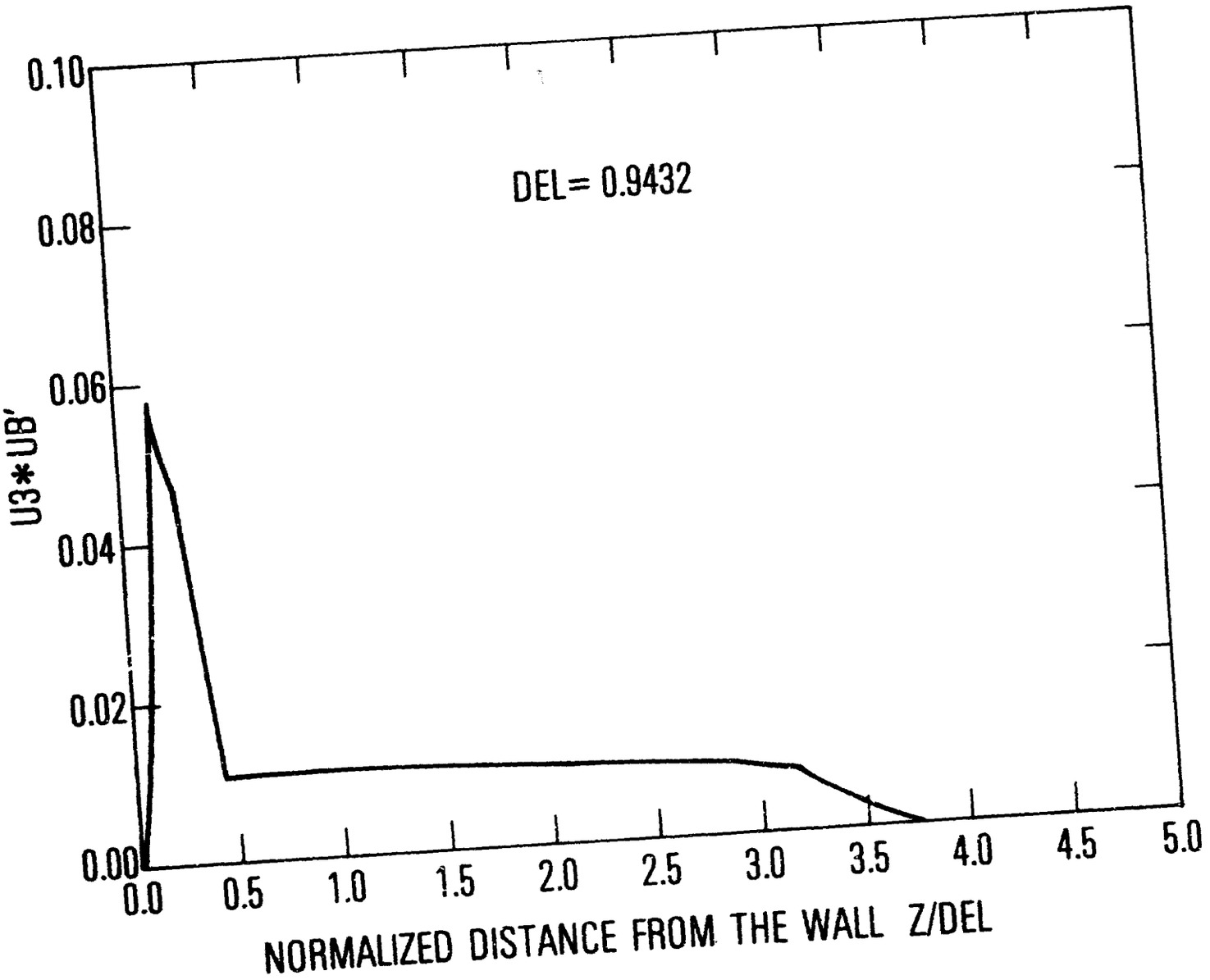

Fig. 6. U3 Turbulent Velocity *UB' - Experimental Boundary Layer

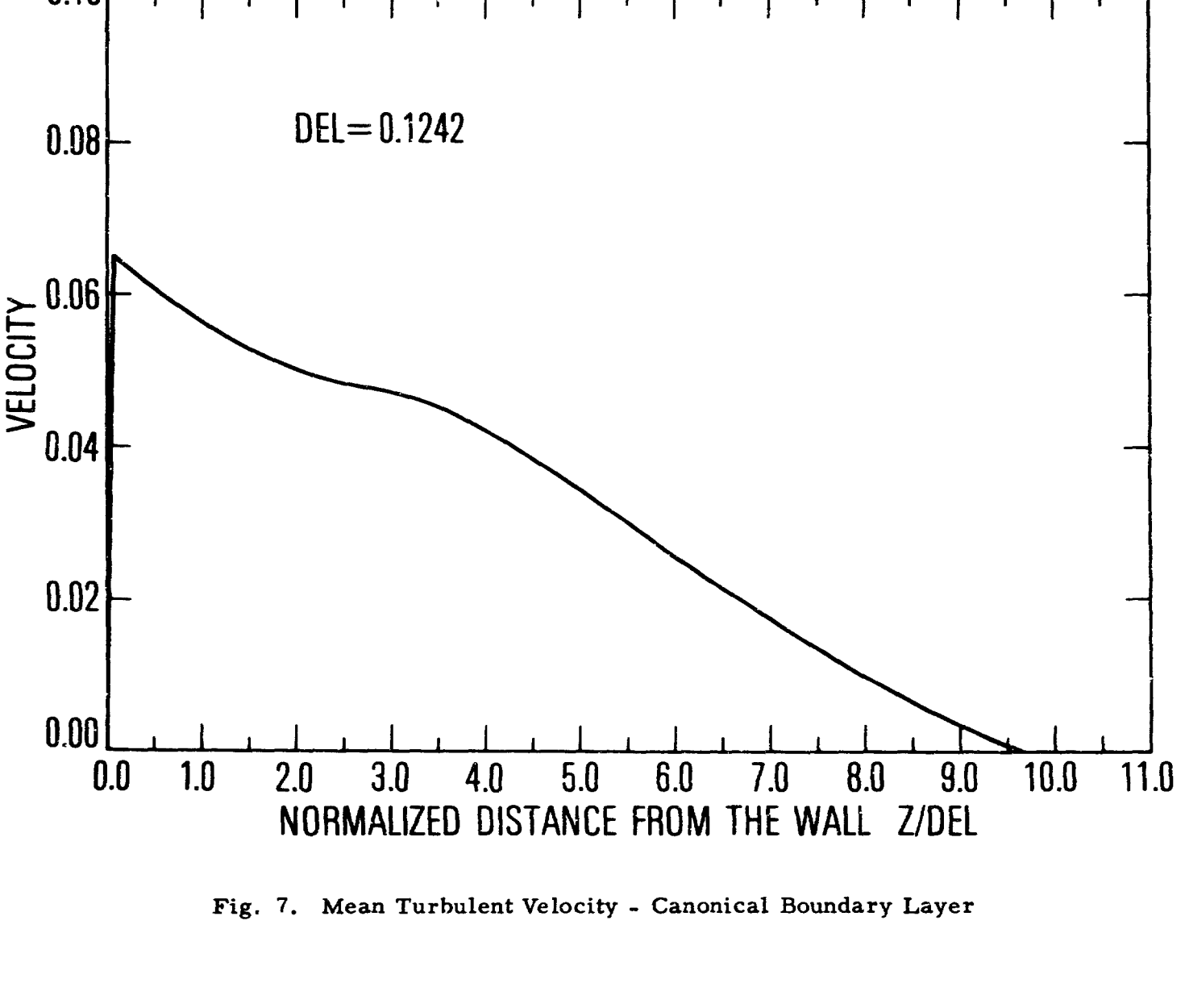

Fig. 7. Mean Turbulent Velocity - Canonical Boundary Layer

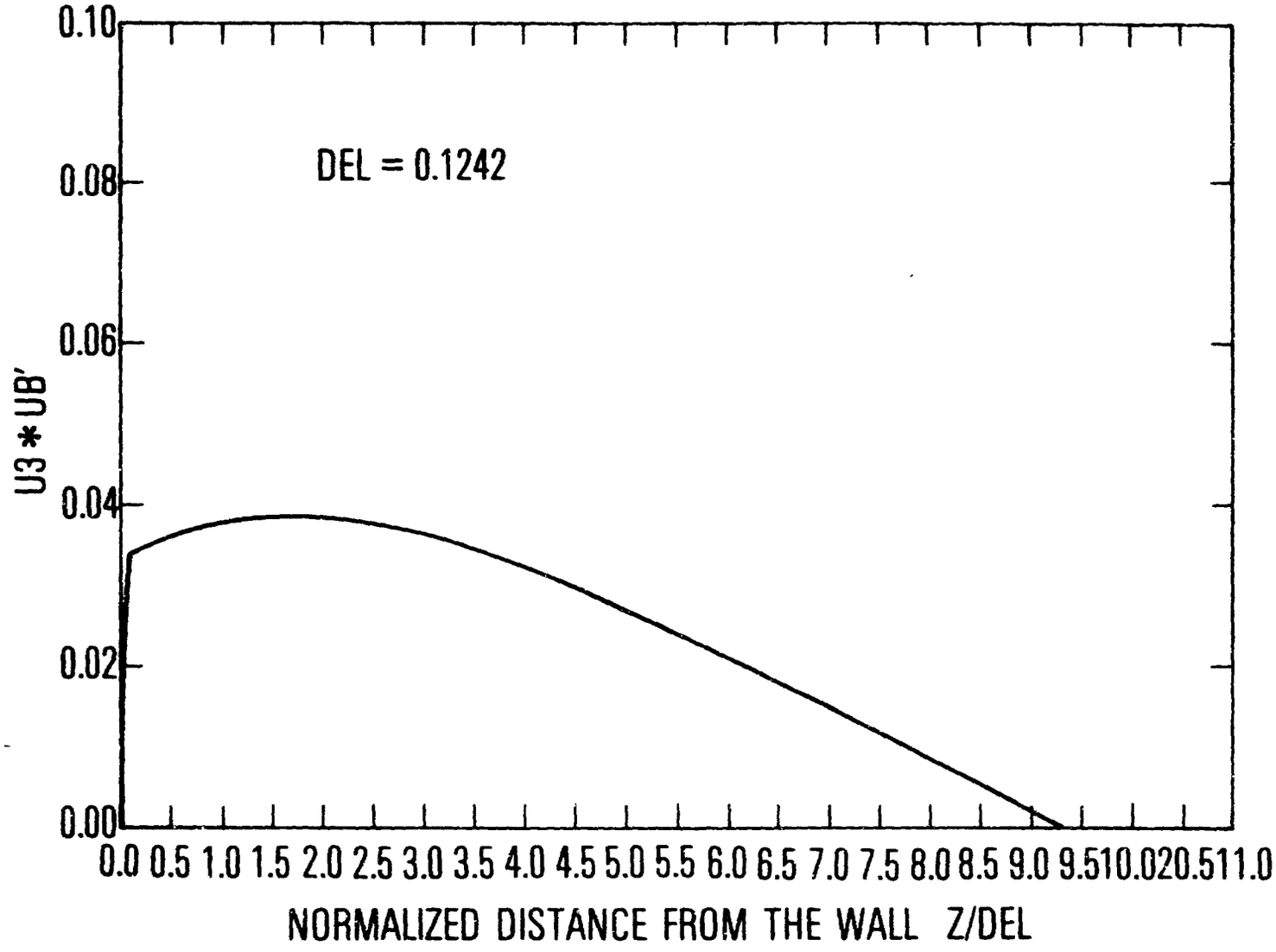

Fig. 8. U3 Turbulent Velocity * UB' - Canonical Boundary Layer

variance and correlation functions are calculated. In Figure 9, the normalized pressure variance for the thickened (experimental) boundary layer is shown. The variance at the wall and at the peak (which here occurs at the distance of about 2.25 displacement boundary layer thicknesses) are larger than the corresponding values (see below) relating to the canonical boundary layer, probably because of the greater value of the turbulent fluctuations farther from the wall. The position of the peak of the variance is considerably farther from the wall for this thickened experimental boundary layer than is the case for the canonical layer. This is probably again a result of the fact that the thickened layer shows greater turbulent fluctuations farther from the wall. It is noted in Fig. 9 that the fourth-order velocity-fluctuation contribution to the pressure variance is slight, amounting to at most but a fraction when compared with the second-order contribution. In Fig. 10 we show the corresponding variance for the canonical layer. The variance is essentially the same as the measured values given in Ref. 7. Here the fourth-order contribution is a considerably larger portion of the total pressure variance than was the case with the thickened boundary layer. The suggestion is that for well developed idealized boundary layers it may not be valid to assume that the fourth-order contributions may be neglected. It is further noted that in this, canonical, case shown in Fig. 10, the peak of the pressure variance occurs extremely close to the wall (0.04 δ), essentially in the vicinity of the laminar sub-layer. This comes about because the velocity fluctuations tend to peak sharply within that layer.[8]

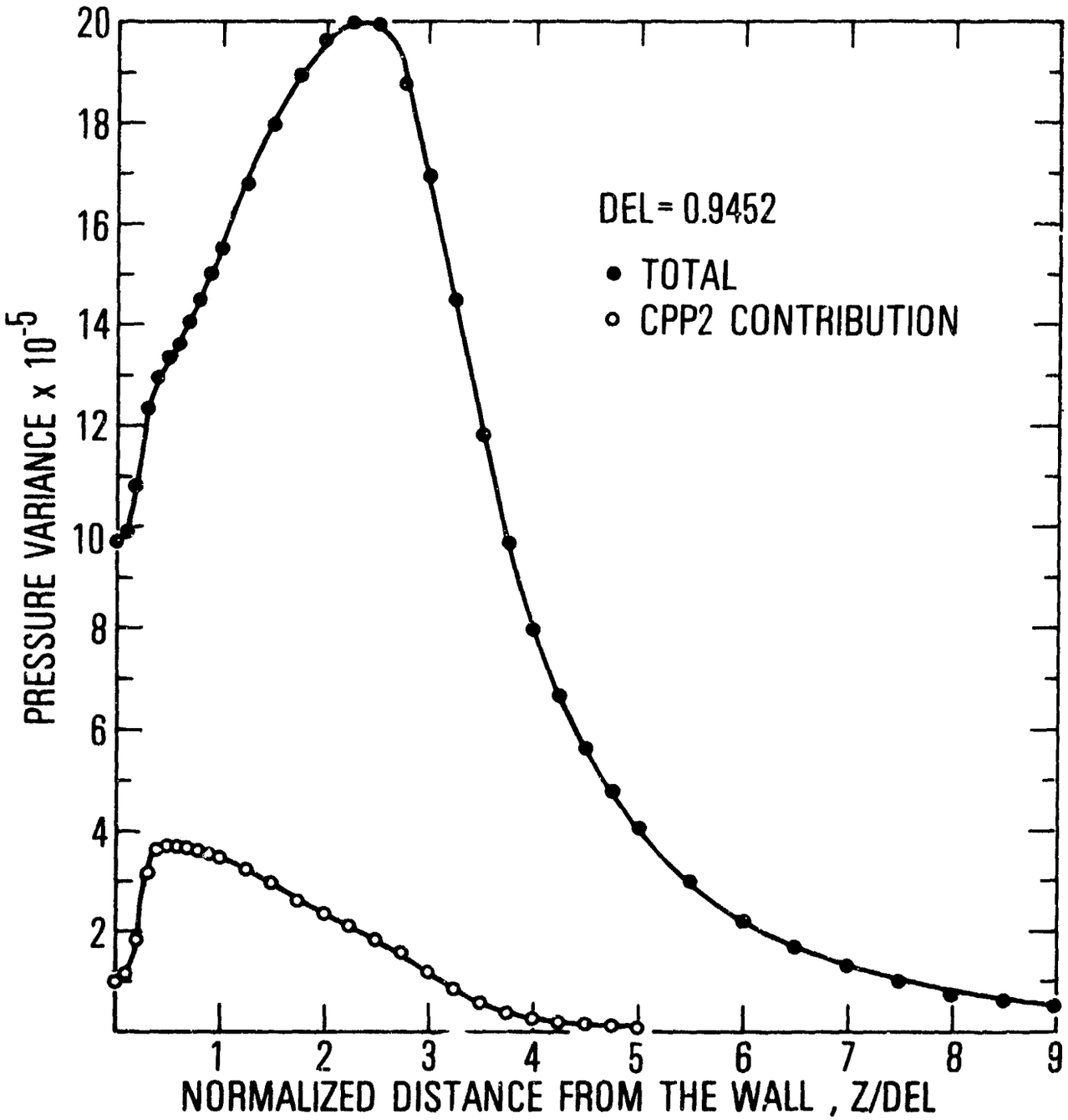

Fig. 9. Normalized Pressure Variance - Experimental Boundary Layer

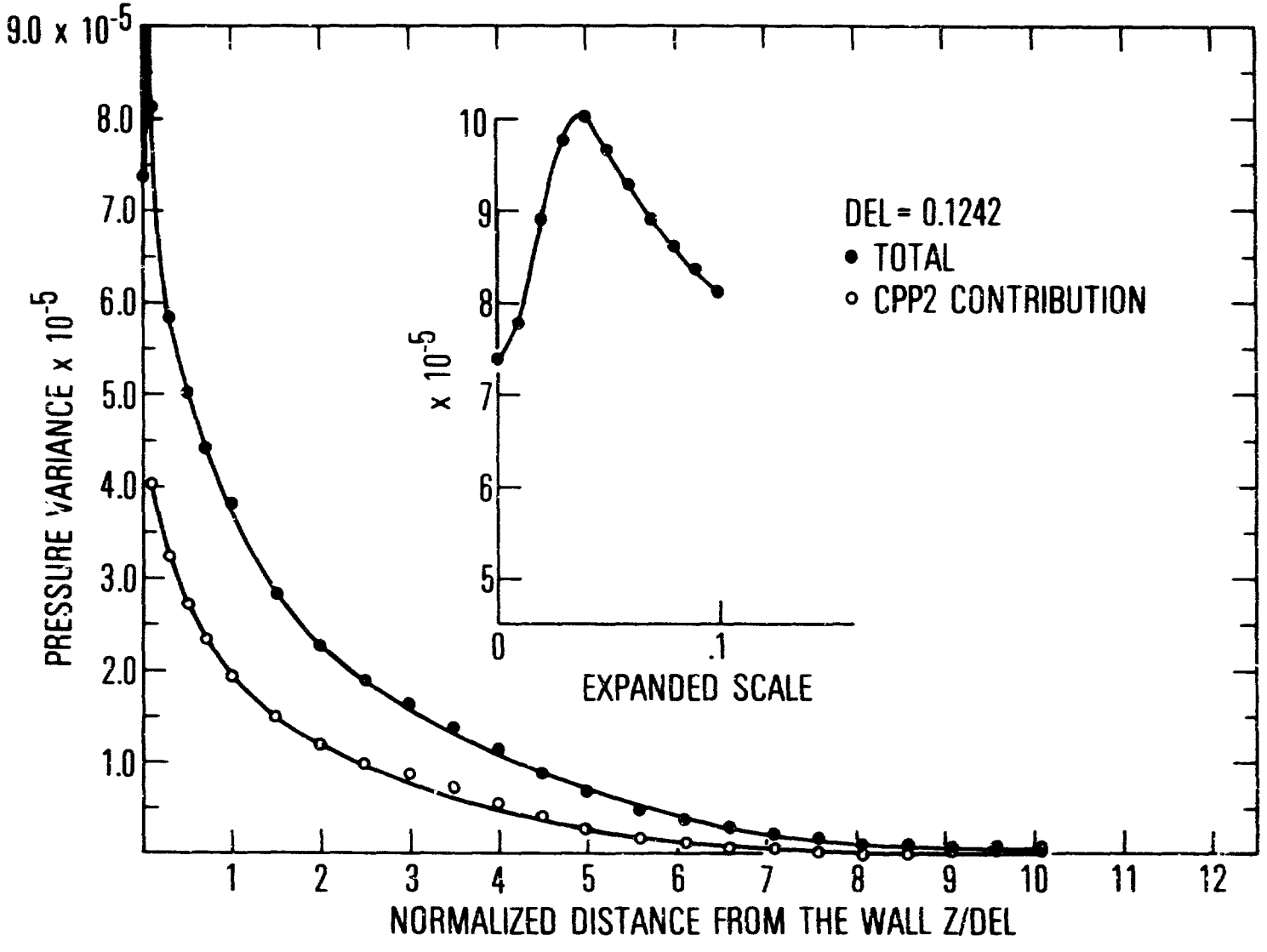

Fig. 10. Normalized Pressure Variance - Canonical Boundary Layer

The normalized correlation functions are shown in Figs. 11-13 for the experimental, thickened boundary layer. In Fig. 11, the correlation in the z-direction normal to the wall is shown for a base position located at the wall and in Fig. 12 the corresponding correlation is shown for a base position located at the position of the peak variance for that boundary layer. In both cases the fourth-order velocity contribution to the pressure correlation is slight. It is noted that the correlations have a long tail, retaining 10% of their value, even out to 9 boundary layer thicknesses. In Fig. 13 the x- and y-correlation functions, that is in the streamwise and transverse (or spanwise) directions are shown for the experimental, thickened boundary layer. It is interesting to note that the x-correlation shows a marked negative lobe; the other correlations remain positive. The scale for the three correlations is essentially the same. In Figs. 14-16 the normalized correlation functions are shown for the canonical layer. It is seen in those figures that (again) the fourth-order velocity-fluctuation contribution to the pressure correlation, though smaller than the second order, is in some ranges appreciable. Scales of the correlation functions in the three directions are essentially the same, the displacement thickness. The x-correlation (in the streamwise direction) shows a slight tendency to go negative, but this is not viewed as reliable. It is interesting that the measured pressure correlations at the wall likewise show no negative lobe (as is found experimentally, see Willmarth and Woolridge, Ref. 9).

To sum up, the fourth-order contribution to the variances and correlations appears to be negligible for the thickened experimental

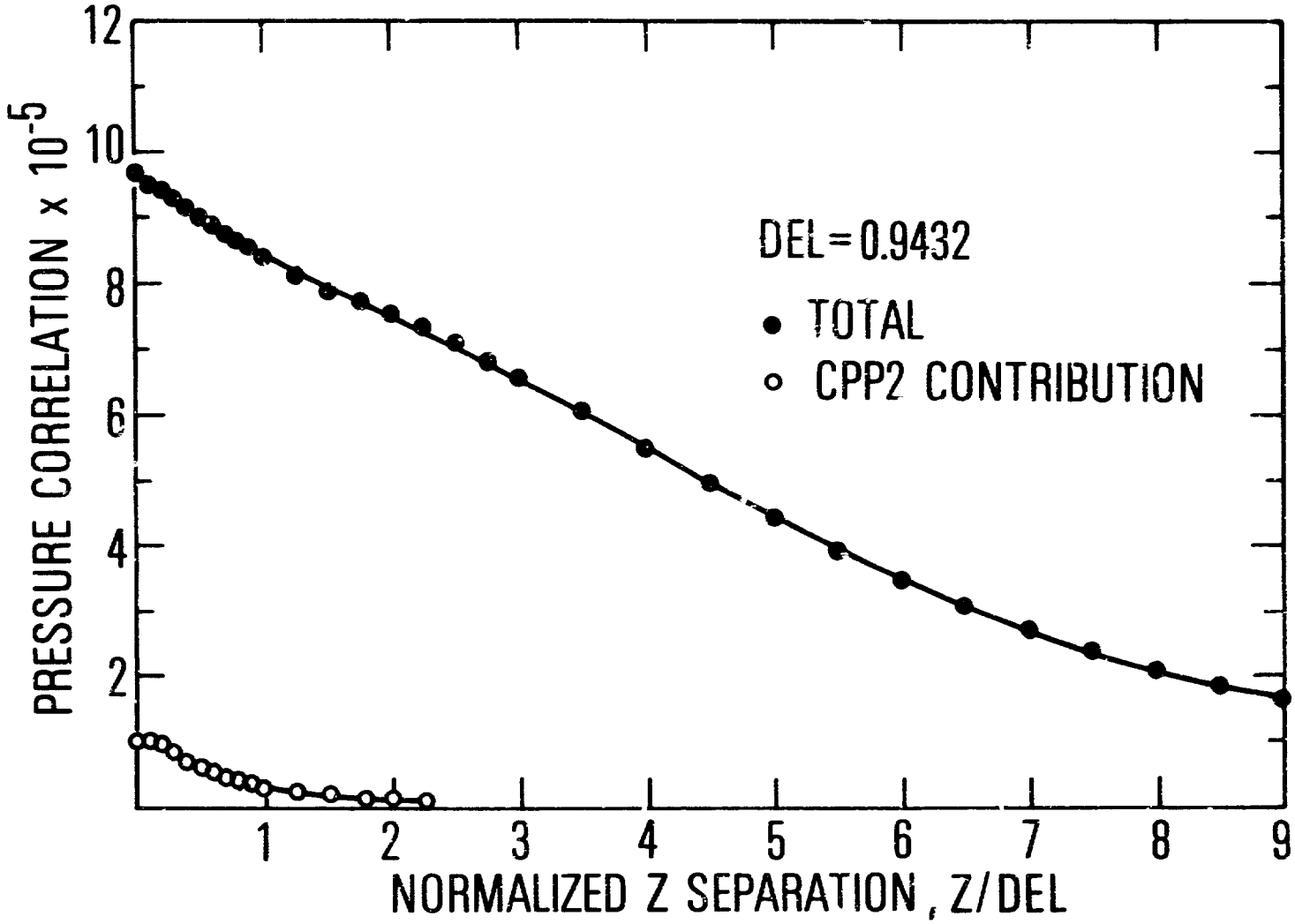

Fig. 11. Normalized Pressure Correlation in the z Direction at the Wall - Experimental Boundary Layer

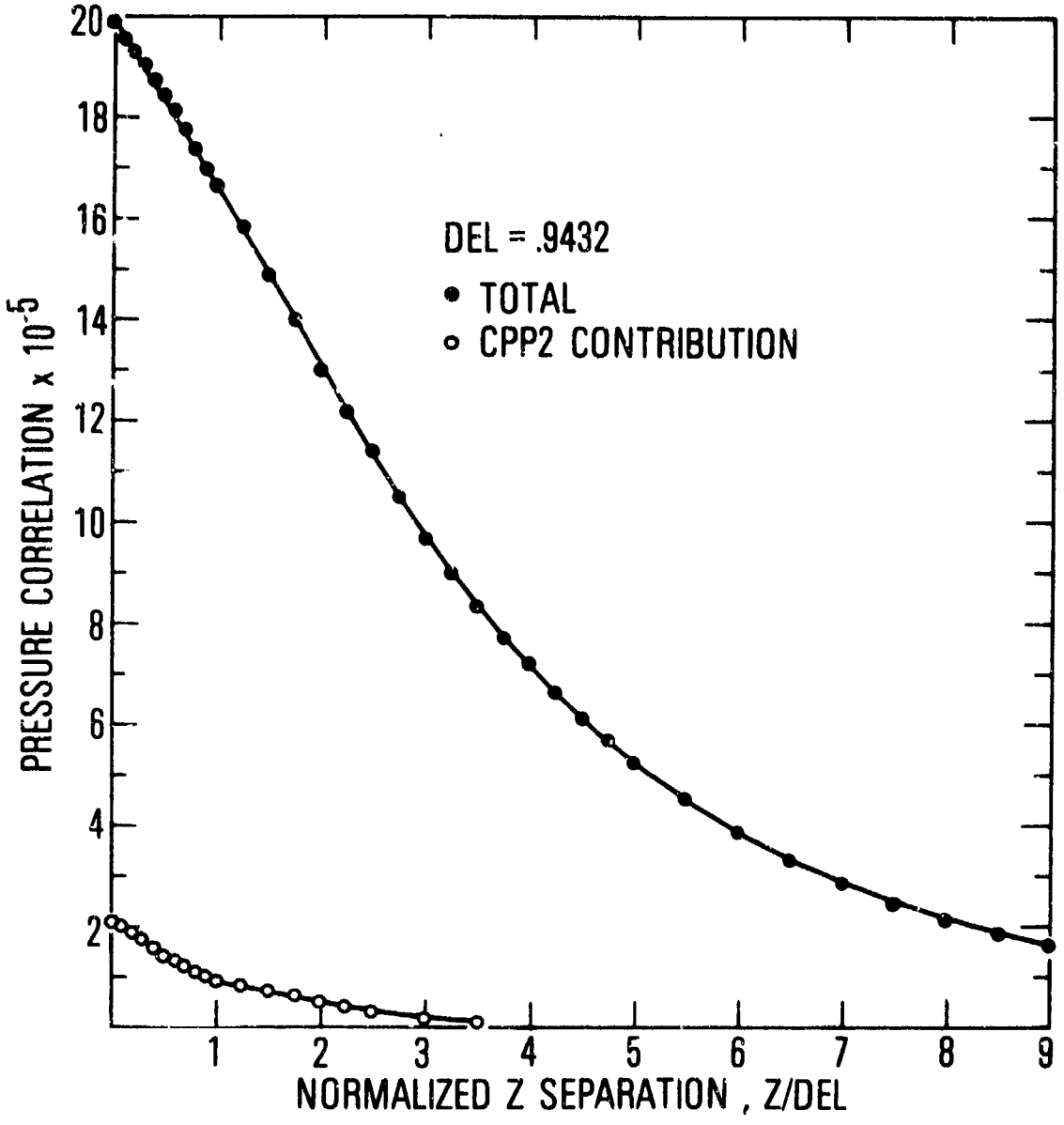

Fig. 12. Normalized Pressure Correlation in the z Direction at 2.25 Del from the Wall - Experimental Boundary Layer

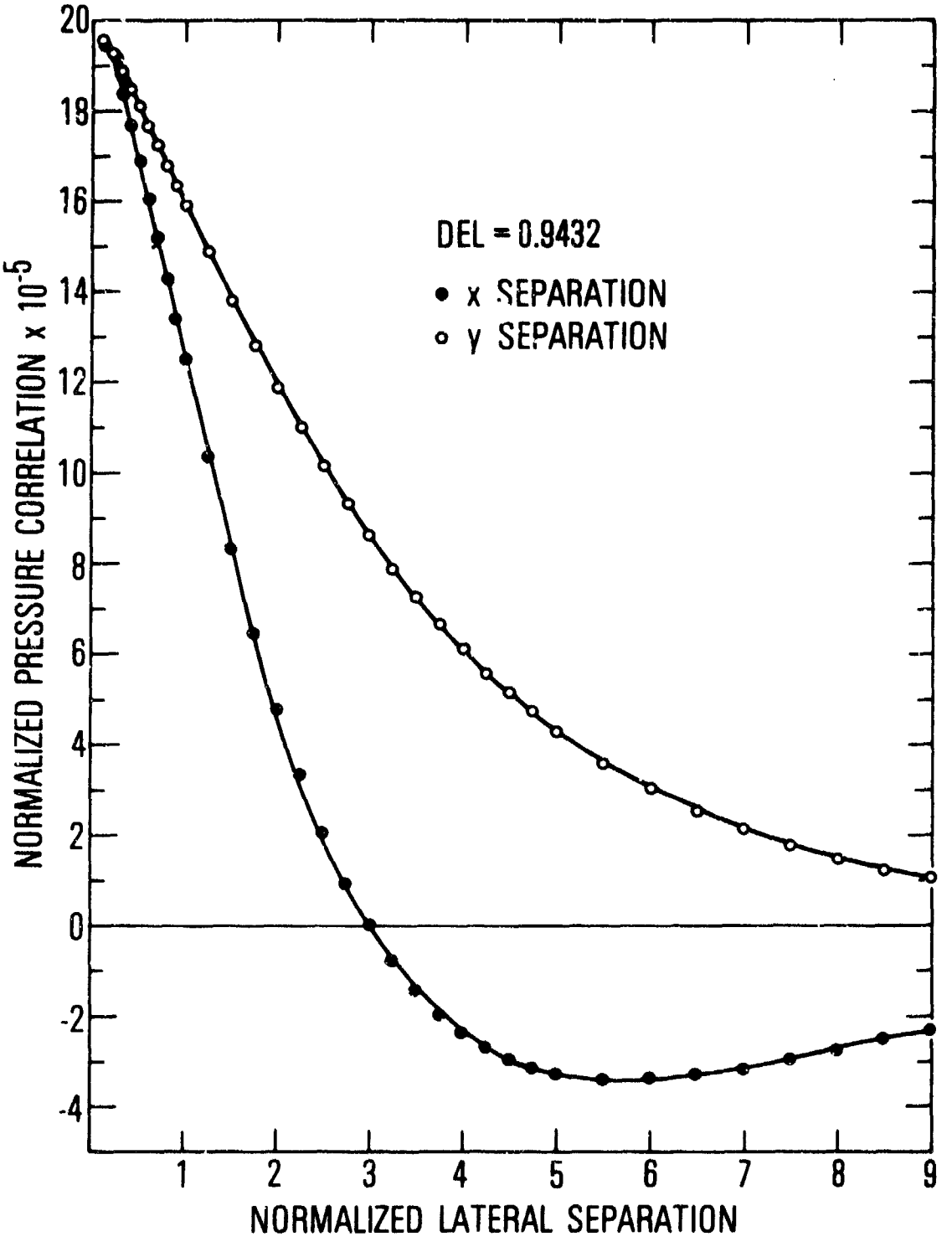

Fig. 13. Normalized Pressure Correlation in the Lateral Direction at 2.25 Del from the Wall - Experimental Boundary Layer

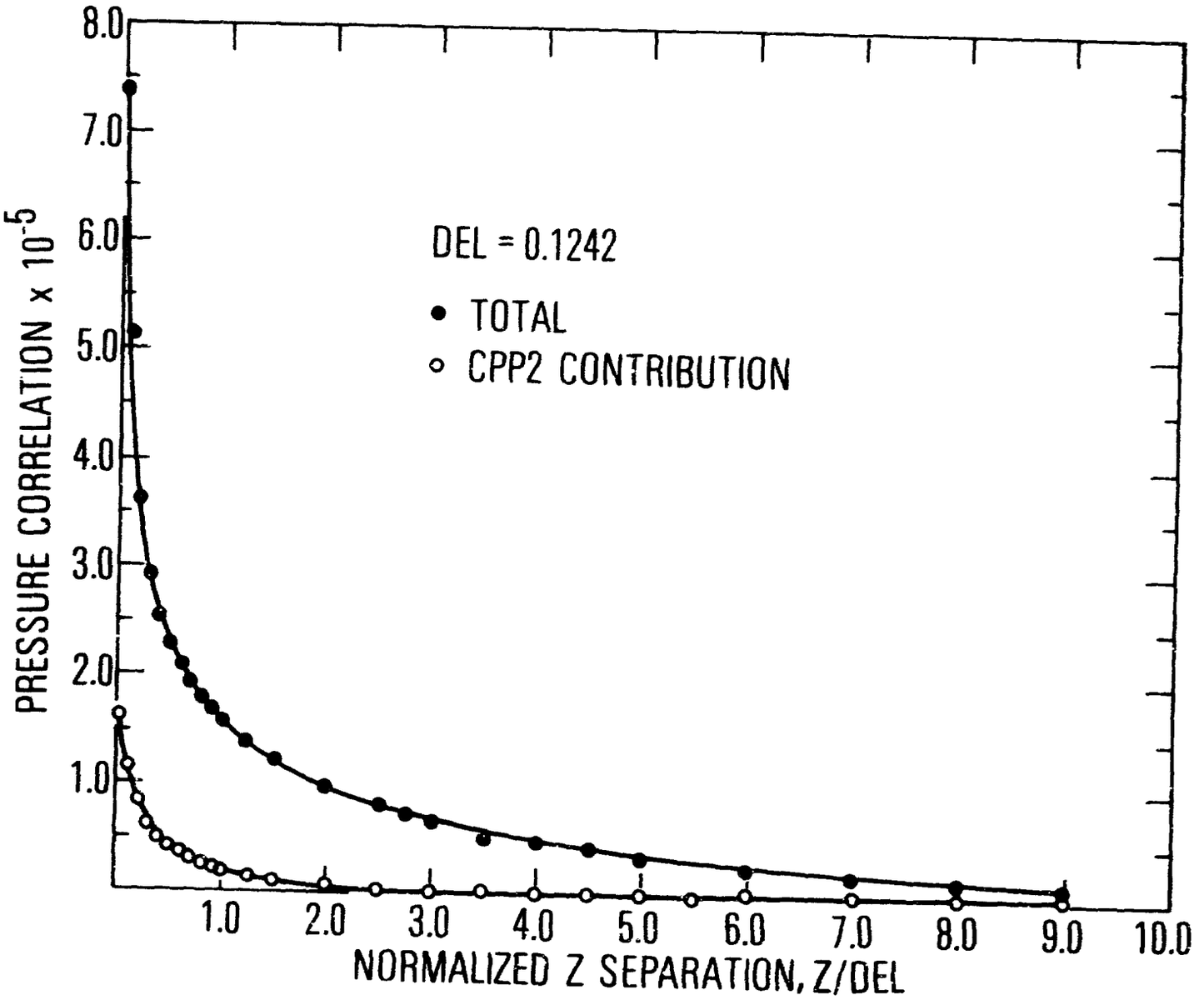

Fig. 14. Normailzed Pressure Correlation in the z Direction at the Wall - Canonical Boundary Layer

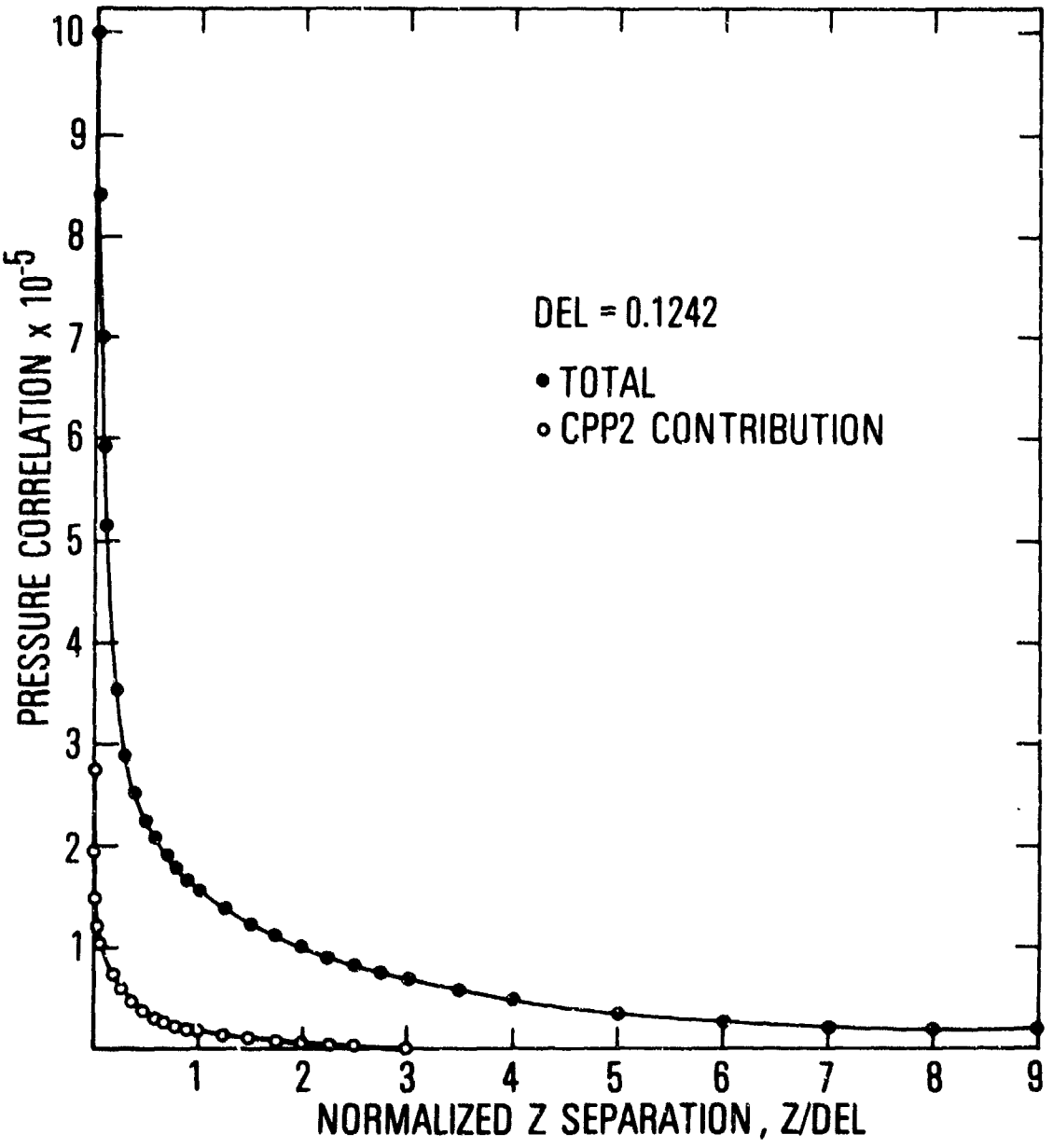

Fig. 15. Normalized Pressure Correlation in the z Direction at .04 Del from the Wall - Canonical Boundary Layer

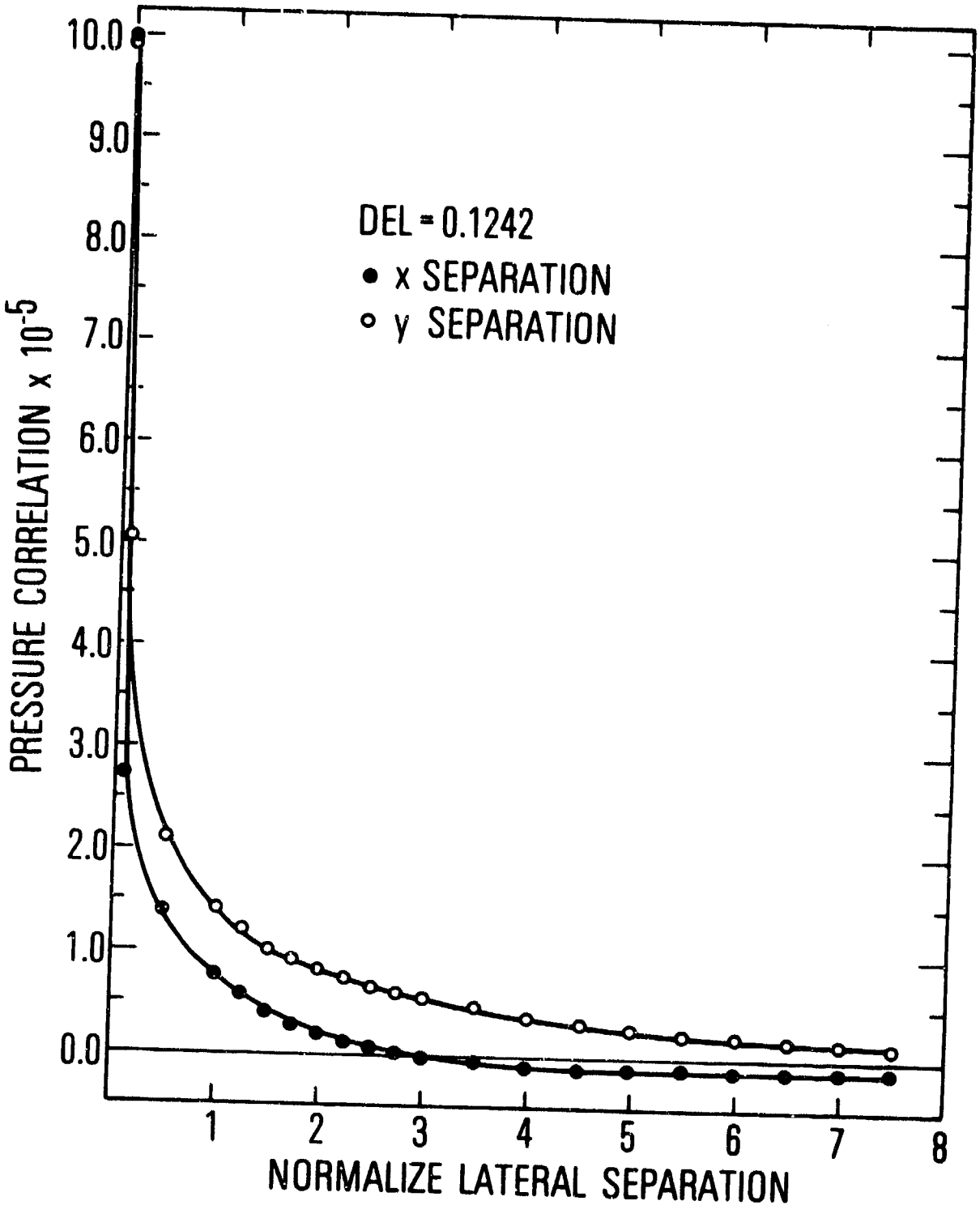

Fig. 16. Normalized Pressure Correlation in the Lateral Direction at .04 Del from the Wall - Canonical Boundary Layer

turbulent boundary layer, though in certain regions it would be necessary to include it for the canonical boundary layer (where the velocity fluctuations are confined for the most part to regions very close to the wall).

REFERENCES

1. R. H. Kraichnan, J. of Acoustical Soc. of Am. 28, 64-72 (1956).
2. R. H. Kraichnan, J. of Acoustical Soc. of Am. 28, 378-390 (1956).
3. W. C. Meecham and M. T. Tavis, Aerospace TR #0078(3606)-2, March 1978.
4. J. A. Stratton, Electromagnetic Theory (McGraw-Hill, New York, 1941).
5. G. K. Batchelor, Homogeneous Turbulence (Cambridge University Press, 1953).
6. W. C. Meecham, to be published.
7. J. Otten, Ames Research Center, Moffett Field Ca., April 1977.
8. J. O. Hinze, Turbulence, McGraw-Hill Book Company, Inc.
9. W. W. Willmarth and C. E. Wooldridge,"Measurements of the Fluctuating Pressure at the Wall Beneath the Thick Turbulent Boundary Layer", College of Engineering, University of Michigan, (April 1962).

Appendix A

POISEUILLE FLOW PROBLEM

There is a problem which exactly satisfies the assumptions made for the single boundary layer problem. It is the flow between parallel plates -- called Poiseuille flow. Consider the turbulent flow between such plates, where the Reynolds' number is large enough to generate two (turbulent) boundary layers, one associated with each of the plates, and a central region of lesser fluctuation intensity between the plates. It is plausible to suppose that each one of the boundary layers is related to a single boundary layer over a single flat plate. There are some differences between the two fluid flow problems; e.g., in the flow between flat plates the central region shows a residual level of turbulent activity which exceeds that observed outside a single boundary layer. Further, we know that a single layer increases (slowly) in thickness downstream; this doesn't occur for the Poiseuille problem, in equilibrium.

In our application we can, as stated, treat the fluid flow as one which is statistically stationary, that is, a flow in which all of the (time) averages are independent of the time at which the average is taken. Furthermore, for the parallel plate problem after the flow has developed, the flow may be assumed to be statistically homogeneous in planes parallel to one of the plates. All averages depend only on z, see Fig. A-1. (It is not assumed that the flow is statistically isotropic.) It will be seen that these conditions permit considerable simplification in the statistical quantities which we need. The geometry of the flow problem is sknown in the sketch.

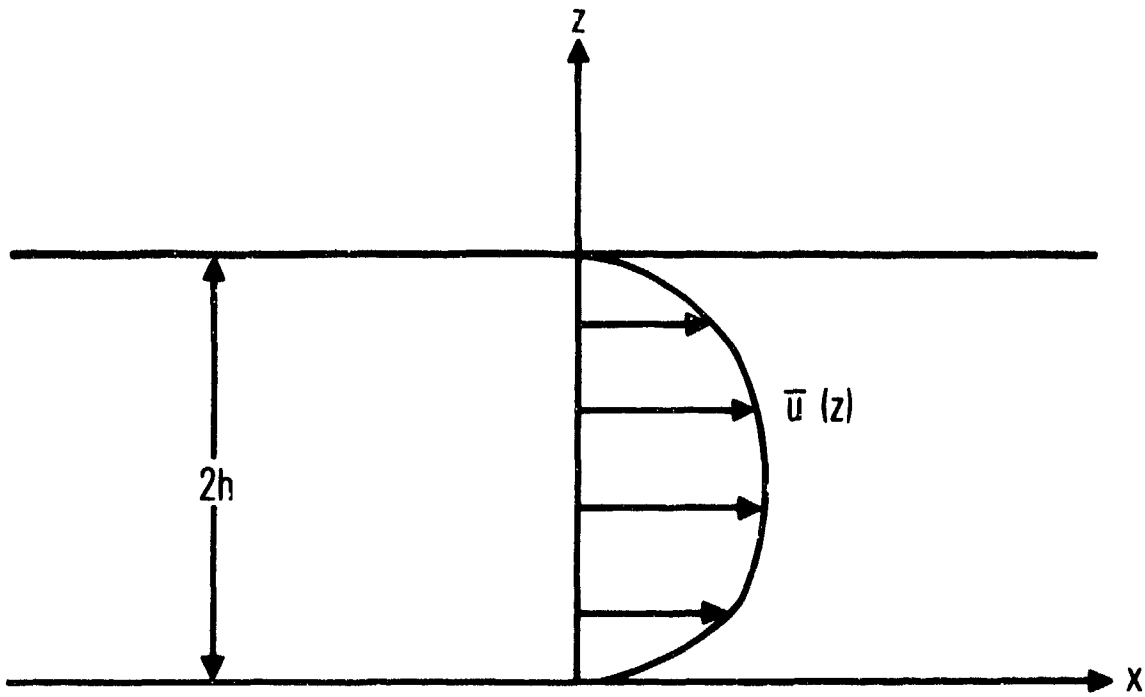

Fig. A-1. Sketch of Turbulent Poiseuille Flow; the y-axis is perpendicular to the page.

We use the notation given in Section I. It is easily shown from Eq. (2) that $\nabla \cdot \overline{\underline{u}} = \nabla \cdot \underline{u}' = 0$. If we substitute Eq. (4) into Eqs. (1) and (2) and use statistical homogeneity (in planes) and statistical stationarity we find after averaging

$$\overline{u}(z) = \frac{1}{\nu} \int_0^z \overline{u' v'(z')}\, dz' + \frac{a}{2\nu} \left[h^2 - (z - h)^2 \right] \tag{A-1}$$

(A-1)

$$\overline{u' w'} = \overline{v' w'} = 0$$

$$\frac{\overline{p}}{\rho} = -ax - \overline{w'^2(z)} \tag{A-2}$$

recalling that averages of terms in Eq. (1) depend at most on z. Here a is the pressure gradient in the downstream direction; it overcomes the viscous drag of the plates upon the flow.

To relate these results for the parallel plate problem to the single boundary layer problem, we replace the parameters a and h by the gradients of the pressure and velocity at the z = 0 plane. Eqs. (A-1) and (A-2) become

$$a = -\overline{p}_x / \rho \tag{A-3}$$

and

$$h = \frac{\nu}{a} \overline{u}_z(0) = -\nu \rho \overline{u}_z(0) / \overline{p}_x(0) \tag{A-4}$$

where the argument equal zero represents the value of the function at the plane z = 0, and the subscripts x and z indicate the derivatives with respect to those coordinates. We can substitute Eqs. (A-3) and (A-4) into Eqs. (A-1) and (A-2) to obtain averages for the related, simple boundary layer.

Appendix B

EVALUATION OF SURFACE FORCES

We begin with the stress on the boundary layer, exerted by the wall on the fluid. The general stress is

$$\sigma_{i3} = p\delta_{i3} - \mu\left(\frac{\partial u_i}{\partial z} + \frac{\partial w}{\partial r_i}\right) \tag{B-1}$$

with the boundary condition

$$\underline{u} = 0, \quad \text{on the wall,}$$

so

$$\frac{\partial u}{\partial x} = \frac{\partial v}{\partial y} = 0, \text{ on the wall.}$$

Thus the continuity equation gives

$$\frac{\partial w}{\partial z} = -\frac{\partial u}{\partial x} - \frac{\partial v}{\partial y} = 0, \quad \text{on the wall}$$

From these relations the force per area exerted by the wall on the fluid is

$$-\mu\frac{\partial u}{\partial z}\,\hat{i} \quad -\mu\frac{\partial v}{\partial z}\,\hat{j} + p\,\hat{k} \tag{B-2}$$

where $\hat{i}$, $\hat{j}$ and $\hat{k}$ are unit vectors in the x, y and z directions.

In the body of the report the image flow is discussed; it is remarked that a force must be added when the wall is removed in the imaging process. Thus a force term must be added to Eq. (1), to represent the drag of the wall; the pr- -ure force is correctly given by the pressure of the imaged flow. The equation for the imaged flow problem, which replaces Eq. (1) is from Eq. (B-2)

$$\dot{\underline{u}} + \underline{u}\cdot\nabla\underline{u} = -\frac{1}{\rho_o}\nabla p + \nu\nabla^2\underline{u} - \nu\left(\frac{\partial u}{\partial z}\,\hat{i} + \frac{\partial v}{\partial z}\,\hat{j}\right)\delta(z). \tag{B-3}$$

with $\delta(z)$ the Dirac delta function. To obtain Eq. (8) we took the divergence of the equation now replaced by Eq. (B-3). Thus the wall stress gives an added term to Eq. (8) which is

$$\frac{\rho_o}{4\pi} \int |\underline{r}' - \underline{r}_0'|^{-1} \nu \left[\frac{\partial^2 u'(\underline{r}_0')}{\partial z_0' \, \partial x_0'} + \frac{\partial^2 v'(\underline{r}_0')}{\partial z_0' \, \partial y_0'} \right] \delta(z_0') \, d\underline{r}_0' \tag{B-4}$$

Suppose we integrate over z_0' and compare estimates of the integrals of (B-4) and of Eq. (8). Near the wall the scale in the x and y directions is of order δ, the thickness of the boundary layer. For (B-4) the scale in the z- direction is the thickness of the laminar sublayer which is of order

$$\left(\frac{\nu \delta}{u'} \right)^{1/2} \tag{B-5}$$

Then, for example, the first term in the integrand of (B-4) is of order, after z_0' integration

$$\nu \frac{\partial^2 u'}{\partial z_0' \, \partial x_0'} \sim \frac{\nu u'}{\delta (\nu \delta / u')^{1/2}} \tag{B-6}$$

The corresponding quantity in Eq. (8), after integration in the z_0' direction, is of order

$$\delta \frac{u'^2}{\delta^2} \tag{B-7}$$

or bigger. The ratio of (B-6) to (B-7) is $(Re')^{-1/2}$

where

$$Re' = \frac{u' \delta}{\nu} \tag{B-8}$$

If we suppose in an application that $\delta = 15$ cm, $u' = 0.1\, c_o$, with c_o the speed of sound (the mean flow, then, near Mach 1) and use $\nu = 0.2$ cm^2/sec, the

ratio of the terms is 0.6×10^{-2}. The contribution of the wall drag is less than 1% of other forces in the flow.

Essentially the contribution of the wall is a viscous force, usually (as here) of less importance than that of inertial forces.

Appendix C

EVALUATION OF A_i, B_i AND C

These functions are needed for the evaluation of the integrals given in Eq. (24). Begin with the functions A_i, and refer to Eqs. (26) and (26a). A simple way to find the functions is the following. Take the cross product of Eqs. (26) and (26a) four times, using the $\underline{\xi}$, and contract indices. Then the only term in Eq. (26a) which doesn't vanish is the third on the right side, thus giving a single equation for A_3. Now continue by taking a cross product of Eqs. (26) and (26a) twice with $\underline{\xi}$, summing on the other two indices. This gives a single equation involving A_2 and A_3; substitute the value for A_3 just found, and determine A_2. To determine A_1, sum on the four indices in pairs in Eqs. (26) and (26a), use the values of A_2 and A_3 already found and determine A_1. From these manipulations, one obtains the following results for these functions.

$$A_1(\xi) = \xi^{-4} \int_0^\infty dr\, r^6\, Q_1^2(r) \left[\frac{3}{8} K_0(\xi, r) - \frac{15}{4} K_2(\xi, r) + \frac{35}{8} K_4(\xi, r) \right]$$

$$A_2(\xi) = \xi^{-2} \int_0^\infty dr\, r^6\, Q_1^2(r) \left[-\frac{1}{8} K_0 + \frac{3}{4} K_2 - \frac{5}{8} K_4 \right] \qquad \text{(C-1)}$$

$$A_3(\xi) = \int_0^\infty dr\, r^6\, Q_1^2(r) \left[\frac{1}{8} K_0 - \frac{1}{4} K_2 + \frac{1}{8} K_4 \right]$$

with (see below)

$$K_n(\xi, r) = 2\pi \int_{-1}^{1} \frac{x^n\, dx}{\sqrt{a + bx}} \quad , \qquad \text{(C-2)}$$

and

$$a = \xi^2 + r^2, \quad b = -2\xi r$$

To find the functions B_1 and B_2 refer to Eqs. (27) and (27a), removing the factor $\delta_{\beta\delta}$. Using those equations take the cross product of both twice with the vector $\underline{\xi}$, yielding a single equation for B_2. Then sum on the two indices giving a single equation for B_1 and B_2 from which B_1 can be found. The result is

$$B_1 = \xi^{-2} \int_0^\infty dr\, r^4\, Q_1(r)\, Q_2(r) \left[\frac{3}{2}\, K_2(\xi, r) - \frac{1}{2} K_0(\xi, r)\right]$$

$$B_2 = \int_0^\infty dr\, r^4\, Q_1(r)\, Q_2(r) \left[\frac{1}{2} K_0 - \frac{1}{2}\, K_2\right] \qquad \text{(C-3)}$$

Finally to determine the function C refer to equation (29a). One simply carries out the integral involved there and obtains the result

$$C = \int_0^\infty dr\, r^2\, Q_2^2(r)\, K_0(\xi, r) \qquad \text{(C-4)}$$

The integrals in (C-2) can be found in terms of elementary functions:

$$K_0(\xi, r) = \frac{4\pi}{r}\,, \quad \xi < r$$

$$K_2(\xi, r) = \frac{4\pi}{15\, r} \left[5 + 2\, \frac{\xi^2}{r^2}\right], \quad \xi < r$$

$$K_4(\xi, r) = \frac{4\pi}{315\, r} \left[63 + 36\, \frac{\xi^2}{r^2} + 8\, \frac{\xi^4}{r^4}\right], \quad \xi < r$$

and are symmetric in ξ and r, as must be so from their definition, (C-2). The functions have discontinuous derivatives, which lead (under two differentiations) to Dirac delta functions in the work.

Appendix D

INTEGRATION BY PARTS, AT A SINGULAR POINT

It will be convenient to integrate Eq. (8) by parts (i.e., use Gauss' theorem). In the process, the singular point at $\underline{r}' - \underline{r}'_0 = 0$ must be treated carefully; we present the reasoning in detail. First note that as it stands, the integrand is integrable at that point. Thus we may set up a small sphere of radius ϵ about the point and delete the integral over sphere-ϵ from the rest of the volume of integration (all space) without changing the result. Let the remaining volume be V-, whereas <u>all</u> space we let be V. Thus we have for Eq. (8)

$$p'(\underline{r}') = \frac{\rho_o}{4\pi} \iiint_{V-} |\underline{r}'_0 - \underline{r}'|^{-1} \frac{\partial^2}{\partial r'_{0\alpha}\, \partial r'_{0\beta}} H_{\alpha\beta}(\underline{r}'_0)\, d\underline{r}'_0 \tag{D-1}$$

$$= \frac{\rho_o}{4\pi} \iiint_{V-} \frac{\partial}{\partial r'_{0\alpha}} \left[|\underline{r}'_0 - \underline{r}'|^{-1} \frac{\partial}{\partial r'_{0\beta}} H_{\alpha\beta}(\underline{r}'_0) \right] d\underline{r}'_0$$

$$- \frac{\rho_o}{4\pi} \iiint_{V-} \left[\frac{\partial}{\partial r'_{0\beta}} H_{\alpha\beta}(\underline{r}'_0) \right] \frac{\partial}{\partial r'_{0\alpha}} |\underline{r}'_0 - \underline{r}'|^{-1} \, d\underline{r}'_0 \tag{D-2}$$

Use Gauss' theorem on the first; we have two surface integrals, one at infinity (i.e., large distance) which vanishes because all fluctuations vanish there, and the other on the ϵ-sphere; that one vanishes as well because the element of surface area is of order ϵ^2, giving an integrand of order ϵ. Thus the first term on the right side of (D-2) vanishes. Consider the second:

$$- \frac{\rho_o}{4\pi} \iiint_{V-} \left[\frac{\partial}{\partial r'_{0\beta}} H_{\alpha\beta}(\underline{r}'_0) \right] \frac{\partial}{\partial r'_{0\alpha}} |\underline{r}'_0 - \underline{r}'|^{-1} \, d\underline{r}'_0$$

$$= - \frac{\rho_o}{4\pi} \iiint_{V-} \frac{\partial}{\partial r'_{0\beta}} \left[H_{\alpha\beta}(\underline{r}'_0) \frac{\partial}{\partial r'_{0\alpha}} |\underline{r}'_0 - \underline{r}'|^{-1} \right] d\underline{r}'_0 \qquad \text{(D-3)}$$

$$+ \frac{\rho_o}{4\pi} \iiint_{V-} H_{\alpha\beta}(\underline{r}'_0) \frac{\partial^2}{\partial r'_{0\alpha} \partial r'_{0\beta}} |\underline{r}'_0 - \underline{r}'|^{-1} \, d\underline{r}'_0 .$$

Use Gauss' theorem on the first term on the right side; it is equal to (recalling that surface integrals at infinity vanish)

$$- \frac{\rho_o}{4\pi} \iint_{\epsilon} (\hat{\eta})_\beta \, H_{\alpha\beta}(\underline{r}'_0) \frac{\partial}{\partial r'_{0\alpha}} |\underline{r}'_0 - \underline{r}'|^{-1} \, dS(\underline{r}'_0) \qquad \text{(D-4)}$$

Let $\underline{\rho} = \underline{r}'_0 - \underline{r}'$ and recall that $\hat{\eta}$ is directed <u>into</u> the surface of the sphere and find for (D-4) for ϵ very small:

$$- \frac{\rho_o}{4\pi} H_{\alpha\beta}(\underline{r}') \iint_{\rho=\epsilon} \left(- \frac{\rho_\beta}{\rho} \right) \left(- \frac{1}{\rho^2} \right) \frac{\rho_\alpha}{\rho} \, \rho^2 \, d\Omega \qquad \text{(D-5)}$$

with $d\Omega$ the element of solid angle. This is easily seen to give $- \frac{\rho_o}{4\pi} \frac{4\pi}{3} H_{\alpha\alpha}(\underline{r}')$. Combining these results we find

$$p'(\underline{r}') = \frac{\rho_o}{4\pi} \iiint_{V-} H_{\alpha\beta}(\underline{r}'_0) \frac{\partial^2}{\partial r'_{0\alpha} \partial r'_{0\beta}} |\underline{r}'_0 - \underline{r}'|^{-1} \, d\underline{r}'_0$$

$$- \frac{\rho_o}{3} H_{\alpha\alpha}(\underline{r}') \qquad \text{(D-6)}$$

Consider now the value of the integral in Eq. (D-6), if carried out within ϵ. We see

$$\frac{\rho_o}{4\pi} \iiint_{\epsilon} H_{\alpha\beta}(\underline{r}'_0) \frac{\partial^2}{\partial r'_{0\alpha}\, \partial r'_{0\beta}} \left| \underline{r}'_0 - \underline{r}' \right|^{-1} d\underline{r}'_0$$

$$\cong \frac{\rho_o}{4\pi} H_{\gamma\beta}(\underline{r}') \iiint_{\epsilon} \frac{\partial^2}{\partial \rho_\alpha\, \partial \rho_\beta} \rho^{-1}\, d\rho \qquad \text{(D-7)}$$

$$= \frac{\rho_o}{4\pi} H_{\alpha\beta}(\underline{r}') \left(-\frac{4\pi}{3}\right) \delta_{\alpha\beta} = -\frac{\rho_o}{3} H_{\alpha\alpha}(\underline{r}')$$

using the vector properties of the integral. Evidently if we (incorrectly) drop the surface integral which gave the added term to Eq. (D-6) and (incorrectly) extend the volume integral in Eq. (D-6) throughout ϵ, we have cancelling errors and the correct result

$$p'(\underline{r}') = \frac{\rho_o}{4\pi} \iiint_{\substack{\text{all} \\ \text{space}}} H_{\alpha\beta}(\underline{r}'_0) \frac{\partial^2}{\partial r'_{0\alpha}\, \partial r'_{0\beta}} \left| \underline{r}'_0 - \underline{r}' \right|^{-1} d\underline{r}'_0 \qquad \text{(D-8)}$$

Some care must be exercised to be sure that the delta-function contribution at $\underline{r}'_0 = \underline{r}'$ is not lost.

Appendix E

TECHNIQUES USED IN EVALUATION OF THE PRESSURE CORRELATION

In order to numerically evaluate the pressure correlations Eqs. (38) and (44) the angular integration is first performed analytically in terms of Hypergeometric functions. From Eq. (38)

$$\int_0^{\pi} d\phi \left\{ \frac{3}{4} \left[\frac{(\xi^2 - r^2)^2}{|\underline{r} - \underline{\xi}|^5} + \frac{2(\xi^2 - r^2)}{|\underline{r} - \underline{\xi}|^3} + \frac{1}{|\underline{r} - \underline{\xi}|} \right] - \frac{\xi^2}{|\underline{r} - \underline{\xi}|^3} \right\} =$$

$$a^{-.5} \left\{ .75 \left[(\xi^2 - r^2)^2 b^{-2} A(x) + 2(\xi^2 - r^2) b^{-1} B(x) + C(x) \right] - \xi^2 b^{-1} B(x) \right\} \qquad \text{(E-1)}$$

where

$$x = \frac{4\eta\rho}{a}, \quad a = (\rho + \eta)^2 + (z - \xi_3)^2, \quad b = (\rho - \eta)^2 + (z - \xi_3)^2$$

and

$$C(x) = 2 \int_0^1 (1 - y^2)^{-.5} (1 - xy^2)^{-.5} dy = 2K(x)$$

$$B(x) = 2 \int_0^1 (1 - y^2)^{-.5} (1 - xy^2)^{-.5} dy = 2E(x)$$

$$A(x) = 2 [(2 - x)B(x) - .5(1 - x)C(x)]/3 \qquad \text{(E-2)}$$

Note that $\xi^2 = \rho^2 + \xi_3^2$ and $r^2 = \eta^2 + z^2$.

Simple polynomial expressions accurate to two parts in 10^8 exist for the complete elliptic integrals[10] K and E. Note that for x = 0 (for example)

calculation of the variance or the correlation for z separation only), $A = B = C = \pi$. For r^2 equal to 0 (i.e. the variance) Eq. (E-1) becomes simply $2\pi/\xi$. This implies that the fourth-order variance is given simply by

$$C_{pp}^{(2)}(z',0) = \frac{\rho_o^2}{2\pi}\left\{-[u'(z')]^4 D_2(0) + \int_{-\infty}^{\infty} d\xi_3 [u'(|z'+\xi_3|]^4 M(xx)m^{-1}\right\} \qquad \text{(E-3)}$$

where

$$M(xx) = \int_{xx}^{\infty} d\xi D_1(\xi) \qquad \text{(E-4)}$$

and

$$xx = \xi_3 M^{-1}$$
$$M = (T^{-1} + |z' + \xi_3|^{-1})^{-1}$$

The function M(xx) is a universal curve independent of the velocity field and should not be confused with the scale factor M. Continue with the calculation of the correlation $C_{pp}^{(2b)}$ by substitution of (E-1) into Eq. (38). Direct numerical integration at this point leads to significant error and large computation times due to the apparent singularity near $\underline{\xi} = \underline{r}$. Instead change integration variables letting

$$\rho = \eta + \Delta$$

$$\xi_3 = z - w$$

Expression (E-1) becomes

$$\left\{\frac{[(\eta^2-z^2)(\Delta^2-\omega^2)-4\eta z\Delta\omega]}{b^2}\,B(x)+\frac{2(\eta^2\Delta^2-2\eta z\Delta\omega+\omega^2z^2}{ab}\;[B(x)-.5C(x)]\right.$$

$$\left.+\frac{(\eta\Delta-\omega z)}{b}\;[3A(x)+B(x)]+[.75A(x)+.5\,B(x)+.75\,C(x)]\right\} \qquad \text{(E-5)}$$

Substitute (E-5) into Eq. (38) and integrate the first term in (E-5) by parts w.r.t. Δ. This gives

$$C_{pp}^{(2b)}(z',\eta,z)=\frac{\rho_o^2}{4\pi^2}\int_{-\infty}^{\infty}\frac{d\omega[u'(|z_0'|)]^4}{M^2}\int_{-\eta}^{\infty}d\Delta\;P(\eta,z,z_0',\Delta,\omega) \qquad \text{(E-6)}$$

where

$$P(\eta,z,z_0',\Delta,\omega)=\left\{\frac{[(\eta^2-z^2)\Delta-2\eta z\omega]}{b}\left[a^{-.5}BD_1+2a^{-1.5}\rho\eta x^{-1}(1-2\rho(\rho+\eta)a^{-1})\right.\right.$$

$$\left.\times(B-C)D_1+\rho^2\xi^{-1}|z_0'|^{-1}a^{-.5}BD_1'-\rho(\rho+\eta)a^{-1.5}BD_1\right]$$

$$+\left[\frac{(\eta\Delta-\omega z)}{b}\;(3A+B)+\frac{2(\eta^2\Delta^2-2\eta z\Delta\omega+\omega^2z^2)}{ab}\;(B-.5C)\right.$$

$$\left.\left.+(.75A+.5B+.75C)\right](a^{-.5}\rho D_1)\right\} \qquad \text{(E-7)}$$

and

$$a = (2\eta + \Delta)^2 + \omega^2$$

$$b = \Delta^2 + \omega^2$$

$$\xi = (\rho^2 + \xi_3^2)^{.5}$$

$$\xi_3 = z - \omega$$

$$x = 4\eta(\eta + \Delta)a^{-1}$$

$$z_0' = z' + \omega$$

The argument of the functions A, B, and C is x while the argument of D_1 and the derivative of D_1 "D_1'" is ξM^{-1}. To complete the numerical evaluation of Eq. (E-6) the integral over Δ was first broken with two terms, one from $-\eta$ to η and the other from η to ∞. Then the integral over Δ from $-\eta$ to η was rewritten in terms of a single integral from 0 to η. Finally the integral over ω from $-\infty$ to ∞ was rewritten as a single integral from 0 to ∞. Note that $[u'(|z_o'|)]^4 M^{-2}$ was brought inside the Δ integral in the final expression. The final results do not give numerical difficulty at $\Delta = \omega = 0$ and typical evaluation times for η, z not too large are of the order of 10 seconds on a CDC 7600. Note that the integral over Δ is a universal function of (η/M, z/M, ω/M). If one knew this function, it would be very easy to evaluate $C_{pp}^{(2)}$ for any velocity field. Unfortunately this function is too complicated to compute and store for all parameter values. Instead one may consider the special cases when either η or z are equal to zero. This results in a two parameter function which can be tabulated and stored. If there are many different boundary layer cases to be considered, there may be a significant advantage of tabulating these

functions. However, even on a CDC 7600, the calculation time required to determine these functions for C_{pp}^{2} and C_{pp}^{1} terms will take approximately one hour. Proceeding now with the case when $\eta = 0$ the fourth-order correlation becomes

$$C_{pp}^{(2)}(z', 0, z) = \frac{\rho_o^2}{4\pi} \int_{-\infty}^{\infty} \frac{d\omega[u'(|z_0'|)]^4}{M} \bar{M}\left(\frac{\omega}{M}, \frac{z}{M}, 0\right) \tag{E-8a}$$

where from Eq. (E-7)

$$\bar{M}(\bar{A}, \bar{B}, 0) = M^{-1} \int_0^{\infty} d\Delta P(0, z, |z_0'|, \Delta, \omega) = \tag{E-8b}$$

$$\int_0^{\infty} \Delta d\Delta[(2-4\bar{A}\bar{B}b^{-1})D_1(\xi) - \Delta^2\bar{B}^2b^{-1}\xi^{-1}D_1'(\xi)]b^{-.5}$$

and a change of variables was made within Eq. (E-8b) so that

$$b = \Delta^2 + \bar{A}^2$$

$$\xi = \sqrt{\Delta^2 + (\bar{B}-\bar{A})^2}$$

$$\bar{A} = \omega/M$$

$$\bar{B} = z/M$$

In obtaining Eq. (E-8) the partial integration proceeded in a slightly different way than discussed after Eq. (E-7) since a = b. Depending on the accuracy required, this function $\bar{M}$ can be stored in tabular form

or the complete double integral Eq. (E-8a) can be calculated. If the first method is used an interpolation is performed for intermediate values of $\bar{A}$ and $\bar{B}$. In a similar manner, for z = 0

$$C_{pp}^{(2)}(z', \eta, 0) = \frac{\rho_o^2}{4\pi^2} \int_{-\infty}^{\infty} \frac{d\omega[u'(|z_0'|)]^4}{M} \bar{M}\left(\frac{\omega}{M}, 0, \frac{\eta}{M}\right) \qquad \text{(E-9a)}$$

where

$$\bar{M}(\bar{A}, 0, \bar{C}) = M^{-1} \int_{-\eta}^{\infty} d\Delta P(\eta, 0, |z_0'|, \Delta, \omega) =$$

$$\int_{-\bar{C}}^{\infty} \Bigg(\bar{C}^2 \Delta b^{-1} a^{-.5} \Big\{ B(x) D_1(\xi) + 2a^{-1}x^{-1}\rho\bar{C}[1-2\rho(\rho+\bar{C})a^{-1}][B(x)-C(x)]D_1(\xi)$$

$$+ \rho^2 \xi^{-1} B(x) D_1'(\xi) - \rho(\rho + \bar{C})a^{-1} B(x) D_1(\xi) \Big\} +$$

$$\Big\{ \bar{C}\Delta b^{-1}[3A(x) + B(x)] + 2\bar{C}^2\Delta^2 b^{-1}a^{-1}[B(x) - .5C(x)] +$$

$$a^{-1}[.75A(x) + .5B(x) + .75C(x)] \Big\} \rho a^{-.5} D_1(\xi) \Bigg) d\Delta \qquad \text{(E-9b)}$$

and

$$\bar{A} = \omega/M$$

$$\bar{C} = \eta/M$$

$$b = \Delta^2 + \bar{A}^2$$

$$\rho = \Delta + \bar{C}$$

$$\xi = \sqrt{\rho^2 + \bar{A}^2}$$

$$a = (\rho + \bar{C})^2 + A^2$$

$$x = 4\rho\bar{C}\,a^{-1}$$

Again the integration over Δ should be broken into two parts, one from 0 to $\bar{C}$ and the other from $\bar{C}$ to ∞ for use of numerical integration.

The calculation of $C_{pp}^{(1)}$ proceeds in a similar way though it is much easier. First the integration is performed over angle. The required scalar integrals are [the underbars do not represent vectors on $\underline{A}(x)$ and $\underline{B}(x)$]

$$a^{-1/2}\,C(x) = \int_0^{\pi} |\underline{r}-\underline{\xi}|^{-1}\,d\phi$$

$$4a^{-1/2}\,\underline{B}(x) = 8a^{-1/2}\int_0^1 y^2(1-y^2)^{1/2}(1-xy)^{-1/2}dy =$$

$$\int_0^{\pi} \sin^2\phi\,|\underline{r}-\underline{\xi}|^{-1}d\phi \qquad \text{(E-10)}$$

$$a^{-1/2}\,\underline{A}(x) = a^{-1/2}[C(x)-4\underline{B}(x)] = \int_0^{\pi} \cos^2\phi\,|\underline{r}-\underline{\xi}|^{-1}d\phi$$

Now $\underline{B}(x)$ is not easily expressed in terms of the elliptic integrals; therefore, $\underline{B}(x)$ is calculated as a function of x for $0 \leq x \leq 1$ and stored for later use. A polynomial fit could also be made. Substituting Eqs. (E-10) into Eqns. (42)-(44) yields

$$C_{pp}^{(1)}(\eta, 0, z, z') = \frac{2\rho_o^2}{\pi} \int_{-\infty}^{\infty} d\omega[\bar{u}'(|z_0'|)u'(|z_0'|)]^2 \int_0^{\infty} \rho d\rho\, N(\rho, \omega, \eta, z, z') \tag{E-11}$$

where

$$N(\rho, \omega, \eta, z, z') = a^{-.5} \left(\frac{\xi_3^2}{M^2} \left\{ \left[7DB\left(\frac{\xi}{M}\right) - Q_1\left(\frac{\xi}{M}\right) \right] \frac{\rho^2}{\xi^2} \underline{A}(x) - \right. \right.$$

$$\left. DB\left(\frac{\xi}{M}\right) C(x) \right\} + \left[f\left(\frac{\xi}{M}\right) - Q_2\left(\frac{\xi}{M}\right) - \frac{\xi^2}{M^2} DB\left(\frac{\xi}{M}\right) \right] \frac{\rho^2}{\xi^2} \underline{A}(x) -$$

$$\left. \left[2f\left(\frac{\xi}{M}\right) \frac{\xi^2}{M^2} DB\left(\frac{\xi}{M}\right) \right] C(x)/5 \right) \tag{E-12}$$

and it is recalled that

$$\xi = (\rho^2 + \xi_3^2)^{.5}$$

$$\xi_3 = z - \omega$$

$$z_0' = z' + \omega$$

$$x = 4\eta\rho/a$$

$$a = (\eta + \rho)^2 + \omega^2$$

$$M = (T^{-1} + |z_0'|^{-1})^{-1}$$

Replace $\underline{A}(x)$ by $\underline{B}(x)$ in $C_{pp}^{(1)}(0, \eta, z, z')$. Direct numerical integration of Eq. (E-11) may follow though there may be a time advantage by replacing the integral over ω from $-\infty$ to ∞ by one from 0 to ∞. When either z, or η is zero, then C_{pp}^{1} can be determined in terms of a two parameter scalar function $\bar{N}$ which is equal to

$$\bar{N}(\bar{A}, \bar{B}, \bar{C}) = M^{-1}\int_0^\infty \rho d\rho\, N(\rho, \omega, \eta, z, |z_0'|) =$$

$$M^{-1}\int_0^\infty \rho d\rho \Big((\bar{B}-\bar{A})^2 \Big| [7DB(\xi) - Q_1(\xi)]\, \rho^2 \xi^{-2} \underline{A}(x) -$$

$$DB(\xi)C(x)\Big| + [f(\xi) - Q_2(\xi) - \xi^2\, DB(\xi)]\, \rho^2 \xi^{-2} \underline{A}(x)$$

$$- [2f(\xi) - \xi^2 DB(\xi)]\, C(x)/5 \Big) a^{-.5} \qquad \text{(E-13)}$$

where

$$\bar{A} = \omega/M$$

$$\bar{B} = z/M$$

$$\bar{C} = \eta/M$$

$$a = (\rho + \bar{C})^2 + \bar{A}^2$$

$$\xi = \sqrt{\rho^2 + (\bar{B} - \bar{A})^2}$$

$$x = 4\rho\bar{C}\, a^{-1}$$

and $\underline{A}(x)$ and $\underline{B}(x)$ are interchangeable depending on whether the x or y correlation function is desired. The variance is easy to determine since then $\bar{N}$ reduces to a one parameter function.

Appendix F

GRAPHICAL REPRESENTATIONS OF VARIOUS FUNCTIONS USED TO CALCULATE THE PRESSURE CORRELATION

Figure F-1 is the plot of the longitudinal velocity coefficient $f(r)$ vs r on a log-log scale. Figure F-2 is the plot of $g(r)$ vs r on a linear scale. A plot of $Q_1(r)$ vs r is shown on a log-log scale in figure F-3. $D_2(r)$ and $-D_1'(r)$ vs r are shown in figs. F-4 and F-5 using log-log scaling. The quantity $\xi^{-7}\bar{E}_6(\xi)$ vs ξ is shown in figure F-6 on a log-log scale. The function $\underline{B}(x)$ vs x is shown in figure F-7 on a linear scale. Note that tabular data is included in figures F-1 through F-7.

As mentioned in Appendix E, it is possible to obtain two parameter functions $\bar{M}$ and $\bar{N}$, when either η or z is equal to zero, from which the correlation functions could be calculated. For a large number of correlation calculations for differing flow field conditions this technique would have a significant computer time advantage over performing a double integral for each desired point. For $\eta = 0$ the function $\bar{M}(\bar{A}, \bar{B}, 0)$ is calculated and shown in perspective in figure F-8. The parameters $\bar{A} = \omega/M$(x axis) and $\bar{B} = z/M$ (y axis) with $M = (T^{-1} + |z' + \omega|^{-1})^{-1}$ with ranges of $-100 \le \bar{A} \le 1$ and $0 \le \bar{B} \le 100$ were used to calculate $\bar{M}$. The parameter interval was varied logarithmicly. Figure F-8 views the function from a location of x = 10, y = 100, z = 100. The plot shown is for the range of values $-5 \le \bar{A} \le 1$ and $0 \le \bar{B} \le 5$. The scaling is reduced by a factor of 5 in the y direction and a factor of 10 in the z direction. Note that there are two sheets to the function - one for positive $\bar{A}$ and the other for negative $\bar{A}$.

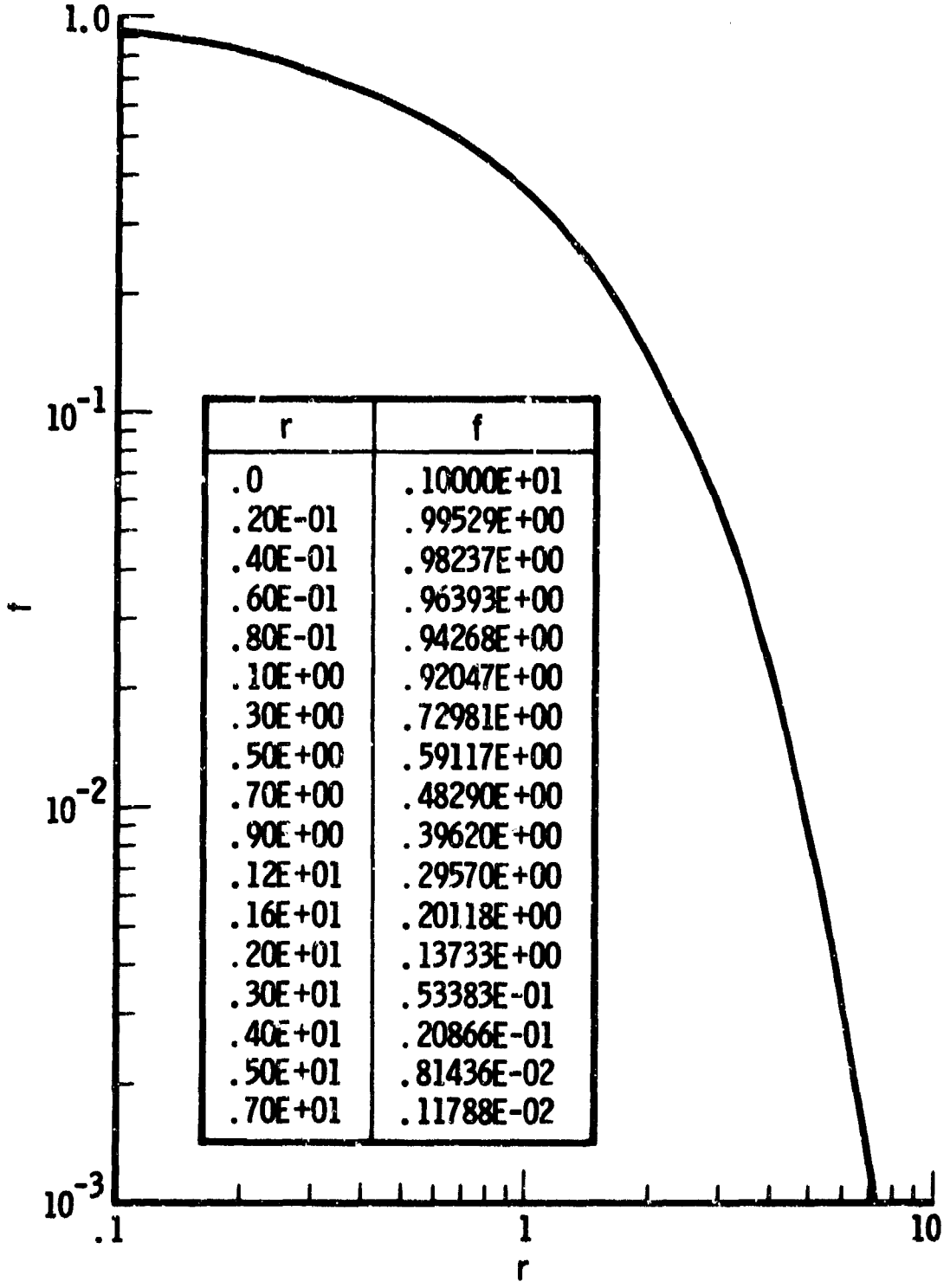

r	f
.0	.10000E+01
.20E-01	.99529E+00
.40E-01	.98237E+00
.60E-01	.96393E+00
.80E-01	.94268E+00
.10E+00	.92047E+00
.30E+00	.72981E+00
.50E+00	.59117E+00
.70E+00	.48290E+00
.90E+00	.39620E+00
.12E+01	.29570E+00
.16E+01	.20118E+00
.20E+01	.13733E+00
.30E+01	.53383E-01
.40E+01	.20866E-01
.50E+01	.81436E-02
.70E+01	.11788E-02

Fig. F-1. Longitudinal Velocity Coefficient

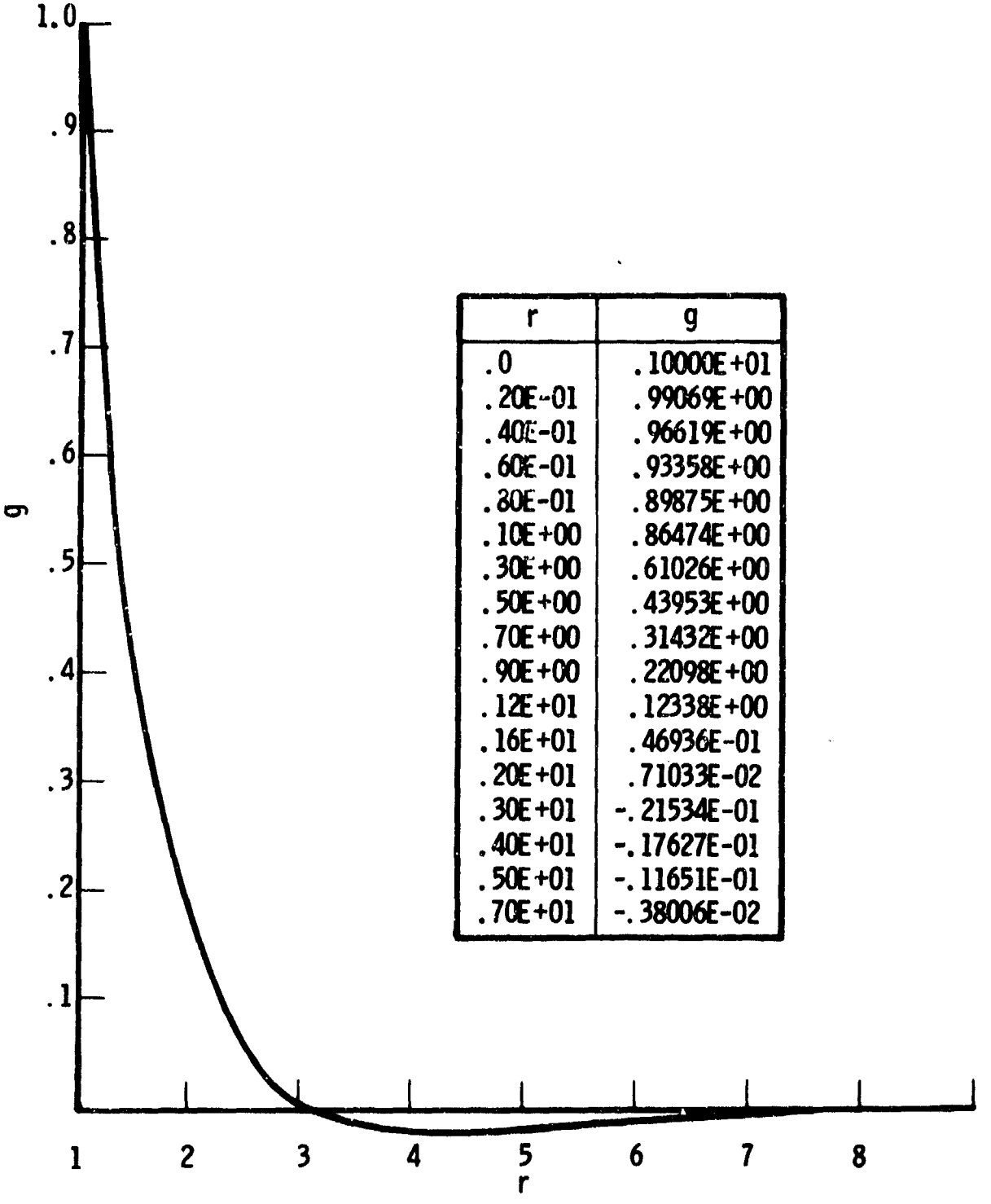

r	g
.0	.10000E+01
.20E-01	.99069E+00
.40E-01	.96619E+00
.60E-01	.93358E+00
.80E-01	.89875E+00
.10E+00	.86474E+00
.30E+00	.61026E+00
.50E+00	.43953E+00
.70E+00	.31432E+00
.90E+00	.22098E+00
.12E+01	.12338E+00
.16E+01	.46936E-01
.20E+01	.71033E-02
.30E+01	-.21534E-01
.40E+01	-.17627E-01
.50E+01	-.11651E-01
.70E+01	-.38006E-02

Fig. F-2. Transverse Velocity Coefficient

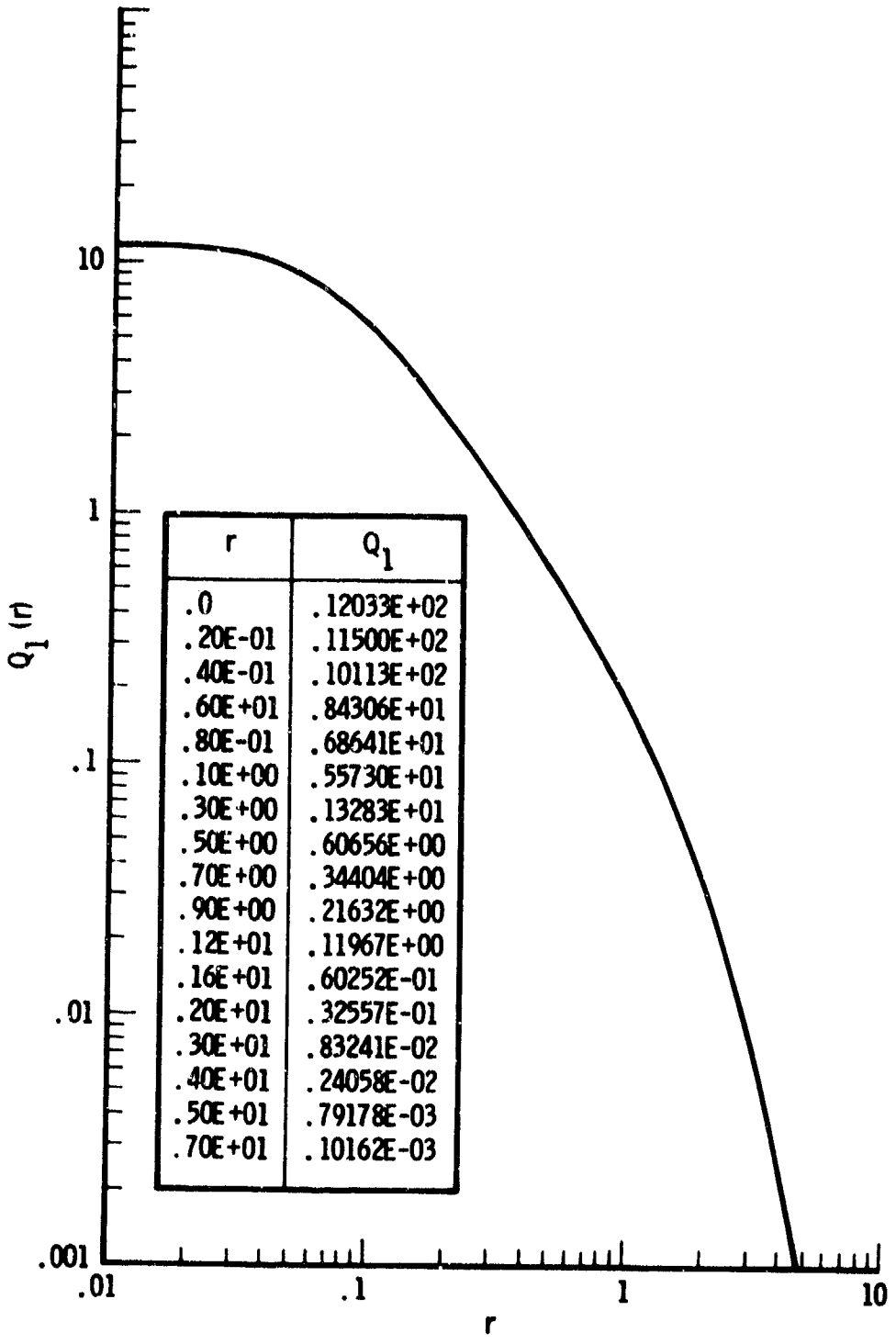

r	Q_1
.0	.12033E+02
.20E-01	.11500E+02
.40E-01	.10113E+02
.60E+01	.84306E+01
.80E-01	.68641E+01
.10E+00	.55730E+01
.30E+00	.13283E+01
.50E+00	.60656E+00
.70E+00	.34404E+00
.90E+00	.21632E+00
.12E+01	.11967E+00
.16E+01	.60252E-01
.20E+01	.32557E-01
.30E+01	.83241E-02
.40E+01	.24058E-02
.50E+01	.79178E-03
.70E+01	.10162E-03

Fig. F-3. Q_1 vs r

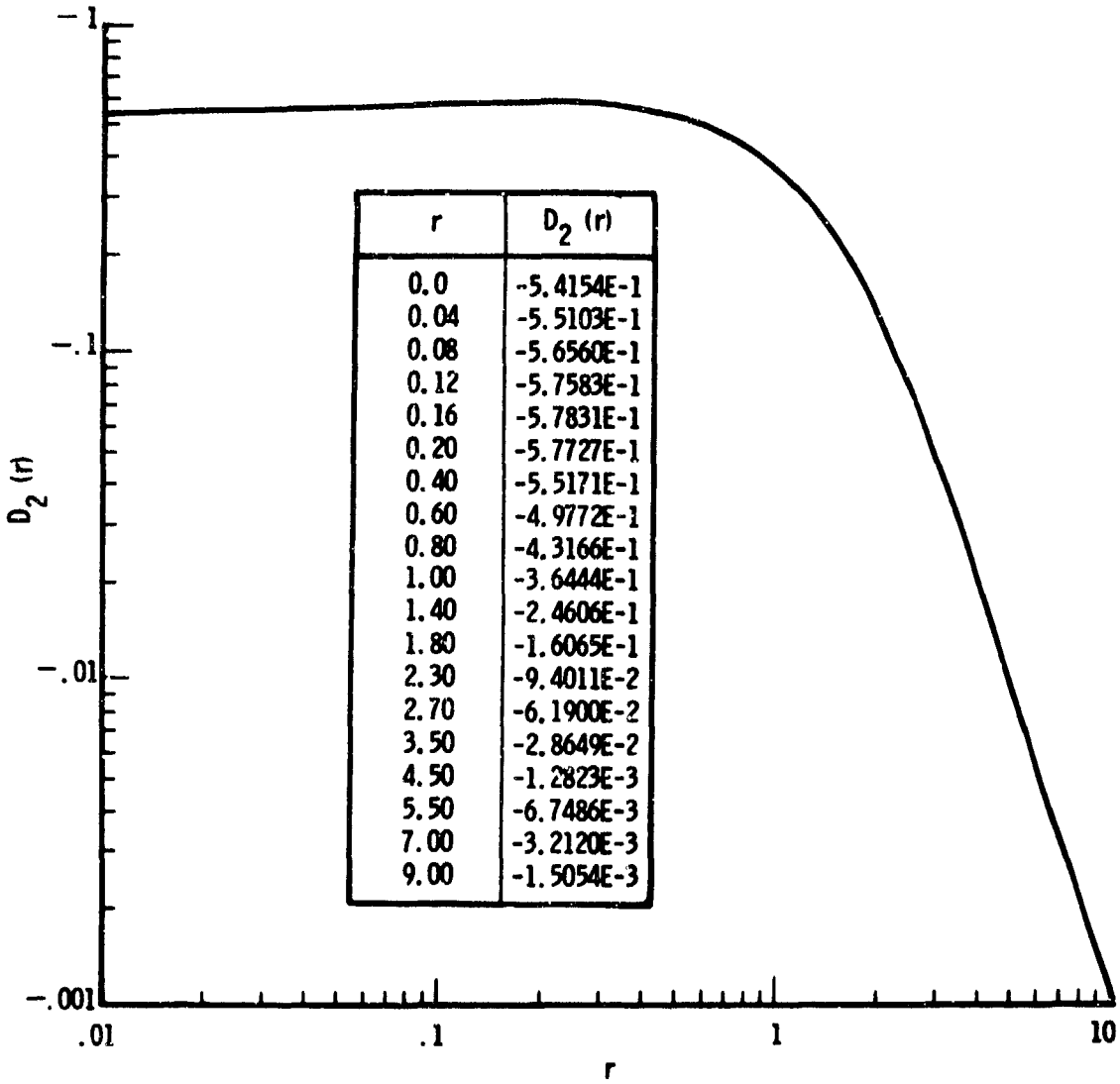

r	D_2 (r)
0.0	-5.4154E-1
0.04	-5.5103E-1
0.08	-5.6560E-1
0.12	-5.7583E-1
0.16	-5.7831E-1
0.20	-5.7727E-1
0.40	-5.5171E-1
0.60	-4.9772E-1
0.80	-4.3166E-1
1.00	-3.6444E-1
1.40	-2.4606E-1
1.80	-1.6065E-1
2.30	-9.4011E-2
2.70	-6.1900E-2
3.50	-2.8649E-2
4.50	-1.2823E-3
5.50	-6.7486E-3
7.00	-3.2120E-3
9.00	-1.5054E-3

Fig. F-4. D_2 (r) vs r

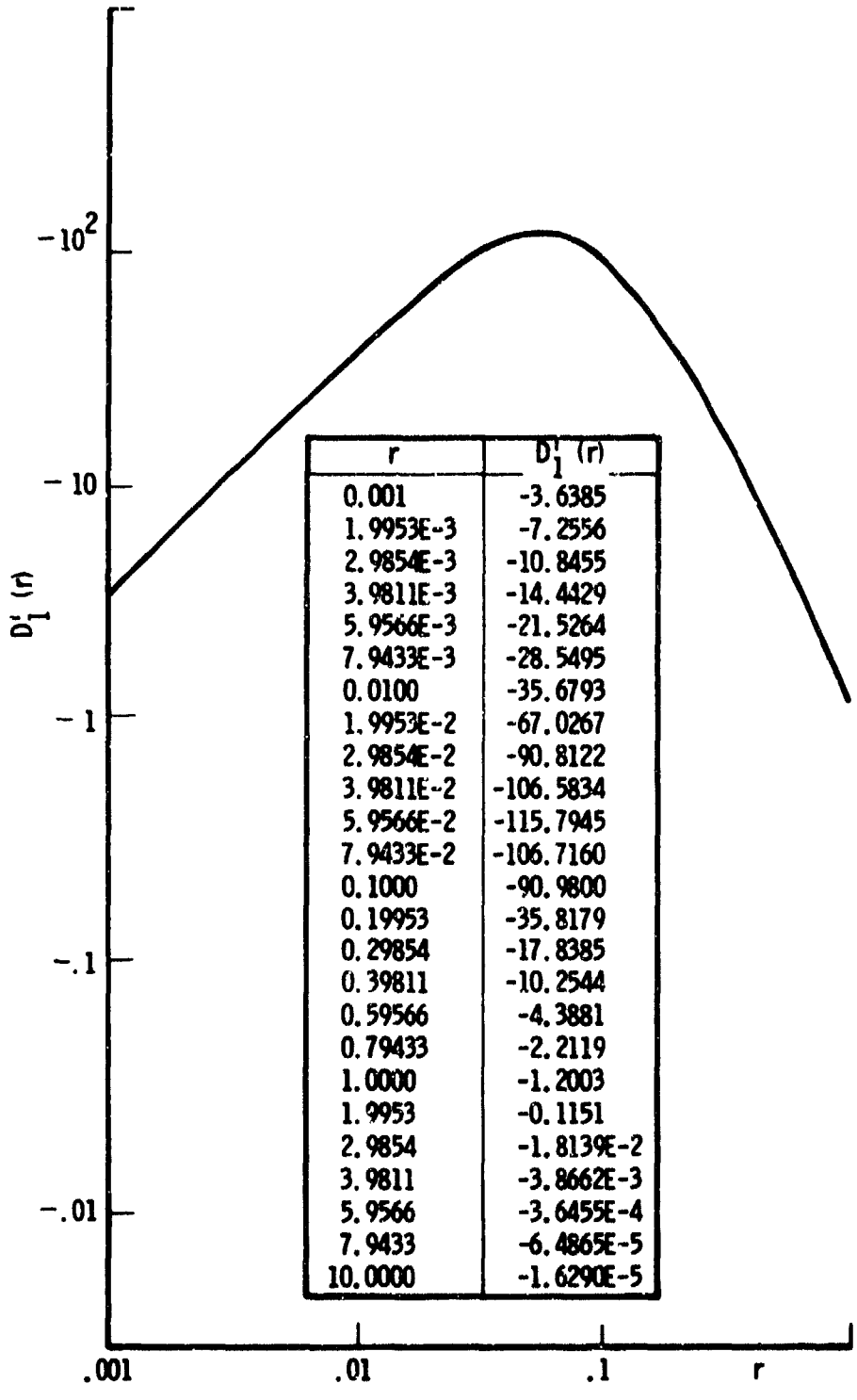

r	$D'_1(r)$
0.001	-3.6385
1.9953E-3	-7.2556
2.9854E-3	-10.8455
3.9811E-3	-14.4429
5.9566E-3	-21.5264
7.9433E-3	-28.5495
0.0100	-35.6793
1.9953E-2	-67.0267
2.9854E-2	-90.8122
3.9811E-2	-106.5834
5.9566E-2	-115.7945
7.9433E-2	-106.7160
0.1000	-90.9800
0.19953	-35.8179
0.29854	-17.8385
0.39811	-10.2544
0.59566	-4.3881
0.79433	-2.2119
1.0000	-1.2003
1.9953	-0.1151
2.9854	-1.8139E-2
3.9811	-3.8662E-3
5.9566	-3.6455E-4
7.9433	-6.4865E-5
10.0000	-1.6290E-5

Fig. F-5. $D'_1(r)$ vs r

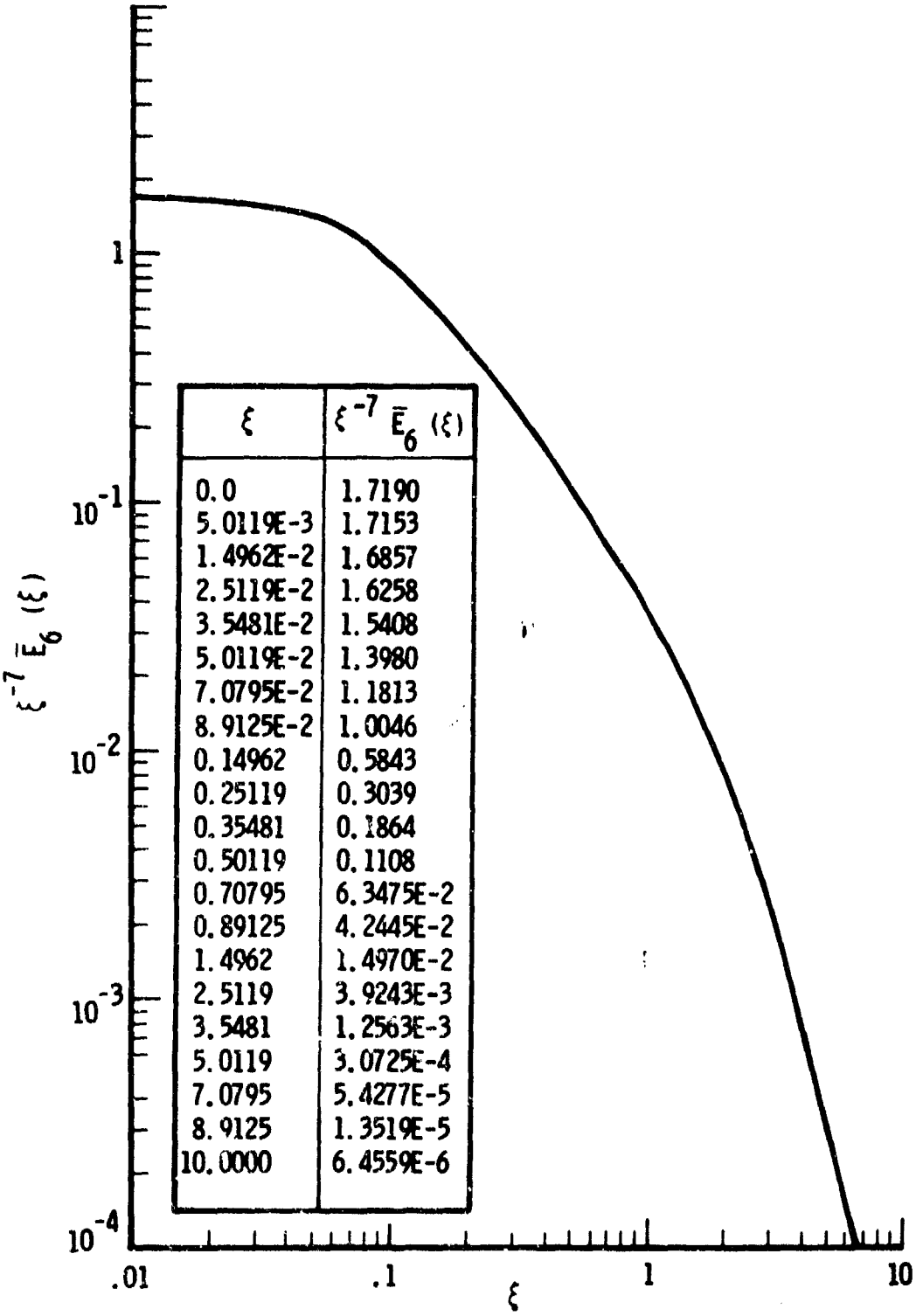

ξ	$\xi^{-7}\bar{E}_6(\xi)$
0.0	1.7190
5.0119E-3	1.7153
1.4962E-2	1.6857
2.5119E-2	1.6258
3.5481E-2	1.5408
5.0119E-2	1.3980
7.0795E-2	1.1813
8.9125E-2	1.0046
0.14962	0.5843
0.25119	0.3039
0.35481	0.1864
0.50119	0.1108
0.70795	6.3475E-2
0.89125	4.2445E-2
1.4962	1.4970E-2
2.5119	3.9243E-3
3.5481	1.2563E-3
5.0119	3.0725E-4
7.0795	5.4277E-5
8.9125	1.3519E-5
10.0000	6.4559E-6

Fig. F-6. $\xi^{-7}\bar{E}_6(\xi)$ vs ξ

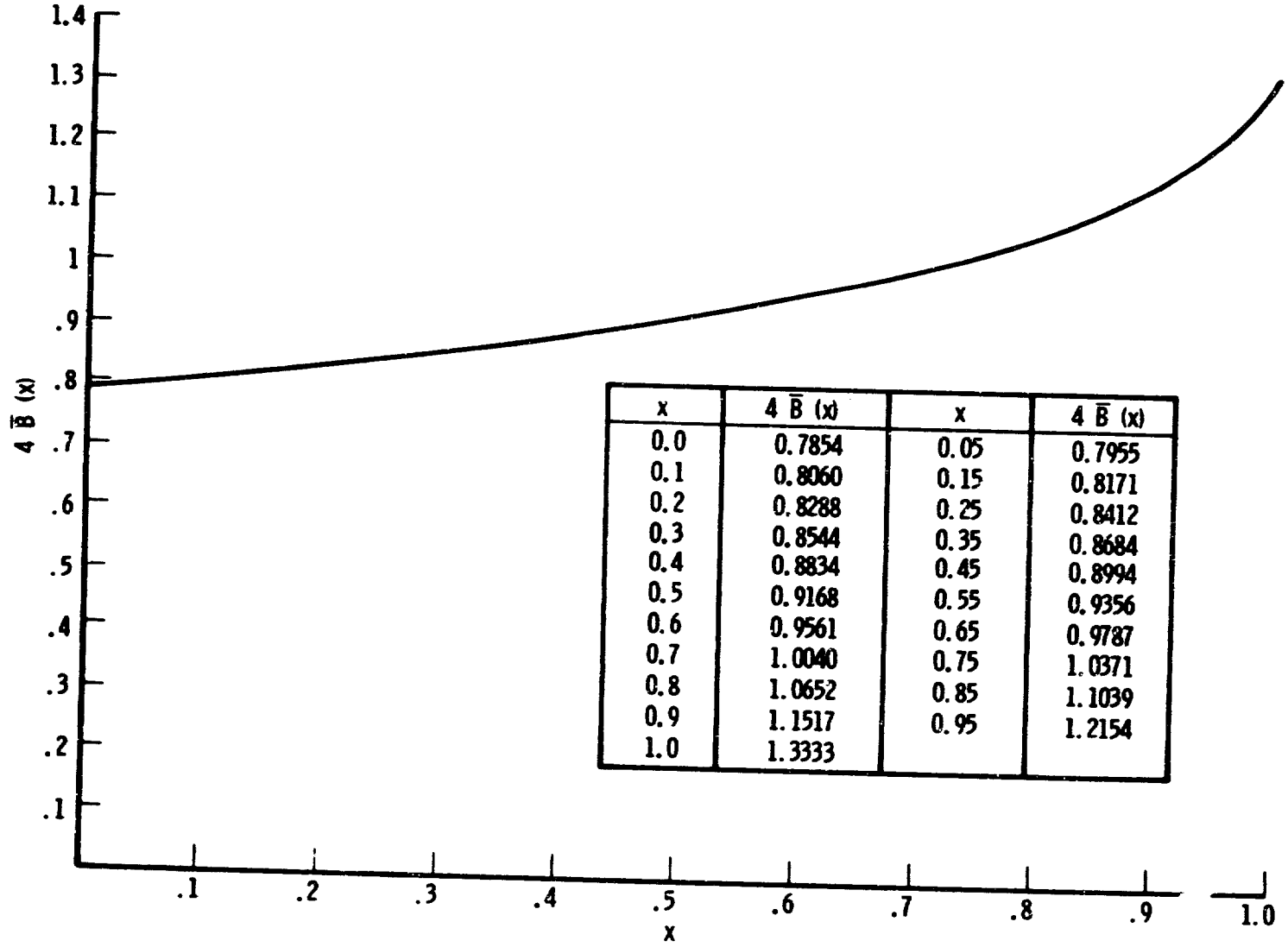

x	4 B̄ (x)	x	4 B̄ (x)
0.0	0.7854	0.05	0.7955
0.1	0.8060	0.15	0.8171
0.2	0.8288	0.25	0.8412
0.3	0.8544	0.35	0.8684
0.4	0.8834	0.45	0.8994
0.5	0.9168	0.55	0.9356
0.6	0.9561	0.65	0.9787
0.7	1.0040	0.75	1.0371
0.8	1.0652	0.85	1.1039
0.9	1.1517	0.95	1.2154
1.0	1.3333		

Fig. F-7. $4\overline{B}(x)$

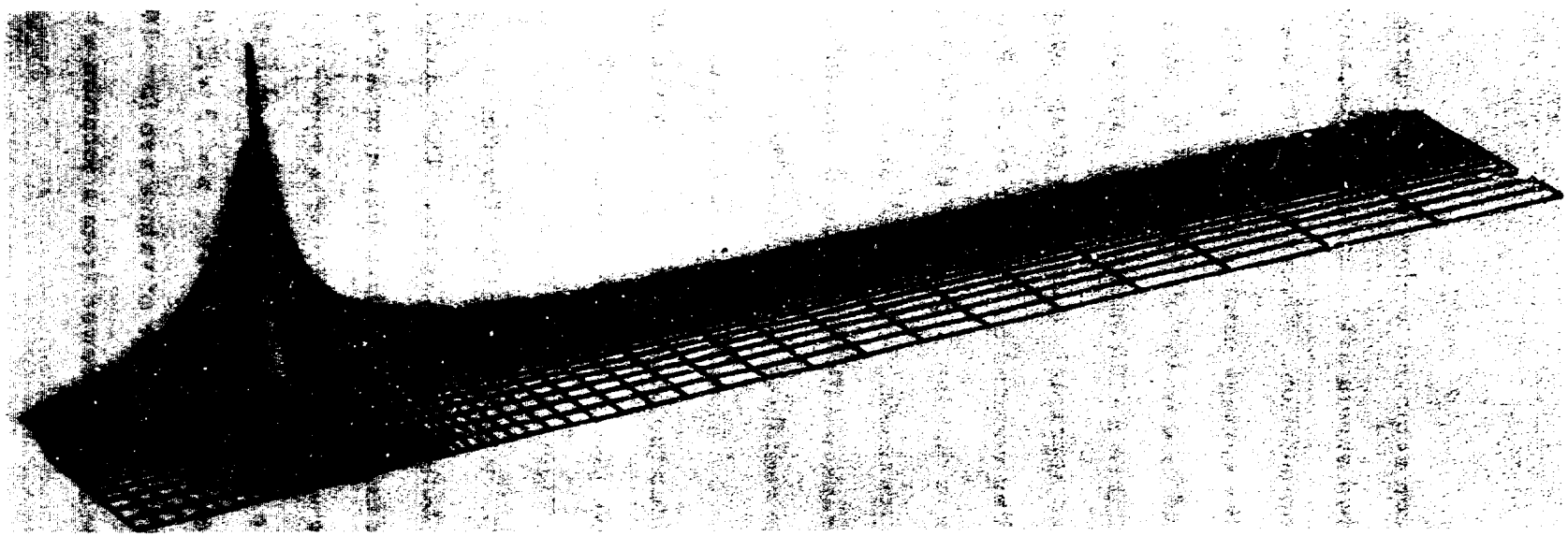

Fig. F-8. Perspective Plot of $\overline{M}$ ($\overline{A}$, $\overline{B}$, 0) from a Location of x = 10, y = 100, z = 100. z scaling reduced by a factor of 10, y scaling by a factor of 5.

The values for $\bar{A} = 0$ have been removed to show a clean figure. If $\bar{M}$ is used to calculate $C_{pp}^{(2b)}$ the two sheets are calculated separately and then added together during the computation. Figure F-9 is the positive sheet of $\bar{M}(\bar{A}, \bar{B}, 0)$ alone from the vantage point of $x = 10$, $y = 10$, $z = 10$. The z scale has been reduced by a factor of 10 and $\bar{M}$ is only plotted for $0 \leq \bar{A} \leq 1$ and $0 \leq \bar{B} \leq 1$. Figure F-10 contains both positive and negative sheets of $\bar{M}(\bar{A}, \bar{B}, 0)$ plotted separately from the vantage point $x = -10$, $y = 10$, $z = 100$ and a z scaling reduced by a factor of 10. From figures F-8, F-9, and F-10 it is seen that the $\bar{A}$ positive sheet is maximum at the origin and falls rapidly for increasing values of $\bar{A}$ or $\bar{B}$. The $\bar{A}$ negative sheet on the other hand increases with increasing $\bar{B}$, reaching a maximum value near $\bar{B} = .1$ then falls rapidly to zero. The other available fourth-order contribution is for $z = 0$. Then $\bar{M}(\bar{A}, 0, \bar{C})$ is required where $\bar{C} = \eta/M$. The function was calculated over the range $0 \leq \bar{A} \leq 10$ and $0 \leq \bar{C} \leq 10$. Figure F-11 is a perspective plot of this function observed from a position of $x = 100$, $y = 100$, $z = 100$. Figure F-12 is the same function observed from $x = 100$, $y = 100$, but $z = 10$. It is seen that the function is highly peaked at $\bar{A} = \bar{C} = 0$ falling rapidly as both $\bar{A}$ and $\bar{C}$ increase. The function falls a bit faster in the $y(\bar{C})$ direction becoming negative then approaching $z = 0$ from the negative values. In the special case that η or z equals zero $\bar{N}$ (Eq. E-13) can be determined. Figure F-13 is a perspective plot of $\bar{N}(\bar{A}, \bar{B}, 0)$ $(\eta = 0)$ viewed from from a location of $x = -20$, $y = 10.$, $z = .3$ with the z scaling increased by a factor of 100. The range of values are for $-10 < x(\bar{A}) \leq 1$ and $0 \leq y(\bar{B}) \leq 10$. The same function is viewed from a location $x = -20$, $y = -20$,

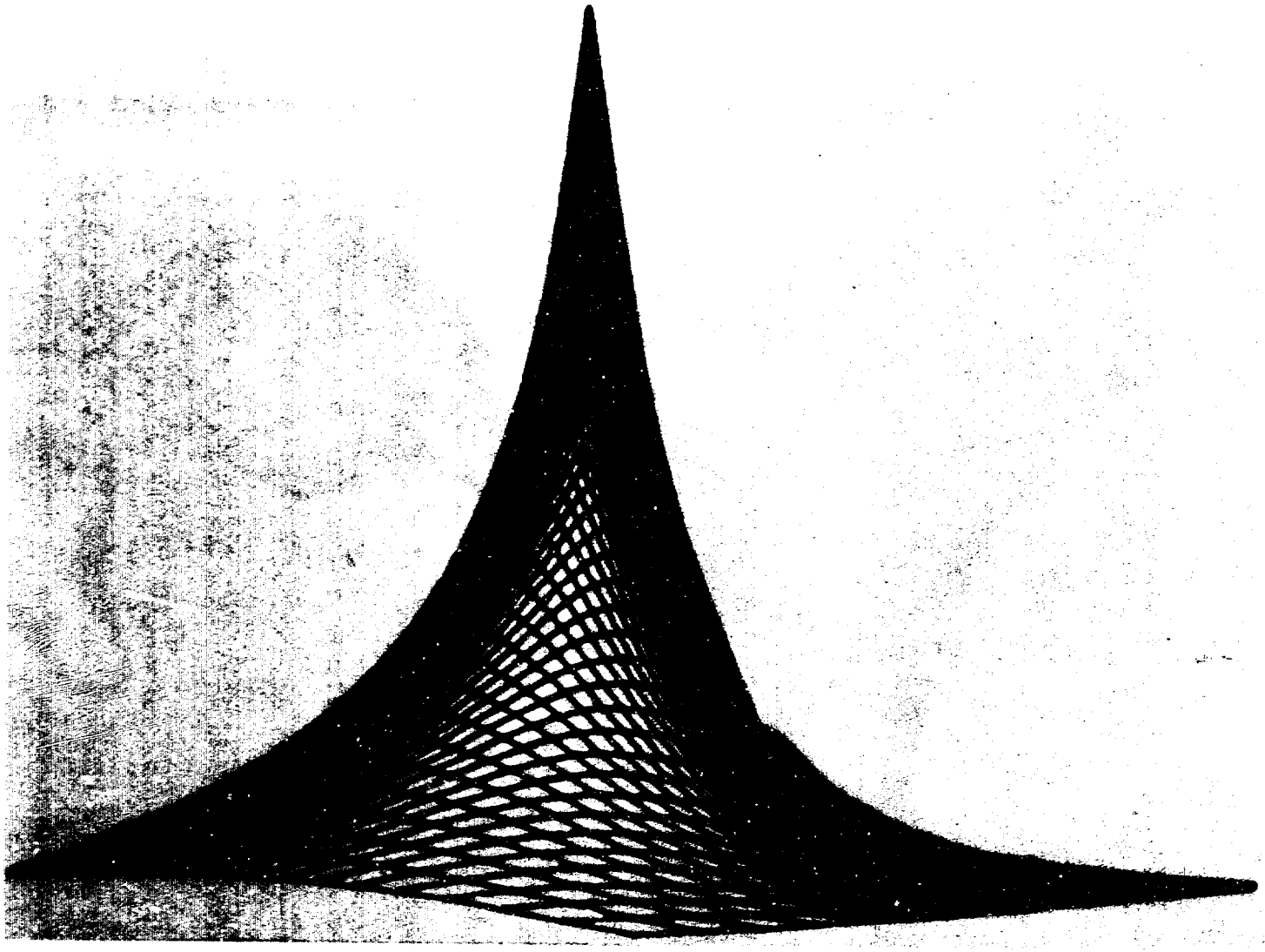

Fig. F-9. Perspective of the Positive $\overline{A}$ sheet of $\overline{M}$ ($\overline{A}$, $\overline{B}$, 0) from a Location ot x = 10, y = 10, z = 10. z scale reduced by a factor 10. $\overline{A}$ and $\overline{B}$ plotted from zero to 1 only.

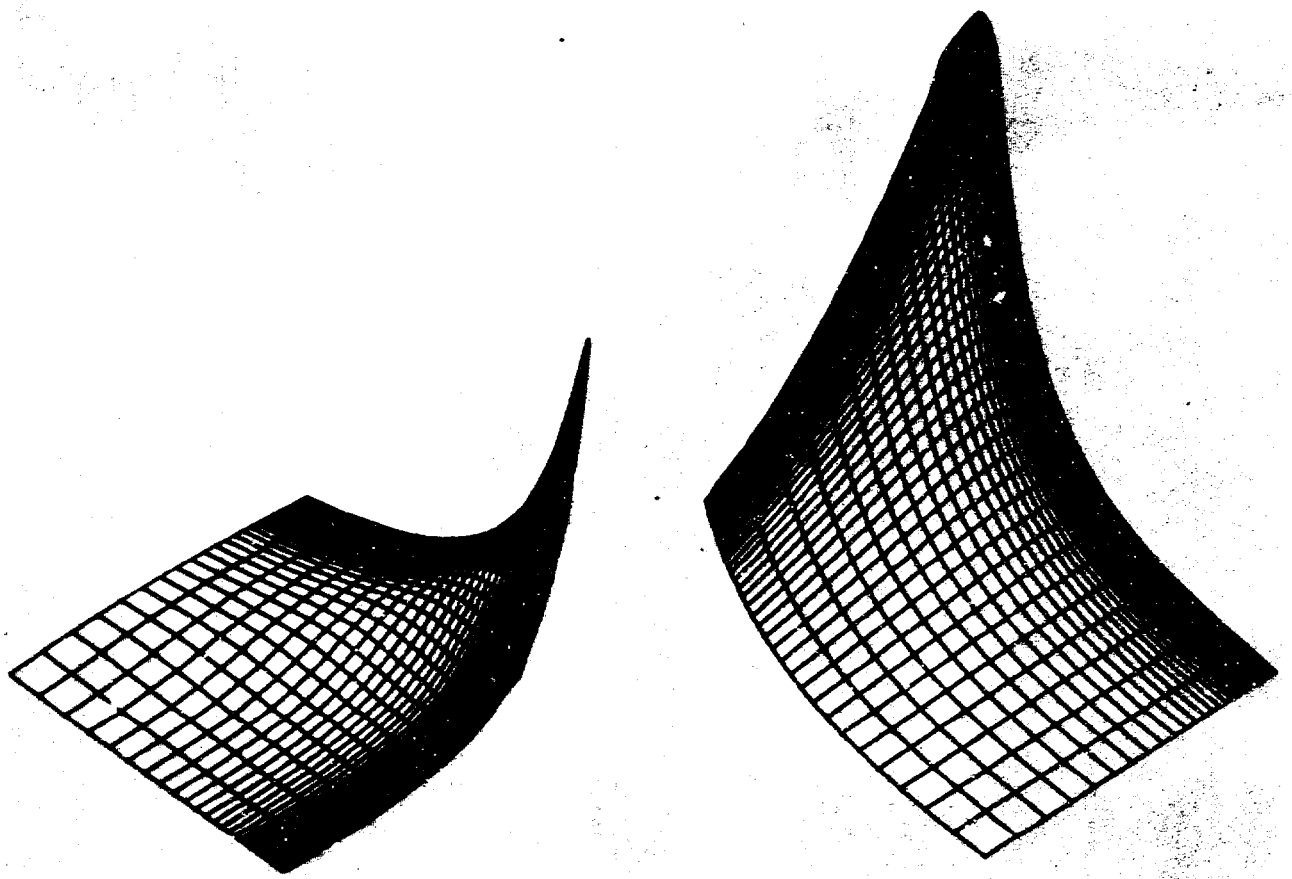

Fig. F-10. Perspective of Positive (left figure) and Negative Sheets of M(A, B, 0) from a Location of x = -10, y = 10, and z = 100. Z scaling reduced by a factor of 10.

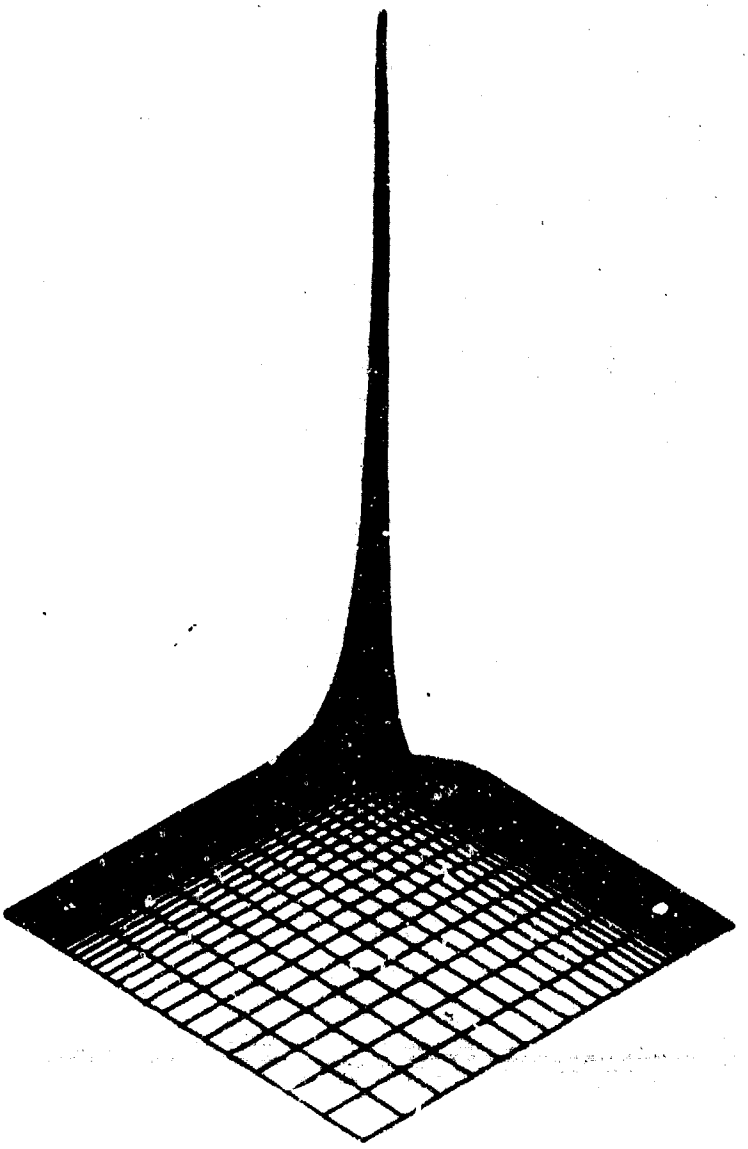

Fig. F-11. Perspective Plot of $\overline{M}(\overline{A}, 0, \overline{C})$ from a Location of 100, 100, 100

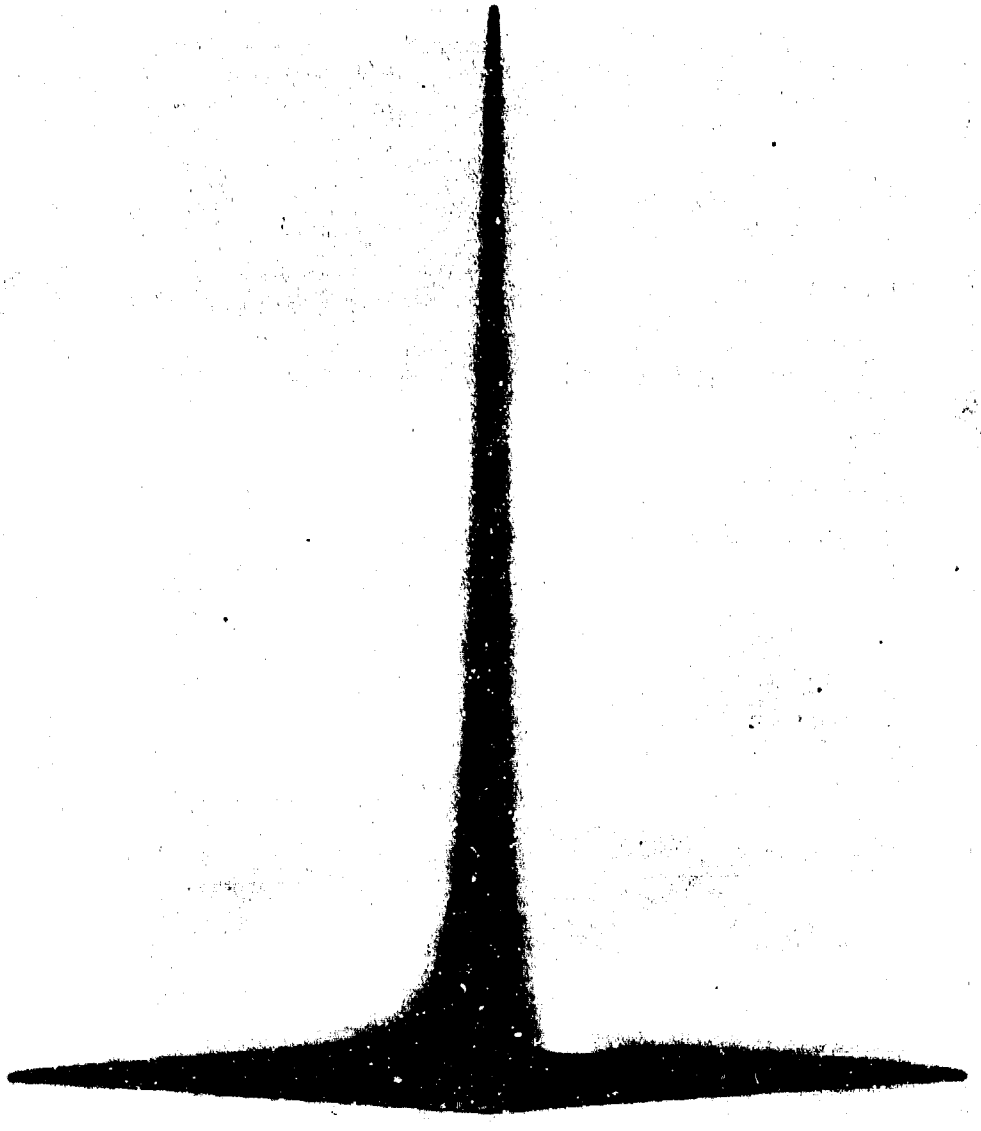

Fig. F-12. Perspective Plot of $\overline{M}(\overline{A}, 0, \overline{J})$ Observed from x = 100, y = 100, z = 10

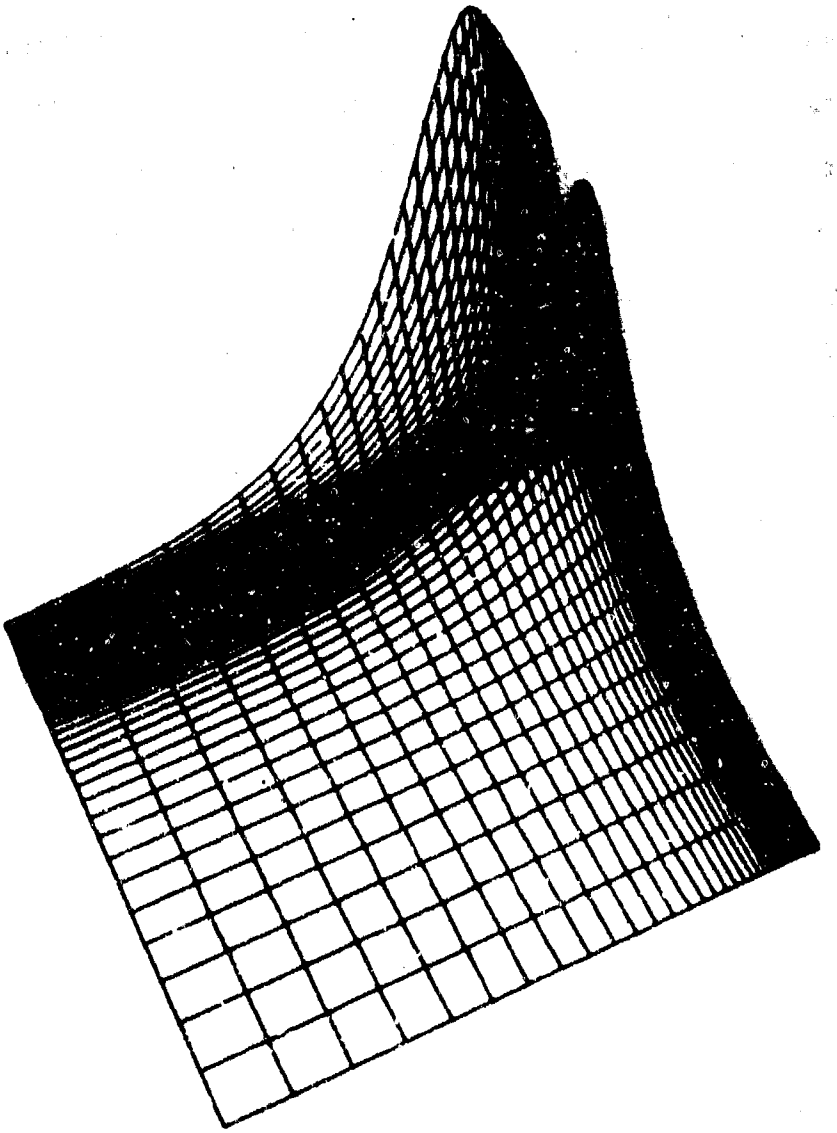

Fig. F-13. Perspective of $\overline{N}(\overline{A}, \overline{B}, 0)$ Viewed from a Location of (-20, 10, .3). The z scaling has been increased by a factor of 100.

$z = 0$ and $x = 0$, $y = 20$, $z = .3$ in figures F-14 and F-15 respectively. Perspective views of $\overline{N}(\overline{A}, 0, \overline{C})$ are given for the x correlation function in figures F-16 and F-17 where the viewing locations are $x = 20$, $y = -20$, $z = .3$ and $x = -20$, $y = -20$, $z = .3$ respectively. The z scaling has been increased by a factor of 50. The perspective views of $\overline{N}(\overline{A}, 0, \overline{C})$ for the y correlation function are given in figures F-18 and F-19. In figures F-16 - F-19 the figures are plotted for $0 \leq x(\overline{A}) \leq 10$ and $0 \leq y(\overline{C}) \leq 10$.

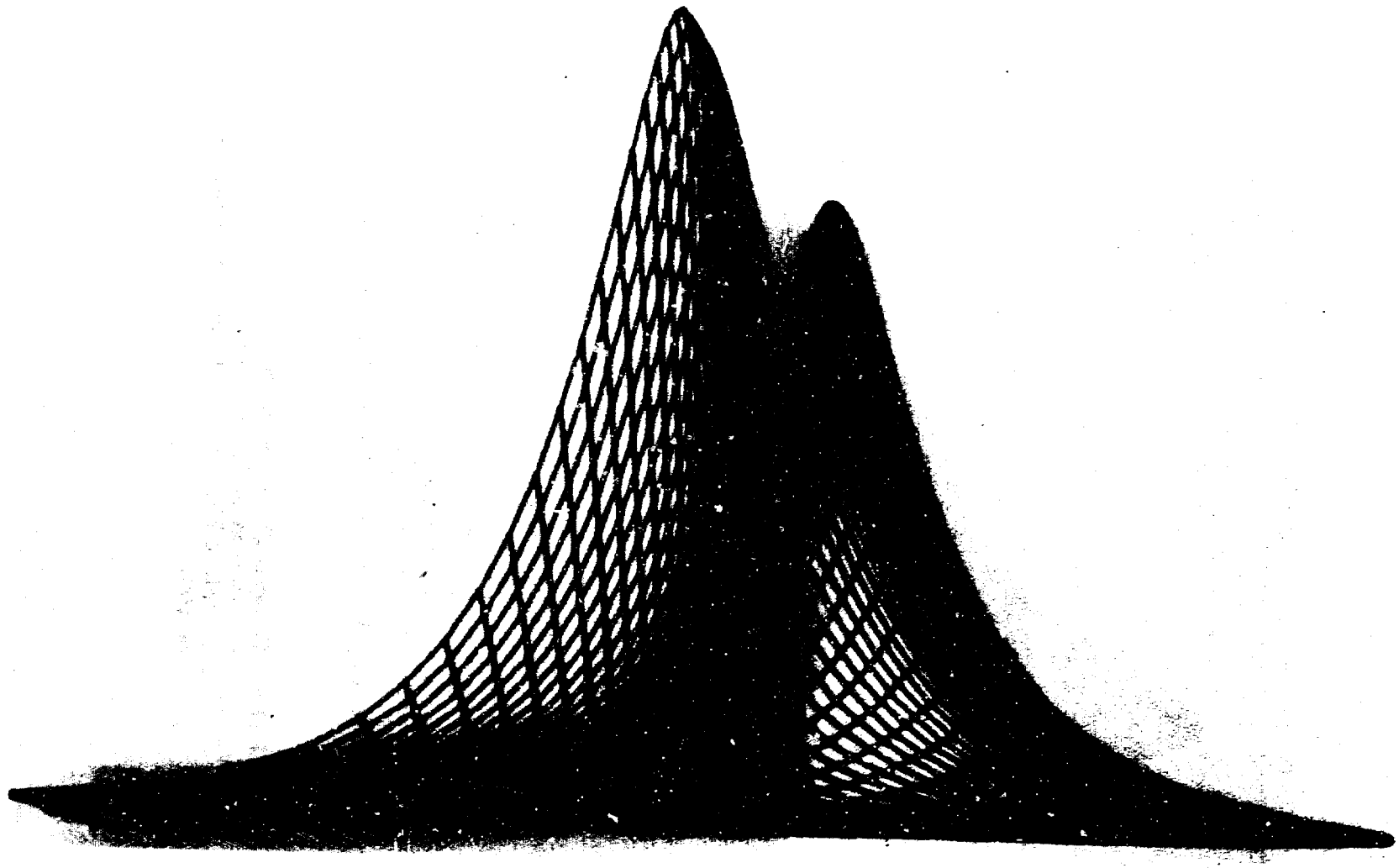

Fig. F-14. Perspective of $\overline{N}(\overline{A}, \overline{B}, 0)$ Viewed from a Location of -20, 20, 0. z scaling increased by a factor of 100.

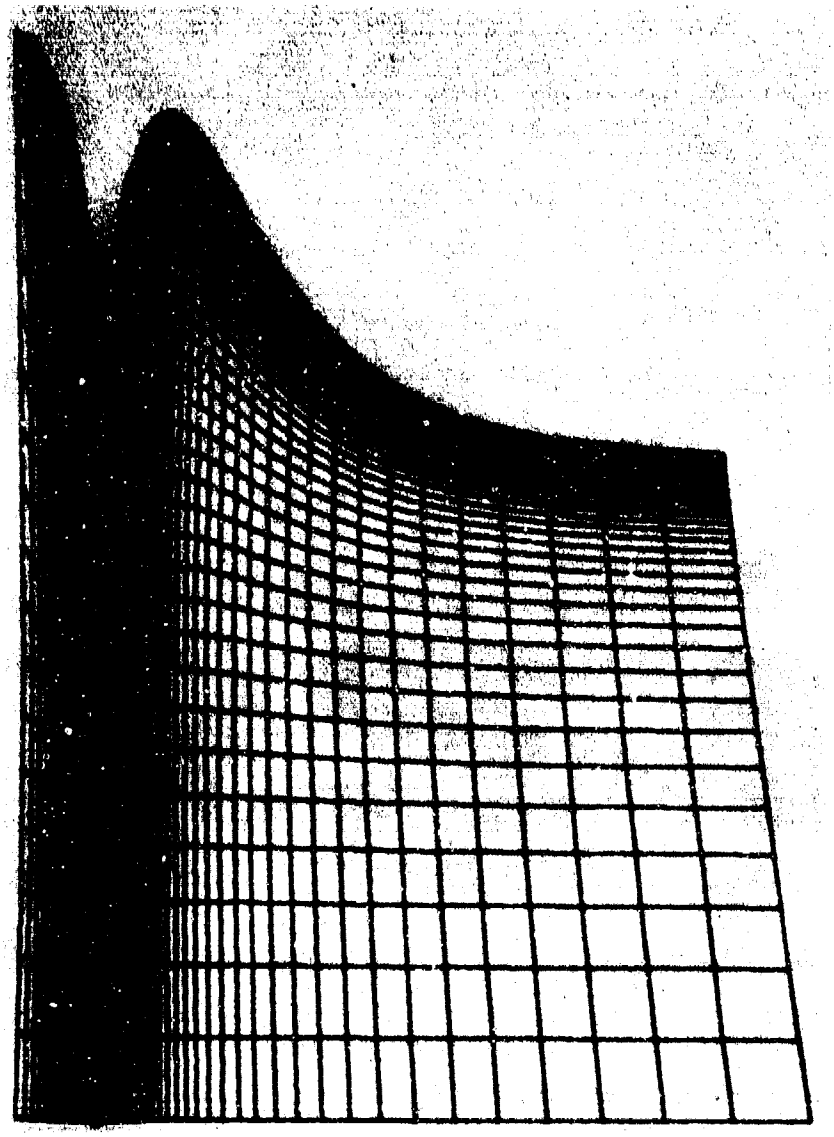

Fig. F-15. Perspective of $\overline{N}(\overline{A}, \overline{B}, 0)$ Viewed from a Location of 0, 20., and 0.3. z scaling has been increased by a factor of 100.

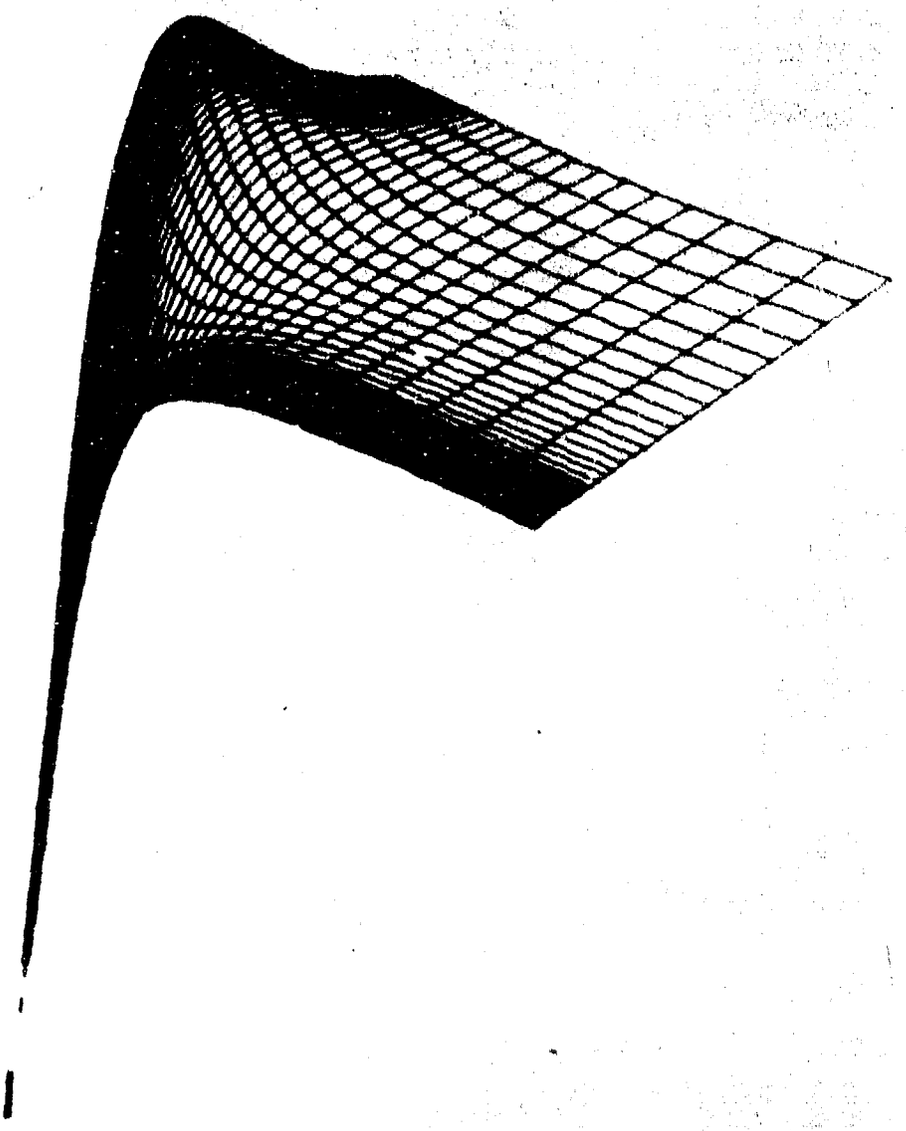

Fig. F-16. Perspective of $\overline{N}(\overline{A}, 0, \overline{C})$ for x Correlation Viewed from a Location of x = 20, y = -20, z = 0.3. z scaling increased by a factor of 50.

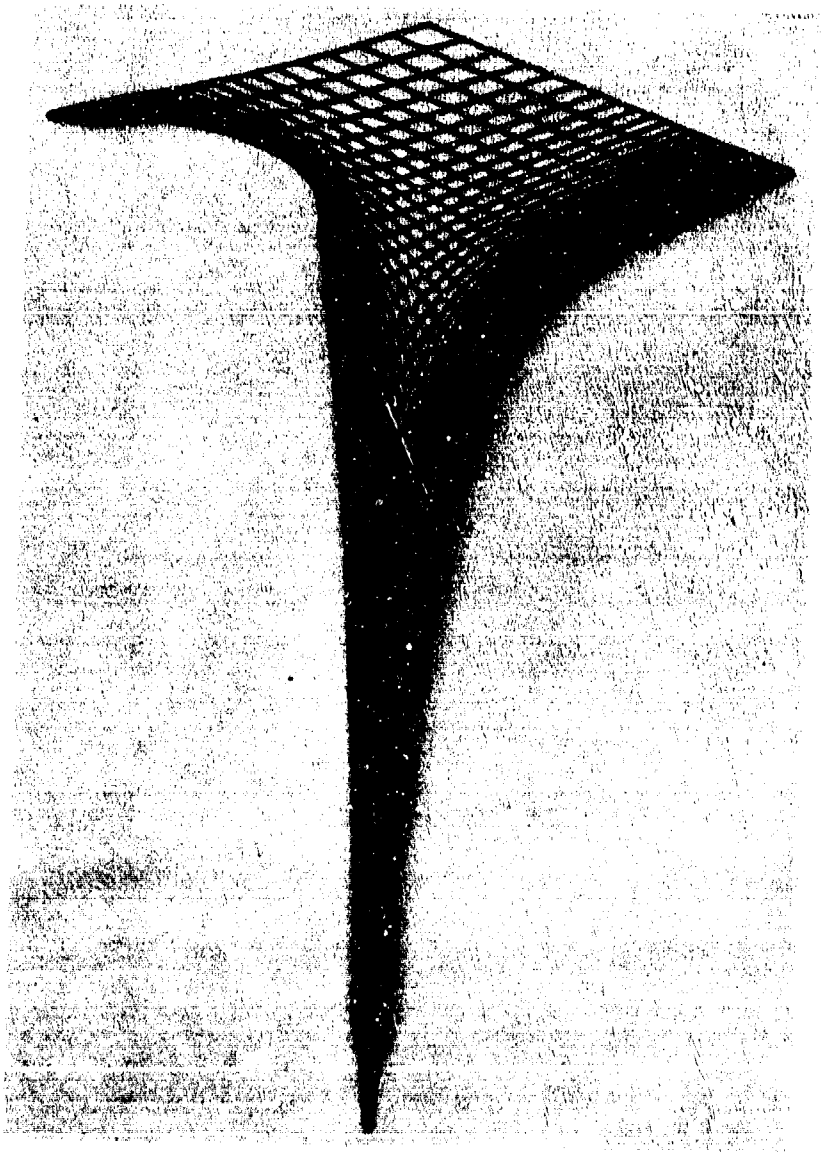

Fig. F-17. Perspective Plot of $\overline{N}(\overline{A}, 0, \overline{C})$ (x correlation) Viewed from a Location of x = -20, y = 20, z = 0.3. z scaling increased by a factor of 50.

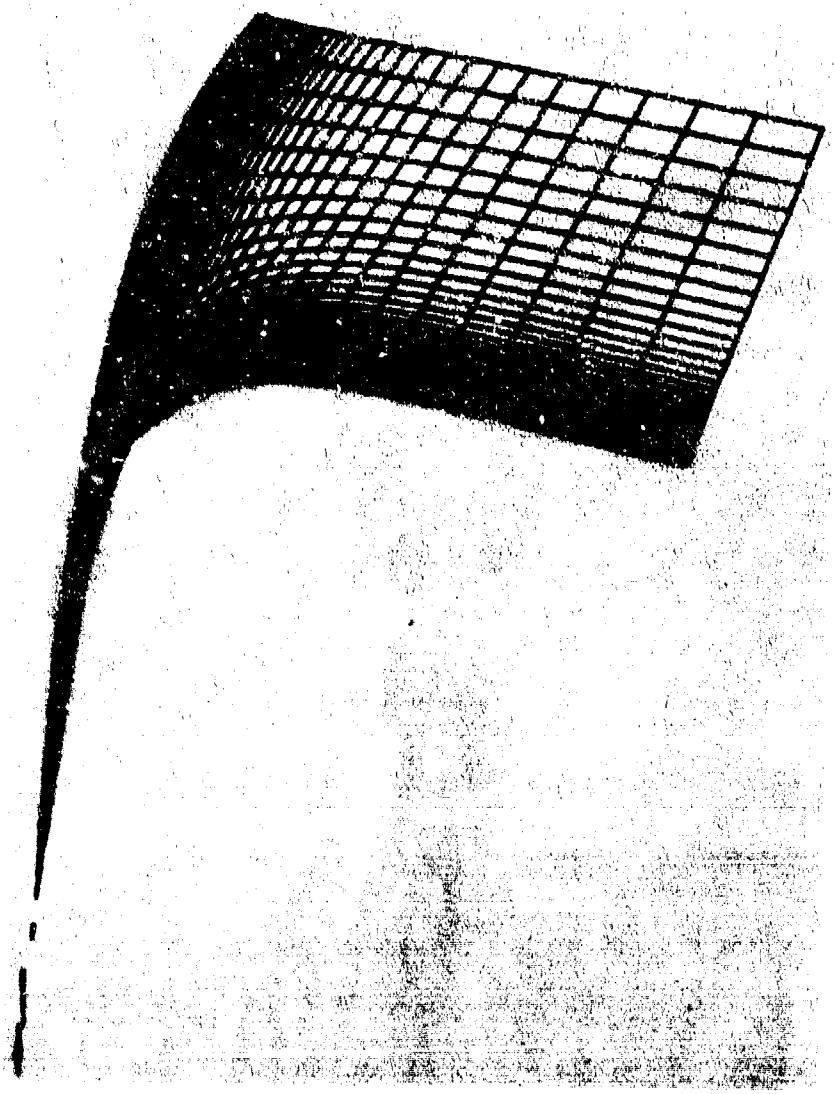

Fig. F-18. Perspective View of $\overline{N}(\overline{A}, 0, \overline{C})$ for the y Correlation Viewed from the Location x = 10, y = -20, z = 0.3. The z scaling is increased by a factor of 50.

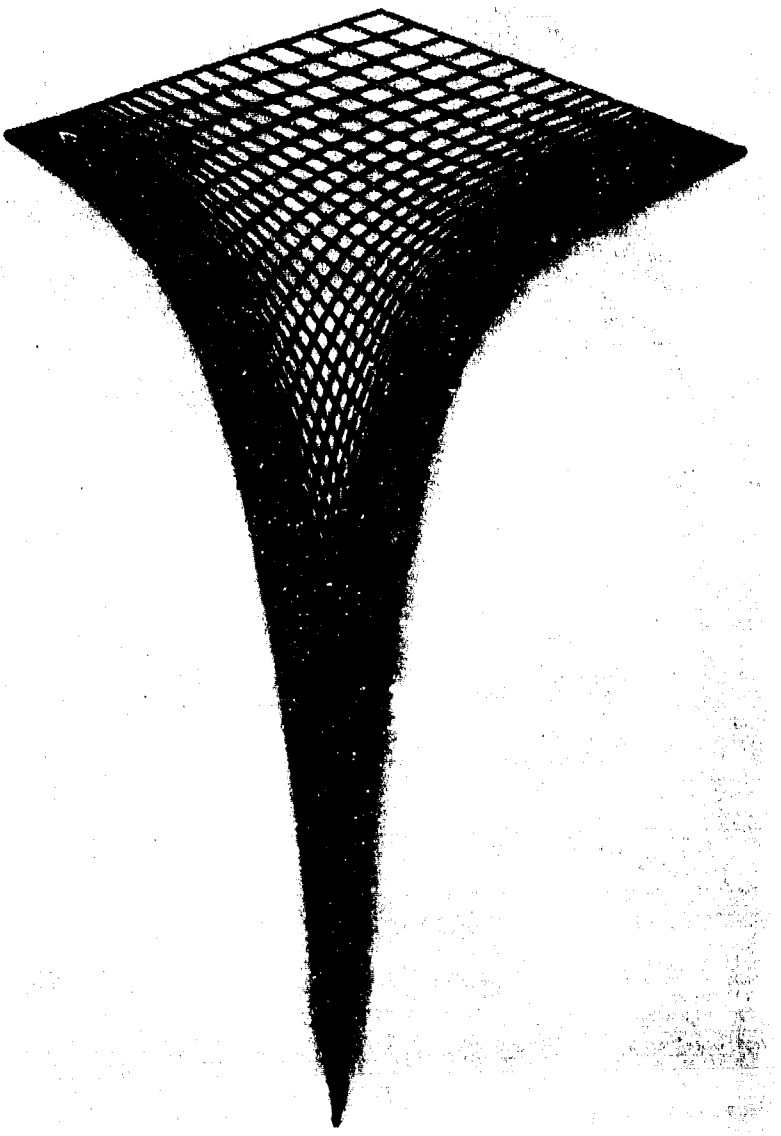

Fig. F-19. Perspective View of $\overline{N}(\overline{A}, 0, \overline{C})$ for the y Correlation Viewed from a Location of x = -20, y = -20, z = 0.3. The z scaling is increased by a factor of 50.

THE IVAN A. GETTING LABORATORIES

The Laboratory Operations of The Aerospace Corporation is conducting experimental and theoretical investigations necessary for the evaluation and application of scientific advances to new military concepts and systems. Versatility and flexibility have been developed to a high degree by the laboratory personnel in dealing with the many problems encountered in the nation's rapidly developing space and missile systems. Expertise in the latest scientific developments is vital to the accomplishment of tasks related to these problems. The laboratories that contribute to this research are:

Aerophysics Laboratory: Launch and reentry aerodynamics, heat transfer, reentry physics, chemical kinetics, structural mechanics, flight dynamics, atmospheric pollution, and high-power gas lasers.

Chemistry and Physics Laboratory: Atmospheric reactions and atmospheric optics, chemical reactions in polluted atmospheres, chemical reactions of excited species in rocket plumes, chemical thermodynamics, plasma and laser-induced reactions, laser chemistry, propulsion chemistry, space vacuum and radiation effects on materials, lubrication and surface phenomena, photosensitive materials and sensors, high precision laser ranging, and the application of physics and chemistry to problems of law enforcement and biomedicine.

Electronics Research Laboratory: Electromagnetic theory, devices, and propagation phenomena, including plasma electromagnetics; quantum electronics, lasers, and electro-optics; communication sciences, applied electronics, semiconducting, superconducting, and crystal device physics, optical and acoustical imaging; atmospheric pollution; millimeter wave and far-infrared technology.

Materials Sciences Laboratory: Development of new materials; metal matrix composites and new forms of carbon; test and evaluation of graphite and ceramics in reentry; spacecraft materials and electronic components in nuclear weapons environment; application of fracture mechanics to stress corrosion and fatigue-induced fractures in structural metals.

Space Sciences Laboratory: Atmospheric and ionospheric physics, radiation from the atmosphere, density and composition of the atmosphere, aurorae and airglow; magnetospheric physics, cosmic rays, generation and propagation of plasma waves in the magnetosphere; solar physics, studies of solar magnetic fields; space astronomy, x-ray astronomy; the effects of nuclear explosions, magnetic storms, and solar activity on the earth's atmosphere, ionosphere, and magnetosphere; the effects of optical, electromagnetic, and particulate radiations in space on space systems.

THE AEROSPACE CORPORATION
El Segundo, California

• • •